Tethering by Uso1 is dispensable: The Uso1 monomeric globular head domain interacts with SNAREs to maintain viability.

Ignacio Bravo-Plaza[1], Víctor G. Tagua[2], Herbert N. Arst, Jr [3], Ana Alonso[1], Mario Pinar[1], Begoña Monterroso[4], Antonio Galindo[5], and Miguel Á. Peñalva[1, $]

Departments of (1) Cellular and Molecular Biology and (4) Structural and Chemical Biology, CSIC Centro de Investigaciones Biológicas, Ramiro de Maeztu 9, 28040 Madrid Spain.

(2) Instituto de Tecnologías Biomédicas, Hospital Universitario Nuestra Señora de Candelaria, Santa Cruz de Tenerife, Spain.

(3) Department of Infectious Diseases, Faculty of Medicine, Flowers Building, Imperial College, Armstrong Road, London, SW7 2AZ, UK

(5) Division of Cell Biology, MRC Laboratory of Molecular Biology, Francis Crick Avenue, Cambridge, CB2 0QH, UK.

($) Corresponding author at the above address

penalva@cib.csis.es
@penalva

phone: +918373112

Summary

Uso1/p115 and RAB1 tether ER-derived vesicles to the Golgi. Uso1/p115 contains a globular-head-domain (GHD), a coiled-coil (CC) mediating dimerization/tethering and a C-terminal region (CTR) interacting with golgins. Uso1/p115 is recruited to vesicles by RAB1. Paradoxically, genetic studies placed Uso1 acting upstream of, or in conjunction with RAB1 (Sapperstein et al., 1996). We selected two missense mutations in *uso1* resulting in E6K and G540S substitutions in the GHD permitting growth of otherwise inviable *rab1*-deficient *Aspergillus nidulans.* Remarkably, the double mutant suppresses the complete absence of RAB1. Full-length Uso1 and CTRΔ proteins are dimeric and the GHD lacking the CC/CTR is monomeric irrespective of whether they carry or not E6K/G540S. Microscopy showed recurrence of Uso1 on puncta (60 sec half-life) colocalizing with RAB1 and less so with early Golgi markers Sed5 and GeaA/Gea1/Gea2. Localization of Uso1 but not of Uso1$^{E6K/G540S}$ to puncta is abolished by compromising RAB1 function, indicating that E6K/G540S creates interactions bypassing RAB1. By S-tag-coprecipitation we demonstrate that Uso1 is an associate of the Sed5/Bos1/Bet1/Sec22 SNARE complex zippering vesicles with the Golgi, with Uso1$^{E6K/G540S}$ showing stronger association. Bos1 and Bet1 bind the Uso1 GHD directly, but Bet1 is a strong E6K/G540S-independent binder, whereas Bos1 is weaker but becomes as strong as Bet1 when the GHD carries E6K/G540S. AlphaFold2 predicts that G540S actually increases binding of GHD to the Bos1 Habc domain. In contrast, E6K seemingly increases membrane targeting of an N-terminal amphipathic α-helix, explaining phenotypic additivity. Overexpression of E6K/G540S and wild-type GHD complemented *uso1*Δ. Thus, a GHD monomer provides the essential Uso1 functions, demonstrating that long-range tethering activity is dispensable. Therefore, when enhanced by E6K/G540S, Uso1 binding to Bos1/Bet1 required to regulate SNAREs bypasses both the contribution of RAB1 to Uso1 recruitment and the reported role of RAB1 in SNARE complex formation (Lupashin and Waters, 1997), suggesting that the latter is consequence of the former.

67 **Introduction**

68 Vesicular traffic at the ER/Golgi interface is the cornerstone of the secretory pathway
69 (Barlowe and Miller, 2013; Weigel et al., 2021). In current models, in which traffic across
70 the Golgi is driven by cisternal maturation (Day et al., 2013; Pantazopoulou and Glick,
71 2019), COPII vesicles generated at specialized domains of the ER fuse homotypically
72 and heterotypically to form and feed the earliest Golgi cisternae (Rexach et al., 1994).
73 As straightforward as this step might seem, it involves a sophisticated circuitry of
74 regulation. Actual fusion is in part mediated by compartmental-specific sets of four-
75 membered SNARE protein complexes (SNARE bundles) (Malsam and Sollner, 2011;
76 Pelham, 2001; Rizo and Sudhof, 2012). Most SNARES are type II single TMD proteins,
77 whose N-terminal cytosolic domain contains nearly all the polypeptide, excepting a few
78 lumenal residues. Like any other transmembrane proteins, SNAREs are synthesized in
79 the ER. This implies that they have to travel to compartments of the cell as distant as the
80 plasma membrane in a conformation that precludes them of catalyzing what would be a
81 calamitous fusion of non-cognate donor and acceptor compartments. Achieving the
82 strictest specificity is particularly challenging in the ER-to-Golgi stage that, as the first
83 step in the secretory pathway, represents an obligate point of transit for each and every
84 transmembrane SNARE. Therefore, the only SNARES acting in this first step are the Qa
85 Sed5, the Qb Bos1, the Qc Bet1 and the R-SNARE Sec22, which form the bundle
86 mediating fusion of carriers that coalesce into cisternae (McNew et al., 2000).
87
88 Given the central role played by the secretory pathway in the physiology of every
89 eukaryotic cell, it is unsurprising that this step involves regulatory factors which are
90 essential for cell survival. One is the SM (Sec1, Munc-18) protein Sly1, which promotes
91 SNARE bundle formation (Bracher and Weissenhorn, 2002; Peng and Gallwitz, 2002;
92 Thomas et al., 2019) Another is the TRAPPIII complex, which interacts with the external
93 coat of COPII carriers and acts as a guanine nucleotide exchange factor (GEF) for RAB1
94 (Bracher and Weissenhorn, 2002; Cai et al., 2007; Galindo et al., 2021; Joiner et al.,
95 2021; Lord et al., 2011; Peng and Gallwitz, 2002; Pinar and Peñalva, 2020; Riedel et al.,
96 2017; Thomas et al., 2018; Thomas et al., 2019). This small GTPase is a key player that
97 transiently recruits protein effectors from the cytosol to donor and acceptor membranes
98 (Sogaard et al., 1994) and regulates SNARE assembly through an as yet undefined
99 mechanism (Lupashin and Waters, 1997; Sapperstein et al., 1996). One RAB1 effector
100 is a fungal protein denoted Uso1, whose highly conserved metazoan homologue is p115.
101 These are homodimers with a globular N-terminal head and a long C-terminal coiled-coil
102 region characteristic of tethering proteins, which bring donor and acceptor membranes
103 into the distance at which v- and t-SNAREs can engage into the productive *trans*-SNARE

complex that mediates membrane fusion (Cao et al., 1998; Nakajima et al., 1991; Sapperstein et al., 1996; Sapperstein et al., 1995; Seog et al., 1994; Yamakawa et al., 1996).

Despite most Golgi tethers are functionally redundant, Uso1 is unique in that it is an essential protein. *uso1-1*, a *S. cerevisiae* amber mutation truncating most, but not all the coiled-coil region, is viable, yet further upstream truncation removing the complete coiled-coil is lethal, which was taken as evidence that tethering is the essential function of Uso1 (Seog et al., 1994). In addition, as the coiled-coil is predicted to mediate dimerization, it is broadly accepted that Uso1 is 'just' an essential homodimer that tethers vesicles to the acceptor membrane. However, genetic evidence stubbornly indicates that Uso1 plays additional functions related with SNAREs. For example, Sapperstein et al showed that SNAREs function downstream of Uso1 (Sapperstein et al., 1996). Notably, the view that Uso1 is a mere RAB1 effector was challenged by the observation that overexpressing Ypt1 (yeast RAB1) rescues lethality of *uso1*Δ, whereas the reciprocal is not true, indicating that Uso1 acts upstream of or in conjunction with RAB1 (Sapperstein et al., 1996).

Our laboratory is interested in deciphering the domains of action of RAB GTPases in the genetic and cell biological model organism *Aspergillus nidulans* (Pinar and Peñalva, 2021). We have previously gained mechanistic insight into the activation of RAB11 by TRAPPII by exploiting a forward genetic screen for mutations bypassing, at the restrictive temperature, the essential role of the key TRAPPII subunit Trs120 (Pinar et al., 2019; Pinar et al., 2015; Pinar and Peñalva, 2020). In this type of screen, a strain carrying a *ts* mutation in the gene-of-interest is mutagenized and strains bypassing lethality at the restrictive temperature are identified and characterized molecularly. A well-characterized, conditionally lethal *rab1* mutation is available (Pinar et al., 2013), enabling us to investigate pathways collaborating with RAB1 in anterograde traffic. We isolated two *uso1* missense mutations causing substitutions in the globular head domain (GHD). When combined together, these rescued the lethality resulting from *rab1*Δ and promoted the localization of the protein to early Golgi cisternae by increasing Uso1 binding to the cytosolic region of the Qa SNARE Bos1 and, potentially, by improving the interaction of an N-terminal amphipathic α-helix with membranes. Importantly, we show that endogenous expression of a protein consisting solely of the double mutant GHD, or overexpression of double mutant or wild-type GHD, rescue the lethality resulting from *uso1*Δ, even though the GHD is monomeric. Our results show that one essential role of RAB1 is recruiting Uso1 to membranes, and that the essential role of Uso1 is not

141 tethering membranes, but rather regulating the formation of the cognate SNARE bundle,
142 indicating that Uso1 is a component of the SNARE fusion machinery .

143 ## Results

144 **Missense mutations in *uso1* rescue the lethality resulting from *rab1*Δ**

145

146 *rab1*^{A136D} (hereby *rab1*^{ts}) mutants do not grow at 37ºC. However, when we plated UV-
147 mutagenized conidiospores of the *rab1*^{ts} mutant at this temperature, we obtained
148 colonies showing different degrees of growth, presumably carrying mutations rescuing
149 the lethality resulting from *rab1*^{ts}. One was chosen for further characterization. By sexual
150 crosses and parasexual genetics this strain was shown to carry a single suppressor
151 mutation, denoted *su1rab1*^{ts}, that co-segregated with chromosome VIII. Meiotic mapping
152 narrowed *su1rab1*^{ts} to the vicinity (2 cM) of *hisC*. 40 kb centromere distal from *hisC* lies
153 AN0706 (Figure 1A) encoding *Aspergillus nidulans* Uso1, a conserved effector of RAB1.
154 Sanger sequencing revealed the presence of a G16A transition (denoted E6K) resulting
155 in Glu6Lys substitution in the *uso1* gene of *su1rab1*^{ts}.

156

157 To determine if the remaining suppressor strains were allelic to *su1rab1*^{ts}, we sequenced
158 *uso1* from a further 13 isolates (Figure 1B). Of these, four were *rab1*^{ts} pseudo-revertants
159 that had acquired a functionally acceptable mutation in the altered codon, and eight
160 carried *uso1* E6K, suggesting that the screen was close to saturation. However, one
161 mutation was found to be a different missense allele, *su85rab1ts* (denoted G540S)
162 resulting in Gly540Ser substitution. Single mutant strains carrying these *uso1* mutations
163 showed no growth defect, indicating that E6K and G540S were unlikely to result in loss-
164 of-function, and suggesting instead that mutant strains had acquired features that made
165 them largely independent of RAB1. These findings were unexpected, because in
166 *Saccharomyces cerevisiae* overexpression of Uso1 does not rescue the lethality of *ypt1*Δ
167 mutants (Ypt1 is the yeast RAB1 homologue)(Sapperstein et al., 1996).

168

169 To demonstrate that *uso1*^{E6K} and *uso1*^{G540S} were causative of the suppression, we
170 reconstructed them by homologous recombination. These reverse-genetic alleles
171 rescued viability of *rab1*^{ts} at 37ºC to a similar extent as *su1rab1*^{ts} and *su85rab1*^{ts} (Figure
172 1C). *uso1*^{G540S} was the strongest suppressor, such that *rab1*^{ts} *uso1*^{G540S} double mutants
173 grew nearly as the wt at 37ºC. Nevertheless, the two alleles showed additivity, and a
174 triple mutant carrying *uso1*^{E6K}, *uso1*^{G540S} and *rab1*^{ts} grew at 42ºC, unlike either single
175 mutant (Figure 1C). These data, together with the genetic mapping above, established
176 that *uso1*^{E6K} and *uso1*^{G540S} are responsible for the suppression phenotype,

177

178 RAB1 recruits Uso1/p115 to uncoated COPII vesicles and early Golgi cisternae (Allan et
179 al., 2000). Therefore, *uso1*$^{E6K/G540S}$ might, by increasing the affinity of Uso1 for RAB1,
180 compensate for the reduction in the amount of the GTPase resulting from *rab1*^{ts}.
181 However, Figure 1D shows that both *uso1*^{E6K} *and uso1*^{G540S} rescue the lethality resulting
182 from the complete ablation of *rab1*Δ at 30ºC, with the strongest *uso1*^{G540S} suppressor
183 rescuing viability even at 37ºC, and the double mutant rescuing *rab1*Δ even at 42ºC
184 (Figure 1D). In contrast, *uso1*$^{E6K/G540S}$ did not rescue the lethality resulting from *arf1*Δ, nor
185 from *sed5*Δ or *sly1*Δ, the syntaxin and the SM protein which are crucial for the formation
186 of the ER/Golgi SNARE bundle (Figure 1—figure supplement 1), indicating that Uso1
187 plays a role acting downstream of RAB1 and upstream of or in conjunction with the
188 SNARE machinery. This role is essential for survival (Figure 1—figure supplement 1).
189

190 **E6K affects a previously undetected N-terminal helix, whereas G540S is located**
191 **in a loop near the end of the armadillo domain.**
192

193 1103-residue *A. nidulans* Uso1 is similar in size to 961-residue p115 (bovine) and notably
194 shorter than *S. cerevisiae* Uso1p (1790 residues) (Yamakawa et al., 1996). Thus far,
195 atomic structures of Uso1/p115 are limited to the 600-700 residue GHD, which consists
196 of a highly conserved α-catenin-like armadillo-fold (An et al., 2009; Heo et al., 2020;
197 Striegl et al., 2009). *In silico* analyses robustly predict that the approximately C-terminal
198 half of Uso1/p115 consists of a coiled-coil that mediates tethering and dimerization, but
199 this region has not been characterized beyond low resolution EM studies (Yamakawa et
200 al., 1996) . Neither crystal structures nor predictions provided information about the N-
201 terminal extension in which Glu6Lys lies.
202

203 Thus, we used AlphaFold2, imposing or not the condition that the protein is a dimer (see
204 below). Figure 2A shows the monomer and dimer models with the highest confidence
205 scores (see Figure 2—figure supplement 1). Like their relatives, Uso1 from *A. nidulans*
206 contains an N-terminal GHD including a previously unnoticed short α-helix in which Glu6
207 affected by E6K lies. This N-terminal extension is followed by ~34 α-helices arranged
208 into 12 tandem repetitions of armadillo repeats (ARM1-ARM12; residues 17 through
209 564), each containing three right-handed α-helices except for the first two repeats.
210 Altogether, the armadillo repeats resemble the shape of a jai alai basket. Downstream
211 of the GHD, AlphaFold2 predicts a long extended coiled-coil (CC) between residues 674
212 through 1082, which would mediate dimerization (see below) (Figure 2A). The CC ends

213 at a conserved C-terminal region (CTR) (Figure 2A and B), which includes an also C-
214 terminal segment rich in acidic residues. In Uso1, twelve out of the last seventeen amino
215 acids are Asp/Glu (Figure 2A and B). The CC and CTR regions will be collectively
216 denoted the CCD domain.
217
218 Even though the GHD contains Glu6 and Gly540 in the N-terminal helix and at the
219 beginning of armadillo α-helix 29, respectively, intramolecular or intermolecular (in the
220 context of a homodimer, see below) distances between these residues are long, arguing
221 against the possibility that they bind a common target as components of the same
222 interaction surface (Figure 2C). Indeed, the synthetic positive effect of the mutations
223 would be consistent with their rescuing viability through different mechanisms. The
224 previously unnoticed short α-helix predicted by AlphaFold between Phe2 and Lys12 is
225 amphipathic (Figure 2D). Glu6 lies on the polar side of this helix, such that Glu6Lys
226 increases its overall positive charge (three of the four polar residues are Lys or Arg). As
227 discussed below, it is tempting to speculate that this helix facilitates membrane
228 recruitment.
229

230 **Coiled-coil mediated dimerization of Uso1: the globular head is monomeric**

231 It has been proposed that p115 alternates between closed and open
232 conformations to hide or expose a RAB1 binding site present in the CCD (Beard et al.,
233 2005). This would be mediated by intramolecular interactions between the globular
234 domain and the C-terminal acidic region, which would be disrupted by the competitive
235 binding of golgins GM130 and giantin to the latter. We addressed whether E6K/G540S
236 promotes a conformational change in Uso1, or, alternatively, a change in the
237 oligomerization status of the protein, by analytical ultracentrifugation. We designed
238 seven constructs carrying a C-terminal His tag (Figure 3). Two corresponded to the full-
239 length protein with or without E6K and G540S substitutions. The second pair included
240 wild-type and doubly-substituted versions of C-terminally truncated Uso1 lacking the
241 CTR (Uso1ΔCTR and Uso1$^{E6K/G540S}\Delta$CTR). The third corresponded to wild-type and
242 doubly-substituted versions of the globular domain, denoted Uso1 GHD and Uso1
243 GHD$^{E6K/G540S}$. The seventh construct corresponded to the CCD domain (i.e. CC + CTR)
244 and was denoted Uso1 CCD. All seven proteins were expressed in bacteria, purified by
245 nickel-affinity and size-exclusion chromatography and analyzed by sedimentation
246 velocity ultracentrifugation. These experiments revealed that all protein preparations
247 were essentially homogeneous, and thus they were used to determine the corresponding
248 Svedberg coefficients. In addition, by dynamic light scattering we determined the

249 translational diffusion coefficients of the constructs. With these values we deduced the
250 molecular mass of the different proteins using Svedberg's equation.
251
252 Wild-type and E6K/G540S full-length Uso1s showed the same sedimentation
253 coefficients, demonstrating that the mutations do not induce a large conformational
254 change that would have been reflected in changes in sedimentation velocity due to
255 differences in frictional forces. Molecular masses deduced from the Svedberg equation
256 indicated that these full-length proteins are homodimers, in agreement with previous
257 literature (Figure 3). Ablation of the conserved C-terminal region (CTR) did not result in
258 any significant change in the sedimentation coefficient (Figure 3, panels 3 and 4 vs. 1
259 and 2), irrespective of the presence or absence of the substitutions, discarding the model
260 in which the CTR would interact with the GHD to maintain a hypothetical closed
261 conformation (Beard et al., 2005). In addition, the molecular masses of the ΔCTR
262 proteins correspond to a dimer, implying that the acidic region is not involved in
263 dimerization either.
264
265 Notably the GHD, whether wild-type or mutant, behaved as a monomer (Figure 3, panels
266 5 and 6), which has important implications described below. In contrast, the coiled-coil
267 domain, with a predicted molecular mass of 52 kDa, behaves as a dimer of *ca.* 100 kDa
268 (Figure 3, panel 7). The sedimentation coefficient of the CCD is markedly slower than
269 that of the 70 kDa monomeric GHD, suggesting an elongated shape. These
270 observations, together with the dimeric nature of the construct lacking the CTR, showed
271 that dimerization is mediated by the CCD. The absence of 443 residues corresponding
272 to the CCD plus CTR domains in the GHD construct and the monomeric nature of the
273 latter compared to full-length Uso1 dimer did not result in a commensurate decrease in
274 sedimentation coefficient, which changed from 4.8 S to 3.7 S in the wild-type (note that
275 the change in *Mr* goes from 246 kDa in full-length Uso1 to only 68 kDa of the
276 GHD)(Figure 3). These data strongly support AlphaFold2 predictions depicting Uso1 as
277 a dimer with a globular head and an extended coiled-coil that would retard sedimentation
278 of the protein very substantially.
279
280 As with full-length Uso1, the double substitution did not alter the sedimentation
281 coefficient of the GHD (Figure 3, panels 5 and 6). To buttress the conclusion that the
282 GHD is a monomer irrespective of the presence or absence of the mutations, we
283 performed sedimentation velocity experiments using different protein concentrations
284 ranging from 0.5 to 5 μM (Figure 3—figure supplement 1, A and B). In all cases the GHD
285 behaved as a monomer. Sedimentation profiles of Uso1 GHD lacking the His-tag showed

286 a similar behavior, establishing that the monomeric state of the mutant is not due to the
287 tag at the C-terminal position hindering dimerization (Figure 3—figure supplement 1,C).
288 Therefore, sedimentation experiments did not detect any change in tertiary or quaternary
289 structures between wild-type and mutant GHD, which is important for the interpretation
290 of genetic data that will be discussed below.

291 In summary, (i) Uso1 is a dimer; (ii) The C-terminal acidic region is dispensable
292 for dimerization and does not mediate an equilibrium between closed and open
293 conformations; (iii) The globular domain of Uso1 is a monomer; (iv) The coiled-coil
294 domain of Uso1 is a dimer; (v) the double E6K G540S substitution does not promote any
295 conformational shift in Uso1, nor does it result in a change in the oligomerization state
296 of the protein.

297 **The punctate pattern of localization of USO1-GFP is dependent on RAB1**

298 The membranous compartments of the Golgi are not generally stacked in fungi,
299 permitting the resolution of cisternae, which appear as punctate structures in different
300 steps of maturation, by wide-field fluorescence microscopy (Losev et al., 2006;
301 Matsuura-Tokita et al., 2006; Pantazopoulou and Peñalva, 2011; Pinar et al., 2013;
302 Wooding and Pelham, 1998). While Uso1 is predicted to localize to the Golgi, studies of
303 its localization in fungi are limited (Cruz-García et al., 2014; Sánchez-León et al., 2015).
304 Therefore, we tagged the *A. nidulans uso1* gene endogenously with GFP

305 Figure 4A and video 1 depicting a software-shadowed 3D reconstruction of a
306 Uso1-GFP hypha, as well as consecutive sections of deconvolved z-stacks in Figure 4B
307 show that Uso1-GFP localizes to puncta polarized towards the tip, often undergoing
308 short-distance movements (see Figure 4C and Figure 4—figure supplement 1). These
309 puncta are smaller and more abundant than those reported for other markers of the
310 Golgi, which suggested that they might represent domains rather than complete
311 cisternae. Notably, 3D (x, y, t) movies revealed that Uso1 puncta are transient,
312 recurrently appearing and disappearing with time (Figure 4C). That this recurrence did
313 not reflect that the puncta go in-and-out of focus was established with 4D (x, y, z, t)
314 movies, which revealed a similar behavior of Uso1 irrespective of whether 3D or 4D
315 microscopy was used (video 2) Uso1 foci with confidence, we constructed movies with
316 middle planes only (i.e. 3D x, y, t series). After careful adjustment of live imaging
317 conditions, we achieved a 2 fps time resolution with relatively low bleaching for time
318 series consisting of 400 photograms (video 3). These conditions sufficed to track Uso1
319 puncta over time using kymographs traced across linear ROIs covering the complete
320 width of the hyphae (Figure 4C). However, as the abundance of Uso1 puncta made
321 automated analysis of Uso1 maturation events troublesome, we tracked them manually

322 with the aid of 3D (x,y,t) representations generated with Imaris software combined with
323 direct observation of photograms in movies (Figure 4C and Figure 4—figure supplement
324 1). The boxed event magnified in Figure 4E (see video 4) illustrates a prototypical
325 example. The right Figure 4E montage shows frames corresponding to this event for
326 comparison. We analyzed *n* = 60 events, which gave an estimation of the average half-
327 life of Uso1 residing in puncta of 60 sec +/- 25.26 S.D. (Figure 4D).
328
329 Nakano and co-workers have proposed that the transfer of lipids and proteins between
330 ER exit sites (ERES) and the early Golgi occurs through a kiss-and-run mechanism
331 (Kurokawa et al., 2014). Because Uso1-GFP punctate structures resemble, in size and
332 abundance, ER exit sites labelled with COPII components, we studied Uso1-GFP cells
333 co-expressing Sec13 endogenously labeled with mCherry (Bravo-Plaza et al., 2019).
334 The maximal intensity projection (MIP) shown on Figure 5A, and video 5 show that the
335 two markers are closely associated, but only in a few instances they showed
336 colocalization. These examples did not represent simple overlap, as they were found to
337 colocalize in the Z dimension using orthogonal views or montages (Figure 5B and C).
338 These observations have not been pursued further with time-resolved sequences, but at
339 the very least we can conclude that the reporters are closely associated in space. In view
340 of this, we determined that Uso1 structures originate downstream of COPII-mediated ER
341 exit. Therefore, we investigated, using *sarA*6, a temperature-sensitive allele of the gene
342 encoding *A. nidulans* SAR1 (Hernández-González et al., 2014), whether the punctate
343 Uso1 structures are dependent on this master GTPase regulating COPII biogenesis.
344 Figure 5D shows that this is indeed the case; the number of Uso1-GFP puncta was
345 significantly reduced relative to the wt when cells were shifted from 28°C to 37°C,
346 indicating that Uso1 populates a membrane compartment with Golgi identity.
347
348 To determine the 'sub-Golgi' localization of Uso1 puncta, we filmed Uso1-GFP along with
349 different Golgi markers (Figure 6). Uso1-GFP showed no overlap (Pearson's coefficient
350 0.17 ± 0.06 S.D., *n* = 16 cells) with cisternae labeled with mCherry-Sec7, the late Golgi
351 ARF1 GEF that is a prototypic marker of the TGN (Arst et al., 2014; Day et al., 2018;
352 Galindo et al., 2016; Halaby and Fromme, 2018; Losev et al., 2006; McDonold and
353 Fromme, 2014; Pantazopoulou, 2016; Pantazopoulou and Glick, 2019; Richardson et
354 al., 2016; Richardson et al., 2012) (Figure 6; video 6). In contrast, visual observation of
355 cells expressing mCh-Sed5 and Uso1-GFP revealed substantial, yet incomplete, overlap
356 of the reporters (Figure 6), reflected in a Pearson's coefficient of 0.44 ± 0.04 S.D., *n* =
357 15 cells (Figure 6). The Qa syntaxin Sed5 drives fusion of COPII vesicles with early Golgi
358 cisternae, with Qb, Qc and R-SNAREs Bet1, Bos1 and Sec22, and mediates intra-Golgi

359 trafficking, with Qb, Qc and R-SNARES Sft1, Gos1 and Ykt6), respectively (Banfield et
360 al., 1995; McNew et al., 2000; Parlati et al., 2002; Pelham, 1999; Wooding and Pelham,
361 1998). These data suggest that Uso1 localizes to a subset of early Golgi
362 cisternae/membranes containing Sed5. GeaA^{Gea1,2} is the only *A. nidulans* homologue of
363 the *S. cerevisiae* early Golgi ARF1 GEFs Gea1 and Gea2 dwelling at the early Golgi
364 (Arst et al., 2014; Gustafson and Fromme, 2017; Muccini et al., 2022; Pantazopoulou,
365 2016; Park et al., 2005; Wright et al., 2014). Overlapping of Uso1 with GeaA^{Gea1,2} was
366 more conspicuous than with Sed5 (Figure 6), which was reflected in an increased
367 Pearson's coefficient to 0.52 ± 0.06 S.D., *n* = 16 cells. Of note, mammalian GeaA (GBF1)
368 and Uso1 (p115) interact (Garcia-Mata and Sztul, 2003). Taken together, these data
369 indicate that Uso1 localizes to Golgi cisternae in early stages of maturation.
370
371 In both mammalian cells and in yeasts Uso1/p115 has been shown to be recruited to
372 early Golgi membranes by RAB1, which is activated by the TRAPPIII GEF on COPII
373 vesicles after they bud from the ER (Allan et al., 2000; Cai et al., 2007; Lord et al., 2011;
374 Yuan et al., 2017). Therefore, we imaged Uso1 and RAB1, which revealed that indeed
375 Uso1 colocalized with RAB1 (Pearson's 0.61 ± 0.07 S.D., *n* = 20 cells) (Figure 6).
376 Altogether, the above microscopy data strongly suggest that Uso1 is transiently recruited
377 to early Golgi membrane domains enriched in RAB1, agreeing with the accepted view
378 that RAB1 acts by recruiting Uso1.
379

380 **Uso1 delocalization after RAB1 impairment rescued by E6K G540S.**
381 We next tested if the subcellular localization of Uso1 is dependent on RAB1, and
382 if this dependency can be bypassed by E6K/G540S. To this end we first showed that in
383 a *RAB1*$^{+}$ background endogenously tagged wild-type and E6K/G540S Uso1-GFP have
384 the same punctate localization pattern (Figure 7A), and that both supported vigorous wt
385 growth (Figure 7B lanes 1, 3, 5 and 7), indicating that the tagged proteins are functional.
386 Next, we introduced in these strains *rab1*^{ts} (Jedd et al., 1995; Pinar et al., 2013) by
387 crossing. This allele, which completely prevents growth at 37ºC, is a hypomorph at
388 permissive (25-30ºC) temperatures, which permitted testing RAB1 dependence under
389 standard microscopy conditions (28ºC). Figure 7A shows that wt Uso1-GFP was largely
390 delocalized to the cytosol by *rab1*^{ts}. This establishes that Uso1 localization to membranes
391 is subordinated to RAB1. Notably, the wt punctate pattern of Uso1 localization was
392 restored by the Uso1 E6K/G540S mutant substitution, correlating with correction of the
393 synthetic growth defect (Figure 7B, compare lanes 2, 4, 6 and 8). All these data indicated
394 that the localization of Uso1 is compromised when RAB1 function is impaired, and that

395 the E6K/G540S substitutions augment Uso1 affinity for a membrane anchor(s)
396 independent of RAB1. They additionally suggest that the principal physiological role of
397 RAB1 is ensuring the proper localization of Uso1.
398
399 Delocalization of Uso1 in the *rab1*^{ts} background was not solely dependent on RAB1.
400 Wild-type *uso1-GFP* displayed a synthetic negative interaction with *rab1*^{ts} (Figure 7B,
401 compare lanes 2 and 4 at 30ºC), suggesting that the presence of GFP in the C-terminus
402 interferes with a RAB1-independent mechanism that facilitates its recruitment to
403 membranes (see below)
404

405 **Genetic evidence that a network involving the CTR and the Grh1/Bug1 golgin**
406 **contributes to the recruitment of Uso1 to membranes.**
407 To follow up the above observation, we focused on golgins. In mammalian cells, the C-
408 terminal region of p115 interacts with GM130, a golgin which is recruited to the early
409 Golgi by GRASP65 (Beard et al., 2005). The equivalent proteins in budding yeast are
410 denoted Bug1 and Grh1 (Behnia et al., 2007)(Figure 8A).
411
412 GRASP65 contains two C-terminal PDZ [post synaptic density protein (PSD95),
413 *Drosophila* disc large tumor suppressor (Dlg1), and zonula occludens-1 protein (zo-1)]
414 domains, which bind an also C-terminal peptide in GM130 (Hu et al., 2015).. Similar to
415 its metazoan counterparts, *Aspergillus* Grh1 contains an N-terminal α-helix and two PDZ
416 domains, in this case followed by ~130 disordered residues (Figure 8B, Figure 8—figure
417 supplement 1A and C). We modelled the Grh1-Bug1 interaction using AlphaFold2.
418 Residues 666-675 of the C-terminal peptide of Bug1 bind to a hydrophobic cleft located
419 between PDZ1 and PDZ2. Bug1 Leu668 and 670 coordinate their side chains with
420 residues from both PDZ domains (e.g. Phe45 and Trp44 in PDZ1 and Trp171 and Val179
421 in PDZ2). A second interaction involves Bug1 C-terminal residues 683-690 fitting within
422 a second groove in PDZ1, such that the four C-terminal residues form a β-strand
423 extending the β-sheet of N-terminal PDZ1 domain (Figure 8B, Figure 8—figure
424 supplement 1B). Further genetic evidence that a network of interactions similar to that
425 acting in yeast and mammalian cells operates in the *A. nidulans* ER-Golgi interface was
426 obtained by constructing strains with combinations of gene-replaced alleles. These
427 consisted of *uso1ΔCTR* encoding Uso1 lacking the C-terminal region (residues 1-1041)
428 and containing or not E6K G540S, *rab1*^{ts}, and deletion alleles of the *Aspergillus BUG1*
429 (AN7680) and *GRH1* (AN11248) genes (Figure 8A). Combining *rab1*^{ts} with *uso1ΔCTR*
430 resulted in a synthetic negative interaction at 30ºC akin to that seen with *uso1-GFP*

431 (lanes 2 and 4 in Figure 8C). That the E6K/G540S double substitution rescued this
432 negative interaction strongly indicates that the CTR cooperates with RAB1 in the
433 recruitment of Uso1 to membranes (Figure 8C, lanes 2, 4, 6 and 8). We note that the
434 control wild-type strain used in these experiments contains a construct completely
435 analogous to the mutant allele, ruling out that the genetic manipulation (for example the
436 introduction, linked to the *uso1* locus, of a selection marker, potentially chromatin-
437 disruptive) is causative of the observed phenotype. Another trivial explanation that we
438 ruled out by Western-blot analysis was that the deletion off the 62 C-terminal residues in
439 *uso1ΔCTR* resulted in increased degradation, which it did not (Figure 8D).
440
441 If interactions involving the CTR of p115 were conserved in fungi, *BUG1* (GM130
442 equivalent) and *GRH1* (GRASP65) should also show a synthetic negative interaction
443 with $rab1^{ts}$. Figure 8E (lanes 1,3 and 5) shows that neither *bug1Δ* nor *grh1Δ* affects
444 growth. However, both deletion alleles showed a strong synthetic negative interaction
445 with $rab1^{ts}$ (Figure 8E, lanes 1,3 and 5). Remarkably, the synthetic negative phenotype
446 was rescued by the presence of E6K/G540S substitutions in Uso1, further suggesting
447 that they promote Uso1 recruitment to its locale of action, compensating for the loss of
448 the Bug1-Uso1 CTR interaction. We conclude that interaction involving the CTR of Uso1
449 and the BUG1/GRH1 complex cooperates with RAB1-mediated mechanisms to recruit
450 Uso1 to membranes.

451 **The globular head domain (GHD) of Uso1 carrying the double E6K/G540S**
452 **substitution supports cell viability**

453 Uso1 has traditionally been considered the archetype of a coiled-coil tether
454 recruiting ER-derived vesicles to the *cis*-Golgi. In *S. cerevisiae*, *uso1-1* (Sapperstein et
455 al., 1996), is a C-terminally truncating, conditionally-lethal *ts* allele whose encoded
456 protein still retains 20% of the coiled-coil region. In contrast, *uso1-12* and *uso1-13*
457 removing the complete coiled-coil region are lethal (Seog et al., 1994). Thus, we asked
458 whether the double E6K/540S substitution bypasses the requirement of the coiled-coil
459 region. To this end, we constructed, by gene replacement, a $uso1^{GHD}$ allele expressing
460 a protein truncated immediately after the GHD, lacking residues 660-1103. By
461 heterokaryon rescue, we demonstrated that this allele is lethal (Figure 9A).
462 Unexpectedly, given that the $rab1^{ts}$ suppressor substitutions lie outside the coiled-coil
463 region, the equivalent allele containing E6K/G540S sufficed for the fungus to survive at
464 30ºC. This result has two key implications: that the coiled-coil of Uso1 is not essential for
465 survival and as the GHD of Uso1 is a monomer in solution, it follows that dimerization of
466 Uso1 is not essential either (see also below).

467

468 In view of these unexpected results we wondered whether the structure of the GHD
469 synthesized in bacteria differed from the physiological form in *Aspergillus*, such that the
470 GHD were a dimer *in vivo.* To address this possibility, we ran an *Aspergillus* cell-free
471 extract expressing HA3-tagged Uso1 GHD through a Sepharose column. As control, we
472 ran in parallel a sample of bacterially-expressed His-tagged GHD used in sedimentation
473 velocity experiments. Western blot analysis of the fractions (Figure 9B) demonstrated
474 that both proteins eluted at the same position, corresponding to that expected for a
475 globular protein with the size of the GHD. As controls we ran in the same column a similar
476 pair of proteins corresponding to full length Uso1. The bacterially-expressed and the
477 native Uso1 proteins also co-eluted (Figure 9B), but this time at a position corresponding
478 to a highly elongated dimer, consistent with sedimentation velocity experiments. Thus,
479 *in vivo*, the GHD, expressed from its own promoter, is a monomer, and it is sufficient to
480 sustain viability if it carries the double mutant substitution that bypasses the requirement
481 for RAB1. These data strongly argue against tethering being *the* essential physiological
482 role that Uso1 plays.

483

484 We next investigated why the E6K/G540S GHD suffices for viability only at 30°C. Often
485 thermo-sensitivity results from protein instability, which is enhanced at high
486 temperatures. Western blot analysis of the allele-replaced strain expressing E6K G540S
487 GHD as the only source of Uso1 revealed that levels of the truncated Uso1 mutant were
488 minuscule relative to the wt or to the equivalent Δ*CTR* allele (Figure 9C). We reasoned
489 that increasing expression would result in E6K/G540S GHD supporting growth over a
490 wider range of temperatures. Thus, we drove its expression with the promoter of the
491 inulinase *inuA* gene, which is inducible by the presence of sucrose in the medium and
492 almost completely shut off on glucose (Hernández-González et al., 2018; Peñalva et al.,
493 2020). Initially we tested wild-type and E6K/G540S GHD in a *uso1+* background. This
494 had no phenotypic consequences despite the fact that western blots confirmed that that
495 the truncated proteins were being overexpressed (Figure 9D; Figure 9E, lanes 1, 3, 5, 7
496 and 10;). Then we proceeded to delete the resident *USO1* gene in the wild-type and
497 mutant GHD overexpressing strains. As expected, neither of the resulting pair of strains
498 was able to grow on medium with glucose as the only carbon source (Figure 9E, lanes
499 2 and 6). Notably, the strain expressing E6K/G540S GHD as sole Uso1 source grew
500 essentially as the wild-type and 30ºC and, although debilitated, was viable at 37ºC,
501 showing a substantial improvement of the growth capacity displayed by the gene-
502 replaced mutant (Figure 9, lanes 7,8 and 9). Thus, if expressed at sufficiently high levels,
503 E6K/G540S GHD maintains viability at the optimal growth temperature.

504

505 Unexpectedly, the wild-type GHD also rescued the viability of the *uso1*Δ mutant when
506 this was cultured with sucrose as carbon source at 30ºC and 37ºC. In fact, at 30ºC, the
507 *uso1*Δ *inuAp::GHD* strain grew like the wt (Figure 9E, lanes 3 and 4)(note that these
508 experiments were carried out in a *RAB1+* background), suggesting that increased
509 binding to a Golgi receptor facilitated by mass action compensated for the loss of the
510 coiled-coil region and associated dimerization. The E6K/G540S GHD would have gained
511 affinity for this receptor, explaining why the doubly substituted GHD suppressed mis-
512 localization of Uso1-GFP when RAB1 is compromised, even when its steady-state levels
513 were very low. Forced expression, combined with a potentially increased binding affinity
514 of E6K/G540S GHD to such a hypothetical receptor might be toxic.

515 **Uso1 is an associate of the early Golgi SNARE machinery, with the double**
516 **substitution E6K/G540S increasing this association**

517

518 What is the nature of this hypothetical receptor? To address this question, we screened
519 for interactors of Uso1 among proteins acting at the same functional level (consumption
520 of COPII vesicles by the early Golgi) using a modified version of the S-tag co-
521 precipitation approach that we used to characterize of TRAPP complexes (Pinar et al.,
522 2019)(Figure 10A). We constructed strains expressing wild-type or mutant Uso1, tagged
523 endogenously with the S-tag and, as negative unrelated control, BapH (an effector of
524 RAB11 acting in late steps of the secretory pathway (Pinar and Peñalva, 2017). Then,
525 derivatives of these three strains co-expressing each of the candidate Uso1 GHD
526 targets, tagged with HA3 (also endogenously), were constructed. The resulting panel
527 (Figure 10B) was screened for HA-tagged proteins co-precipitating more efficiently with
528 the E6K/G540S version of Uso1 than with the wild-type, and satisfying the criterium of
529 not co-purifying with BapH. To this end cell-free extracts of these strains were incubated
530 with S-agarose beads that were recovered by centrifugation. Proteins associating with
531 the S-baits were revealed by anti-HA western blotting.

532

533 That not every protein specifically co-purified with Uso1 baits was demonstrated by the
534 results obtained with the COG component COG2, which did not associate with any of
535 the three baits (Figure 10C, 10). In contrast, β-COP was a promiscuous non-specific
536 interactor pulled down by all three baits (Figure 10C, 11). Notably, the screen identified
537 the Golgi syntaxin Sed5 within the specific Uso1 associates (Figure 10C, 1), an
538 association reported previously by others for both p115 and fungal Uso1 (Allan et al.,
539 2000; Sapperstein et al., 1996). That the PM SNARE Sso1 did not interact at all with any

540 of the S-baits demonstrated that Uso1 does not bind promiscuously to syntaxins (Figure
541 10C, 5). Importantly, Sed5 was brought down more efficiently by E6K/G540S Uso1, and
542 not at all by BapH, even though levels of this unrelated bait, as assessed by silver
543 staining of pull-downs, were markedly higher than those of either Uso1 version.
544 Therefore, Sed5 (or its associates) might represent a potential anchor bound by
545 E6K/G540S Uso1 with increased affinity to compensate for the lack of RAB1-mediated
546 recruitment.
547
548 This analysis was extended to other members of the SNARE bundle forming in the
549 ER/Golgi interface with the Qa Sed5: the Qb Bos1, the Qc Bet1 and the R-SNARE Sec22
550 (Parlati et al., 2002; Pelham, 1999; Tsui et al., 2001). Sec22 was slightly enriched in the
551 E6K/G540S pull-down relative to wild-type Uso1 (Figure 10C, 4). The results with Bos1
552 and Bet1 were most noteworthy (Figure 10C2 and 3). Both were markedly increased in
553 the E6K/G540S pull-downs, with Bet1 increased most. The AAA ATPase Sec18
554 disassembling *cis*-SNARE complexes also bound Uso1 and was slightly enriched in the
555 sample of E6K/G540S associates, as was the Uso1-interacting Golgin Bug1, but not its
556 membrane anchor Grh1 (Figure 10, C6-8). We conclude that Uso1 is a component of
557 the SNARE machinery and that this association is augmented by E6K/G540S.
558
559 S-tag-coprecipitations in Figure 10 clearly singled out Bet1 (Qc) and Bos1(Qb) as the
560 preys that were most strongly enriched with the mutant E6K/G540S bait relative to wild-
561 type, and therefore with the highest probability of being direct interactors bound with
562 greater affinity by the doubly substituted Uso1 mutant.
563
564 During these analyses we also addressed the physiological role of golgins, which were
565 expected to be dispensable for growth, given their functional redundancy (Gillingham,
566 2018; Gillingham and Munro, 2016; Muschalik and Munro, 2018). We examined the role
567 of three golgins acting at the early Golgi: The Grh1 (AN11248)/Bug1(AN7680) complex,
568 discussed above, Coy1 (the product of AN0762) and Rud3 (AN10186). Consistent with
569 their roles, AlphaFold2 predicts that they form long coiled-coils carrying C-terminal
570 membrane anchors, characteristics of golgins. Coy1 contains a C-terminal TMD anchor
571 and an adjacent CLASP domain that, according to AlphaFold2, consists of α-helices
572 (Figure 10—figure supplement 1). Rud3 is a dimer consisting of a long coiled-coil with a
573 ARF1-binding GRIP domain composed of four short helices, near its C-terminus (Figure
574 10—figure supplemental 1). Ablation of *grh1*, *bug1*, *coy1* or *rud3* did not prevent growth
575 of the corresponding mutants, with only *coy1*Δ displaying a minor growth phenotype
576 (Figure 10—figure supplement 2). Next, we deleted the corresponding genes in a *rab1*Δ

577 *uso1*$^{E6K\ G540S}$ and tested whether any of the golgins was required for viability rescue. Grh1
578 and Bug1 were partially required, as their absence precluded rescue at 42° (Figure 10—
579 figure supplement 2). In contrast, RUD3 was not required. With regard to COY1, the fact
580 that combining *coy1*Δ and *rab1*Δ *uso1*$^{E6K\ G540S}$ results in lethality at 30ºC, 37ºC and 42ºC
581 precluded conclusions on the role of COY1 in suppression. However, we can conclude
582 that proper assembly of *A. nidulans* Golgi cisternae is supported by a redundant set of
583 tethers (Behnia et al., 2007), of which in Coy1 appears to be the least redundant of those
584 tested. Coy1 has been implicated in retrograde traffic within the Golgi itself (Anderson et
585 al., 2017)
586

587 **Golgi SNAREs bind directly to the Uso1 GHD; effects of Uso1 E6K/G540S**
588 Work by others implicated Uso1 in the assembly of the early Golgi SNARE bundle
589 (Sapperstein et al., 1996). Thus, prompted by co-association experiments, we predicted
590 that Uso1 would bind directly Bet1, Bos1 and perhaps other SNAREs implicated in the
591 biogenesis of the early Golgi. We anticipated that binding to Bet1 and Bos1 would be
592 insufficient to recruit Uso1 to membranes in the absence of RAB1, but that once
593 reinforced by E6K/G540S, Uso1 would not require RAB1 for its recruitment. To test this
594 possibility, we searched for direct and E6K/G540S-enhanced interactions between the
595 GHD and SNAREs with pull down assays carried out with purified SNARE-GST fusion
596 proteins as baits and Uso1-His6 constructs as preys.
597

598 Full-length Uso1 bound, weakly, to the Sec22 R-SNARE and to the Qb Bos1, and very
599 efficiently [with *circa* 70% of the prey being pulled down (Figure 11A, B)] to the Qc Bet1.
600 In contrast, Uso1 did not bind the Qa syntaxins tested, Sed5 and Sso1 (Figure 11A). The
601 absence of interaction between Sed5 and Uso1, be it the wild-type or the E6K/G540S
602 mutant version, strongly indicated that the association detected with S-tag pull-downs
603 between Uso1 and Sed5 is bridged by other protein(s). This absence of binding cannot
604 be attributed to Sed5-GST being incompetent for binding because Sed5-GST was
605 competent in pulling-down highly efficiently its cognate SM protein Sly1, an interaction
606 that did not occur with Sso1-GST (Figure 11C). Notably, the presence of the E6K/G540S
607 double substitution in Uso1 (indicated with ** for simplicity on Fig 11) increased five times
608 the amount of protein retained by the Qb Bos1 bait (Figure 11A and B), whereas
609 interaction with Bet1 did not change (Figure 11A and B) . The double substitution in Uso1
610 did not promote interaction with Sed5 either. Thus, under normal circumstances Uso1 is
611 able to bind directly to three of the four SNAREs in the ER/Golgi interface, with binding
612 to Bet1 being the strongest. The double E6K/G540S substitution increases binding to

613 Bos1 very markedly and specifically, bringing it to up to the levels of Bet1 without
614 affecting, for example, binding to Bet1 or Sec22. Consistently, the GHD is sufficient to
615 mediate interaction with Bet1 and Bos1, as well as, if E6K G540S-substituted, the
616 increased binding of Bos1 to Uso1 (Figure 11D and E). The GHD did not interact with
617 Sec22, suggesting either that this R-SNARE is recruited by other parts of the protein or
618 that binding is dimerization dependent.
619
620 Besides the Sed5/Bos1/Bet1/Sec22 combination ( ), across cisternal maturation Sed5
621 forms SNARE bundles in Golgi compartments located downstream of Uso1 domains
622 (Pelham, 1999). In fungi, membrane fusion in the medial Golgi involves the Sed5
623 partners Gos1 (Qb) and Sft1 (Qc) substituting for Bos1 and Bet1, respectively, but
624 neither Gos1 nor Sft1 bound wild-type or E6K/G540 Uso1 GHD (Figure 11F),
625 demonstrating that interaction of Uso1 with Bos1 and Bet1 is highly specific. Therefore,
626 it seems fair to conclude that increased binding for a SNARE receptor underlies the
627 mechanism by which mutant Uso1 bypasses the need for RAB1 in the ER/Golgi
628 interface.
629
630 In summary, Uso1 is an essential protein acting in the ER/Golgi interface, and we report
631 here several important findings. We show that (i) the Golgi GTPase RAB1, which is
632 essential for viability, becomes dispensable if there is an alternative method to recruit
633 Uso1 to Golgi membranes; (ii) the coiled-coil region of Uso1 is dispensable to sustain
634 viability, implying that the tethering role of the protein is not essential either, consistent
635 with the redundant roles of other Golgin tethers; (iii) the Uso1 GHD is essential for
636 viability; (iv) the Uso1 GHD monomer, if present at suitably high levels, is sufficient to
637 maintain viability; (v) that the Uso1 GHD is a direct and specific binder of the Qb SNARE
638 Bos1, and a strong binder of the Qc Bet1; (vi) the mutation bypassing the need for RAB1
639 markedly increases the affinity of the GHD for Bos1, indicating that *rab1*Δ viability rescue
640 by E6K/G540S Uso1 occurs because SNARE anchoring provides an alternative mode
641 of recruitment to Golgi membranes to that provided physiologically by RAB1.
642

643 **Mechanistic insights guided by AlphaFold2 predictions**

644
645 To gain further insight into the mechanisms by which the double E6K/G540S bypasses
646 RAB1 we exploited AlphaFold2 to model the Uso1^{GHD} domain alone, or together with
647 each of the individual SNAREs, with both Bos1 and Bet1 simultaneously, and with RAB1.
648

649 Consistent with biochemical data, in the predicted model Bet1 and Bos1 interact with a
650 medial and a C-terminal region, respectively, of Uso1^{GHD}. (Figure 12; Figure 12—
651 supplement 1 and —supplement 2). Bet1 docks against a region of the GHD that is not
652 affected by the mutations. In contrast, Gly540 and its environs dock against the N-
653 terminal, triple α-helical Habc domain of Bos1. In all likelihood Gly540Ser mediates the
654 increased binding of mutant Uso1^{GHD} to Bos1. AlphaFold2 predicts that Uso1^{GHD}
655 interacts with Bos1 through a surface composed by the N-terminal part of the first Bos1
656 Habc α-helix and the loop between α-helices 2 and 3 (Figure 12A and B). The binding
657 surface in Uso1^{GHD} involves the second α-helices of the ARM10 and ARM11 repeats,
658 (α-helices 26 and 29), and the loop connecting the first two α-helices of ARM10 (Figure
659 12B). In AlphaFold2 models, Uso1 Gly504 (wild-type) is located at the beginning of
660 Uso1^{GHD} α-helix 29, at the heart of the interaction surface, contributing to the Uso1-Bos1
661 interaction by coordinating the amide group of the Uso1 backbone with the Bos1 Glu58
662 carboxylate to create a hydrogen bond (Figure 12C). According to the most confident
663 prediction, Gly504Ser results in the hydroxymethyl side chain protruding into a small
664 pocket rimmed by the side chains of Bos1 Leu59 and Ile60, such that the Uso1 Ser504
665 hydroxyl group hydrogen-bonds the amide group of Bos1 Glu58 (Figure 12C). Besides
666 creating a new hydrogen bond, Gly540Ser would increase the surface of interaction
667 slightly, from ~825.2 Å^2 to ~831.1 Å^2, implying that these alterations, together with a
668 minor shift in the environs of Gly540 detected by models (which might facilitate additional
669 interactions), would strengthen the binding of the Uso1^{GHD} to the Bos1 surface.
670
671 The mechanism by which Glu6Lys contributes to increase the recruitment of Uso1 to
672 Golgi membranes appears to be different. This glutamate is located in a region with low
673 pLDDT score which shows different conformations depending on the model (Figure 2D,
674 boxed), suggesting that this region is difficult to predict due to flexibility. However,
675 models concur in the prediction of an amphipatic N-terminal α-helix containing Glu6,
676 whose substitution by Lys (as in E6K) reinforces the positive charge of this α-helix, which
677 would be inserted into the vesicle membrane, potentially contributing to Uso1 recruitment
678 to COPII vesicles
679
680 In the case of the strong Uso1^{GHD}-Bet1 interaction (Figure 12—figure supplement 1), the
681 N-terminal region of Bet1 consisting of *circa* 80 amino acids is disordered, and the
682 pLDDT score of the different models is understandably low. However, all structural
683 models depicting Bet1 interacting with Uso1^{GHD} (e.g. in the context of the whole SNARE

complex, Bet1 alone or the isolated Bet1 N-terminal) consistently show a region where the pLDDT is higher. This region forms a kink in this N-terminal part of the Bet1 that protrudes into the surface created by the α-helices 13 and 16 of ARM4 and ARM5 (Figure 12—figure supplement 1). Surface representations show that this section of the Bet1 polypeptide covers ~ 1300 Å^2 of the GHD, docking against the same side of the boomerang-shaped solenoid as Bos1, which is consistent with the orientation that these SNAREs should take during the formation of the SNARE pin (Figure 12—figure supplement 2)

We next modelled RAB1 binding to the GHD in the absence and presence of Uso1 binders Bos1 and Bet1. AlphaFold2 predicts that the GHD interacts with RAB1 through a binding surface formed by the ARM3-5. repeats. On the other hand, the interactive region of RAB1 conforms to canons, as Uso1 α-helices 8 and 9 (ARM3) interact with the Switch II region while α-helices 11 (ARM-4) and 14 (ARM-5) interact with the Switch I) (Figure 12—figure supplement 2, A and B). Importantly, the model indicates that within the Uso1-GHD jai alai basket, RAB1 binds to the opposite (convex) side of the Bet1 interacting area at the concave side, and away from the C-terminal helix where the Bos1 Habc domain predictably binds, which would allow Uso1 to bind these three interactors simultaneously (Figure 12—figure supplement 2C). In addition, the predicted models supported two highly suggestive but as yet speculative implications. One is that the position of the RAB1 hypervariable domain, which anchors the GTPase to the membrane through is prenylated C-terminus, is compatible whith the hypothetical membrane binding of the N-terminal Uso1 amphipatic helix (Figure 12—figure supplement 2D); The second is that Uso1-RAB1 would be in an orientation that facilitates the docking of RAB1-loaded ER-derived vesicles with an acceptor membrane where SNARE zippering occurs (see discussion); this orientation implies that the donor membrane (the position of the N-terminal Uso1 helix) and the acceptor membrane (the TMDs of the SNAREs) is compatible with the Uso1 CTR contributing to tethering through interaction with Bug1/Grh1.

Discussion

RAB1 regulates transport at the ER/Golgi interface. Using an unbiased forward genetic screen to identify subordinated genes accounting for its essential role, we isolated two extragenic mutations resulting in single-residue substitutions in the RAB1 effector Uso1,

719 usually regarded as a tether. The single-residue substitutions lie at opposite ends of the
720 jai alai basket-shaped GHD; both are individually able to rescue viability of *rab1Δ* strains
721 at 30ºC and, when combined, even at 42ºC. Subcellular localization experiments hinted
722 at the mechanism by which the double mutation rescues *rab1*Δ lethality. Uso1 plays its
723 physiological role on an early Golgi compartment, where it largely colocalizes with RAB1,
724 with relocation to the cytosol in a RAB1-deficient background. Under normal
725 circumstances, the Uso1 CTR acts in concert with RAB1 to recruit the protein to the
726 Golgi. Genetic evidence (Figure 8) showed that this contribution requires the Golgi-
727 localized tether composed of the membrane anchor Grh1 and its associated golgin
728 BUG1 (Behnia et al., 2007), homologues of human GRASP65 and GM130, respectively.
729 In the absence of RAB1, engagement of the CTR with BUG1 is insufficient to stabilize
730 wild-type Uso1 on membranes. However, the double E6K/G540S substitution relocalizes
731 Uso1 to Golgi structures, suggesting that mutant Uso1 GHD had gained affinity for
732 another element, thereby compensating for the loss of RAB1.
733
734 By S-tag co-precipitation experiments we identified proteins associating with wild-type
735 and E6K/G540S Uso1 baits. Prominent among these were the four SNAREs, Sed5,
736 Bos1, Bet1 and Sec22, mediating fusion events at the ER/ Golgi interface, and the
737 SNARE regulator Sec18, indicating that Uso1 is a component of the SNARE fusion
738 machinery. This was suggested by previous studies with *S. cerevisiae* showing that
739 overexpression of Bet1, Bos1 and Sec22 suppresses *uso1-1* and that of Sec22 and Bet1
740 weakly suppresses *uso1Δ* (Sapperstein et al., 1996). Moreover, in mammalian cells
741 crosslinking studies with p115 identified Sed5, membrin (Bos1) and mBet1 as its weak
742 interactors (Allan et al., 2000), suggesting that contributing to the ER/Golgi SNARE
743 machinery is a conserved feature of Uso1/p115 family members. Of the above four *A.*
744 *nidulans* SNAREs, Bet1 and Bos1, which co-precipitated weakly with the wild-type, were
745 dramatically enriched with the mutant. Pull-down assays showed that full-length
746 *Aspergillus* Uso1 interacts weakly with Sec22 and strongly with Bet1, irrespective of
747 whether the bait was wild-type or E6K/G540S, indicating that they are direct
748 physiological interactors. In sharp contrast, the interaction of E6K/G540S Uso1 with the
749 Qb Bos1 was markedly augmented, strongly suggesting that this increase contributes
750 substantially to bypass RAB1. Both the high levels of binding to Bet1, and the marked
751 increase in binding to Bos1 resulting from E6K/G540S were tracked down to the GHD,
752 which is sufficient to bind these SNAREs.
753

754 AlphaFold2 models predicting the regions of interaction of the GHD with Bos1 and Bet1
755 showed that, of the two Uso1 residue substitutions, only Gly540Ser maps to the region
756 mediating the interaction with Bos1, whereas neither affected the interacting region with
757 Bet1, agreeing with GST pull-downs. Interaction with this SNARE is predicted to involve
758 a large surface, consistent with the strong "constitutive" binding of Bet1 with the GHD.
759 AlphaFold2 also predicted that RAB1 binds to the convex face of the GHD solenoid, in a
760 position that would permit the simultaneous binding of Qb and Qc SNARES and the
761 GTPase. In addition, AlphaFold2 also detected a previously unnoticed amphipathic α-
762 helix in the N-terminal region of Uso1. The Glu6Lys substitution falls within this helix,
763 making its global positive charge even greater, strongly suggesting that this substitution
764 increases Uso1 GHD binding to membranes. That the two residue substitutions act by
765 different mechanisms is coherent with their showing additivity to suppress RAB1 deficit.
766
767 The Uso1/p115 family has been implicated in the regulation of SNARE complexes (Allan
768 et al., 2000). (Shorter et al., 2002) first reported that p115 binds to SNAREs and
769 proposed that they would 'catalyze' the formation of the ER/Golgi SNARE bundle. The
770 direct interaction of p115 with unassembled mBet1 and Sec22 agrees with this role
771 (Wang et al., 2014). However, there are significant gaps in this model: Uso1
772 overexpression suppresses a partial deficit of *ypt1/RAB1*, but not *ypt1*Δ*, whereas* Ypt1
773 overexpression suppresses *uso1*Δ, indicating that Uso1 acts and in concert or upstream
774 of RAB1. [Of note, overexpression of Uso1 also suppresses *bet3-1*, a *ts* allele
775 inactivating the TRAPPIII complex, which is the RAB1 GEF (Galindo et al., 2021; Jiang
776 et al., 1998; Pinar et al., 2019; Riedel et al., 2017; Thomas et al., 2018)]. The grid of
777 reported genetic interactions strongly indicates that RAB1 regulates SNAREs (Brandon
778 et al., 2006; Lupashin and Waters, 1997; Sapperstein et al., 1996). Notably, our viability
779 rescue experiments show that E6K/G540S bypasses this non-canonical, yet essential
780 role of RAB1. As the double mutant substitution increases the recruitment of USO1 to
781 the SNARE machinery and as E6K/G540S suppresses *rab1Δ*, the most parsimonic
782 interpretation of the data is that the role of RAB1is cooperating to recruit Uso1 to the
783 SNARE complexes, a cooperation that is no longer needed when recruitment is ensured
784 by other means. That p115 regulates SNAREs' assembly was proposed by (Shorter et
785 al., 2002). However, a fundamental difference with our conclusions is that they attributed
786 this role to the CCD, whereas we identify here the GHD as the positively-acting player.
787
788 We also note that our experiments provide a mechanistic interpretation as to why
789 overexpression of Bet1, Bos1, Sec22 and Ypt1/RAB1 rescue the viability of *uso1-1*

790 removing a substantial portion of the yeast Uso1 CCD (Sapperstein et al., 1996; Seog
791 et al., 1994). A similar *Aspergillus* allele results in marked protein instability (Figure 9).
792 Thus, in all likelihood, suppression by overexpression of known direct interactors
793 involves stabilization of the *uso1-1* product.
794
795 In summary, our work firmly establishes that the essential role of Uso1 resides not in its
796 CCD domain tethering donor and acceptor membranes, but in the GHD. When
797 expressed at sufficient levels this domain is capable of fully complementing *uso1Δ*, which
798 is definitive evidence that neither the tethering function of Uso1 nor dimerization (the
799 GHD is monomeric) is required for the protein to play its essential role. As the GHD binds
800 two of the four SNAREs of the bundle, the simplest interpretation is that the essential
801 role of Uso1 is regulating SNAREs.
802

803 **Ideas and Speculation**

804 While the molecular details of this regulation will be addressed in future, it is tempting to
805 speculate that the GHD contributes, with Sly1, to orientate SNAREs to form a productive
806 bundle, acting as chaperones, similarly to the HOPS SM component Vps33, which
807 appears to align SNAREs in a pre-zippering stage, facilitating their assembly (Baker and
808 Hughson, 2016; Baker et al., 2015; Ren et al., 2009; Yu and Hughson, 2010; Zhang and
809 Hughson, 2021; Zhang and Yang, 2020). A second speculative interpretation is that
810 tethering occurs in two steps, with golgins acting at long distances, approximating
811 vesicles to the vicinity of SNAREs. Then SNAREs would engage RAB1–Uso1 to serve
812 as short-range tether preceding the zippering up of membranes. The > 700 Å-long Uso1
813 CCD would cooperate with Bug1 in the first step, whereas the Uso1 GHD would
814 cooperate with RAB1 and Bet1/Bos1 in the second, exploiting the fact that GHD binders
815 use surfaces located at opposite sides of the α-solenoid (Figure 12—figure supplement
816 2). Such arrangement implies that RAB1 C-terminal isoprenoids inserting into the donor
817 vesicle membrane would be *circa* 220 Å apart from the C-termini of the SNAREs inserted
818 in the acceptor membrane. Two-step tethering might impose one additional level of
819 specificity, preventing unproductive fusion events mediated by other SNARES circulating
820 through the ER/ interface and directing, by way of Uso1 interactions, incoming vesicles
821 to fusion-competent areas enriched in target SNAREs (Bentley et al., 2006).
822
823
824

825 # Materials and Methods

826 ***Aspergillus* techniques**

827 Standard *A. nidulans* media were used for growth tests, strain maintenance and
828 conidiospore harvesting (Cove, 1966). GFP-, HA3- and S-tagged alleles were
829 introduced by homologous recombination-mediated gene replacement, using
830 transformation (Tilburn et al., 1983) of recipient *nkuA*Δ strains deficient in the non-
831 homologous end joining pathway (Nayak et al., 2005). Complete strain genotypes are
832 listed in supplemental table I. These alleles were usually mobilized into the different
833 genetic backgrounds by meiotic recombination (Todd et al., 2007).
834
835 Null mutant strains were constructed by transformation-mediated gene replacement,
836 using as donor DNA cassettes made by fusion PCR (primers detailed in supplemental
837 table II) carrying appropriate selectable markers (Szewczyk et al., 2006). Integration
838 events were confirmed by PCR with external primers. When allele combinations were
839 expected to be synthetically lethal or severely debilitating, the corresponding strains
840 were constructed by sequential transformation, but the second such manipulation was
841 always carried out using $pyrG^{Af}$ as selective marker, which favors the formation of
842 heterokaryons in which untransformed nuclei supported growth (Osmani et al., 1988).
843 Conidiospores, in which single nuclei had segregated (i.e., homokaryotic nuclei), were
844 scrapped and streaked onto plates carrying doubly-selective medium. Absence of
845 growth or appearance of microcolonies, combined with a positive PCR diagnostic of
846 heterokaryosis of the primary transformants, was taken as indication of lethality.
847 Whenever possible, colony PCR of microcolonies was always used to genotype the
848 desired genetic intervention
849
850 The following proteins were C- or N-terminally tagged endogenously, using cassettes
851 constructed by fusion PCR (Nayak et al., 2005; Szewczyk et al., 2006): Uso1-GFP and
852 $Uso1^{E6K/G540S}$-GFP, Uso1-HA3 and $Uso1^{E6K/G540S}$-HA3; Uso1-S and $Uso1^{E6K/G540S}$-S;
853 BapH-S (Pinar and Peñalva, 2017), Sec13-mCherry (Bravo-Plaza et al., 2019;
854 Hernández-González et al., 2019), Gea1-mCherry and Sec7-mCherry (Arst et al., 2014),
855 mCherry-Sed5 (Pantazopoulou and Peñalva, 2011), mCherry-RAB1 (Pinar et al., 2013),
856 HA3-Sed5, HA3-Bet1, HA3-Bos1, HA3-Sec22, Sec18-HA3, Grh1-HA3, Bug1-HA3,
857 Coy1-HA3, COG2-HA3, and β-COP-HA3.
858
859

860 **Antibodies for western blotting**

Antibody	dilution	Origin	Reference
Primary			
α-HA	1:1000	rat	3F10 clone, Roche
α-His6x tag	1:10 000	mouse	#631212, Clontech
α-tubulin	1:5000	mouse	DM1A clone, Sigma
α-Uso1	1:1000	rabbit	Polyclonal antiserum, Davids Biotechnologie
Secondary (HRP-conjugated)			
α-rat IgG	1:4000	goat	#3010-05, Southern Biotech
α-mouse IgG	1:5000	goat	#A9044, Sigma
α-rabbit IgG	1:2000	donkey	#NA934, Amersham

861 Antiserum against Uso1 was raised in rabbits by Davids Biotechnology. Animals were
862 immunized with the Uso1 GHD (residues 1-659), tagged with His6x. Recombinant
863 expression in *E. coli* and Ni^{2+} affinity purification is described below. Target antibodies
864 were purified from raw antiserum by affinity chromatography through Hi-Trap NHS
865 columns (#17-0716-01, Cytiva) charged with Uso1 antigen following the manufacturer's
866 instructions. Affinity-bound antibodies were eluted with 100 mM glycine (pH 3.0), then
867 neutralized with 2 M Tris to a pH of 7.5 and stored at -20ºC.

868 ***inuA* promoter-driven expression of Uso1 GHD in *Aspergillus***

869 The Uso1 GHD was expressed in a sucrose-inducible manner from an *in locus*
870 replacement of the *inuA* gene (AN11778) ORF encoding inulinase by the GHD coding
871 sequence, such that its expression was driven by the *inuA* promoter, which is induced
872 on sucrose and non-induced on glucose (Hernández-González et al., 2018). The gene
873 replacement cassette was assembled through fusion PCR of 4 different elements, listed
874 here from 5' to 3': (1) inuA promoter, (2) cDNA sequence encoding Uso1 wt or mutant
875 E6K/G540S GHD (residues 1 – 659), (3) *Aspergillus fumigatus riboB* gene as selection
876 marker and (4) *inuA* gene 3'-flanking region. A *pyrG*89, *nkuA*Δ::bar, *riboB*2 *A. nidulans*
877 strain was transformed with this cassette, replacing the inuA gene. The resulting strain
878 was subsequently transformed with a *uso1*Δ deletion cassette (*A. fumigatus pyrG* as
879 selection marker) to ablate endogenous of Uso1, such that the GHD was the only moiety
880 of Uso1 present.

881 **Plasmids for protein expression in *E. coli***

882

883 **(I) His6x-tagging constructs**

884 pET21b-Uso1-His6x and pET21b-Uso1(E6K/G540S)-His6x: cDNA encoding full length
885 Uso1 (residues 1 -1103) was cloned into a pET21b *Nde*I/*Not*I linearized vector.

886 pET21b-Uso1ΔCTR-His6x and pET21b-Uso1(E6K/G540S)ΔCTR-His6x: lacking the C-
887 Terminal Region of the Coiled Coil Domain (residues 1 – 1040)

888 pET21b-Uso1GHD-His6x and pET21b-Uso1(E6K/G540S)GHD-His6x: cDNA encoding
889 the Globular Head Domain of Uso1 (residues 1 - 659) was cloned as a *Nde*I/*Xho*I insert
890 into a pET21b *Nde*I/*Xho*I linearized vector.

891 pET21b-Uso1 CCD-His6x: cDNA encoding Uso1 Coiled Coil Domain (residues 660-
892 1103) was cloned as a *Nde*I/*Not*I insert into a pET21b *Nde*I/*Not*I linearized vector.

893 **(II) TNT® expression plasmids**

894 pSP64-Sly1-HA: this plasmid carries cDNA encoding full length Sly1 (AN2518) C-
895 terminally tagged with a HA3x epitope, cloned as an *Nsi*I/*Sac*I insert into *Pst*I/*Sac*I
896 pSP64(PolyA) vector

897 **(III) GST-tagging constructs**

898 pET21b-Sed5-GST: cDNA encoding Sed5/AN9526 cytoplasmic domain (residues 1–
899 322) C-terminally tagged with GST, was cloned as a *Nde*I/*Sal*I insert into a pET21b
900 *Nde*I/*Xho*I linearized vector.

901 pET21b-Bos1-GST: cDNA encoding Bos1/AN11900 cytoplasmic domain (residues 1–
902 219) C-terminally tagged with GST, was cloned as a *Nde*I/*Sal*I insert into a pET21b
903 *Nde*I/*Xho*I linearized vector.

904 pET21b-Bet1-GST: cDNA encoding Bos1/AN5127 cytoplasmic domain (residues 1–71)
905 C-terminally tagged with GST, was cloned as a *Nde*I/*Sal*I insert into a pET21b *Nde*I/*Xho*I
906 linearized vector.

907 pET21b-Sec22-GST: cDNA encoding Sec22/ ASPND00903 cytoplasmic domain
908 (residues 1–198) C-terminally tagged with GST, was cloned as a *Nhe*I/*Sal*I insert into a
909 pET21b *Nhe*I/*Xho*I linearized vector.

910 pET21b-Sso1-GST: cDNA encoding Sso1/AN3416 cytoplasmic domain (residues 1–
911 271) C-terminally tagged with GST, was cloned as a *Nde*I/*Sac*I insert into a pET21b
912 *Nde*I/*Sac*I linearized vector.

913 pET21b-Gos1-GST: cDNA encoding Gos1/AN1229 cytoplasmic domain (residues 1–
914 208) C-terminally tagged with GST, was cloned as a *Nde*I/*Sal*I insert into a pET21b
915 *Nde*I/*Xho*I linearized vector.

916 pET21b-Sft1-GST: cDNA encoding Sft1/AN10508 cytoplasmic domain (residues 1–73)
917 C-terminally tagged with GST, was cloned as a *Nde*I/*Sal*I insert into a pET21b *Nde*I/*Xho*I
918 linearized vector.

919 **Co-precipitation experiments with total cell extracts**

920 Preparation of *Aspergillus* total cell extracts was done as described, with minor
921 modifications (Pinar et al., 2019) (Pinar et al., 2019). 70 mg of lyophilized mycelium were
922 ground with a ceramic bead in a Fast Prep (settings: 20 sec, power 4). The resulting fine
923 powder was resuspended in 1.5 ml of extraction buffer [25 mM HEPES-KOH (pH 7.5),
924 200 mM KCl, 4 mM EDTA, 1% (v/v) IGEPAL CA-630 (NP-40 substitute, #I8896, Sigma),
925 1 mM DTT, 2 µM MG-132 proteasome inhibitor (#S2619, SelleckChem) and cOmplete®
926 ULTRA EDTA-free inhibitor cocktail (#5892953001, Roche). Approximately 0.1 ml of 0.6
927 mm glass beads were added and thoroughly mixed. This suspension was homogenized
928 with a 10 sec pulse at the Fast Prep (power 6) followed by a 10 min incubation at 4ºC.
929 This homogenization step was repeated two times before clarifying the extract by
930 centrifugation at 4ºC and 15,000 × *g* in a microcentrifuge. Total protein concentration of
931 the extracts was determined by Bradford. Bovine Serum-Albumin BSA was then added
932 as a blocking agent to the cell extract (final concentration 1% (w/v)). Binding reactions
933 were carried out in 0.8 ml Pierce centrifuge columns (#89869, ThermoFisher): 9 mg of
934 protein were mixed with 20 µL of S-protein Agarose beads (#69704, Novagen), that had
935 been previously washed in extraction buffer with 1% (w/v) BSA. This buffer was also
936 added to complete final reaction volume of 0.6 ml. The mix was incubated for 3 h at 4°C
937 in a rotating wheel. Columns were then opened at the bottom and gently centrifuged to
938 remove the supernatant and collect the protein-bound beads. These were resuspended
939 in extraction buffer without inhibitors and incubated in rotation for 10 min at 4ºC, followed
940 by two more washing steps in extraction buffer without detergent and inhibitors. To elute
941 proteins bound to the beads, 30 µl of Laemmli loading buffer [62.5 mM Tris-HCl (pH 6.0),
942 6 M urea, 2% (w/v) SDS and 5% (v/v) β-mercaptoethanol] were added and the columns
943 incubated at 90ºC for 2 min. The columns were centrifuged to collect the eluate, of which
944 a 40% of the final volume were resolved in a SDS-polyacrylamide gel and then
945 transferred to nitrocellulose for α-HA (#3F10, Roche) western blotting.

946 **Purification of Uso1 constructs tagged with His6x**

947 Full-length His6-tagged Uso1, Uso1ΔCTR, Uso1 GTD and Uso1 CCD constructs, wild
948 type and mutant versions, were expressed in *E. coli* BL21(DE3) cells harboring pET21b-
949 His6 derivatives and pRIL. Bacteria were cultured at 37ºC in LB medium containing
950 ampicillin and chloramphenicol until reaching an OD_{600nm} of 0.6. Then, IPTG was added
951 to a final concentration of 0.1 mM. Cultures were shifted to 15ºC and incubated for 20 h.

952 Bacterial cells were collected by centrifugation and pellets stored at -80ºC. For
953 purification, frozen pellets were thawed in ice and resuspended in ice-cold bacterial cell
954 lysis buffer [20 mM sodium phosphate buffer, pH 7.4, 500 mM KCl, 30 mM imidazole,
955 5% (v/v) glycerol, 1 mM β-mercaptoethanol, 1 mM $MgCl_2$, 0.2 mg/ml lysozyme and 1
956 µg/ml of DNAse I and cOmplete® protease inhibitor cocktail (#11873580001, Sigma)].
957 This cell suspension was mechanically lysed in a French press (1500 kg/cm^2) and the
958 resulting lysate was centrifuged at 10,000 × *g* and 4ºC for 20 min to remove the cell
959 debris. The supernatant was then transferred to polycarbonate tubes and centrifuged at
960 100,000 × *g* and 4ºC for 1 h in a XL-90 ultracentrifuge (Beckman Coulter) . 50 ml of
961 cleared lysate were incubated with 400 µL of Ni-Sepharose High Performance beads
962 (#17526801, Cytiva) for 2 h at 4ºC. After this step, His-tagged protein-bound beads were
963 pelleted at low-speed centrifugation and washed three times in lysis buffer [20 mM
964 sodium phosphate buffer, pH 7.4, 500 mM KCl, 5% (v/v) glycerol, 1 mM β-
965 mercaptoethanol] with increasing concentrations of imidazole. Finally, Ni2+bound His6
966 proteins were eluted 0.5 M imidazole buffer. 5 ml of eluted protein were loaded onto a
967 HiLoad 16/600 Superdex 200 column (Cytiva) and run at 1 ml/min flow rate on an AKTA
968 HPLC system, using phosphate buffered saline PBS containing 5% (v/v) glycerol and 1
969 mM β-mercaptoethanol. Fractions containing protein were pooled, analyzed for purity by
970 SDS-PAGE followed by Coomassie staining, and finally quantified on a UV-Vis
971 spectrophotometer before being stored at -80ºC.

972 **Purification of SNARE constructs tagged with GST**

973 cDNAs encoding the cytosolic domains of SNAREs fused to a C-terminal GST were
974 cloned into pET21b. Bacterial cultures and protein expression conditions were as
975 described above for Uso1-His6 constructs. Frozen pellets were thawed in ice and
976 resuspended in chilled bacterial cell lysis buffer [25 mM Tris-HCl (pH 7.4), 300 mM KCl,
977 5 mM $MgCl_2$, 1 mM DTT, 0.5 mg/ml lysozyme, 1 µg/ml of DNAse I and cOmplete®
978 protease inhibitor cocktail (#11873580001, Sigma)]. This cell suspension was incubated
979 for 30 min in ice before being mechanically lysed in a French press (1500 kg/cm^2). The
980 lysate was incubated for a further 30 min on ice and centrifuged at 20,000 × *g* and 4ºC
981 for 30 min. After adding 10 mM EDTA to the clarified supernatant to stop DNAse I activity,
982 it was transferred to a 50 ml tube, mixed with 500 µL of glutathione Sepharose beads 4B
983 (#17075601, Cytiva) and rotated for 2 h at 4ºC. After incubation, SNARE-GST-bound
984 beads were pelleted by gentle centrifugation and washed three times for 10 min at 4ºC
985 in 25 mM Tris-HCl (pH 7.4), 500 mM KCl, 5 mM EDTA, 1 mM DTT and subsequently
986 transferred to a 0.8 ml Pierce column. Beads were washed 6 times (10 min at RT) in 200
987 µL of elution buffer [50 mM Tris-HCl (pH 8.0), 200 mM KCl, 10 mM glutathione and 1

988 mM DTT]. These fractions were collected and pooled (~1 ml), then buffer-exchanged to
989 storage buffer (PBS, 5% (v/v) glycerol and 0.1 mM DTT) in a PD MidiTrap G-25 column.
990 Protein concentration and purity was assessed by spectrophotometry and SDS-PAGE
991 followed by Coomassie staining. Protein stocks were kept frozen at -80ºC.

992 **SNARE-GST pull-downs with purified Uso1-His6 constructs (Uso1, Uso1 GHD)**
993 Binding reactions were performed in 0.8 ml Pierce centrifuge columns. 75 µg of purified
994 SNARE-GST were mixed with 15 µL of glutathione Sepharose 4B beads and storage
995 buffer to a final volume of 0.3 ml. Columns were rotated at 4ºC for 2 h before the
996 supernatant was removed after low speed centrifugation. Subsequently, His6 preys were
997 added to a final concentration of 0.2 µM in a total volume of 0.4 ml of pull-down binding
998 buffer [25 mM HEPES-KOH (pH 7.5), 150 mM NaCl, 10% (v/v) glycerol, 0.1% (v/v) Triton
999 X-100 and 0.1 mM DTT]. Columns were rotated overnight at 4ºC. Beads were collected
1000 by gentle centrifugation and washed three times for 10 min with ice-cold binding buffer,
1001 before eluting bound proteins with 30 µL of Laemmli loading buffer pre-heated at 90ºC.
1002 0.5 % of the samples (eluted material or flow-through) were run onto 8% SDS-
1003 polyacrylamide gels that were transferred to nitrocellulose membranes which were
1004 reacted with α-His tag antibody (#631212, Clontech). Quantitation of band intensities
1005 was done with ImageLab software (BioRad). In parallel, 4% of the elution sample volume
1006 was loaded onto 10% SDS-polyacrylamide gel and stained with coomassie dye
1007 (BlueSafe, NZY) to confirm recovery of SNARE-GST baits.
1008

1009 **Pull-down of TNT®-expressed Sly1-HA3**
1010 Sly1-HA3 was synthesized with the TNT® SP6 Quick Coupled Transcription/Translation
1011 system (#L2080, Promega), according to the instructions of the manufacturer. The
1012 reaction was primed with 1 µg of pSP64::Sly1-HA3 cDNA. 10 µL of the resulting mix
1013 were combined with 15 µL of glutathione-Sepharose beads, previously loaded with
1014 SNARE-GST baits as described above, in 0.4 ml of pull-down binding buffer, using 0.8
1015 ml Pierce columns that were rotated overnight at 4ºC before beads and flow-through
1016 were recovered after gentle centrifugation. Beads were washed three times for 10 min
1017 at 4ºC in pull-down binding buffer before eluting bound material with 30 µL of Laemmli
1018 loading buffer for 2 min at 90ºC. 20% of the elution sample volume was analyzed by
1019 western blotting with α-HA tag antibody (#3F10, Roche) for Sly1-HA immunodetection.

1020 **Size exclusion chromatography of HA-tagged cell extracts**
1021 Gel filtration experiments were performed as described (Bravo-Plaza et al., 2019).
1022 Briefly, 200 µL of cell extract were loaded onto a Superose 6 10/300 column (Pharmacia)

1023 equilibrated with running buffer [25 mM Tris-HCl (pH 7.5), 600 mM KCl, 4 mM EDTA, 1
1024 mM DTT]. Fractions of 0.5 ml were collected, from which 80 µL were mixed with 40 µL
1025 of Laemmli loading buffer and denatured at 90ºC. 25 µL of these samples were resolved
1026 by SDS-PAGE and analyzed by western blotting with α-HA3 tag antibody (#3F10,
1027 Roche) for western blotting. Sizing standards were myoglobin (17 kDa), BSA (67 kDa),
1028 aldolase (158 kDa) ferritin (449 kDa), thyroglobulin (669 kDa) and dextran blue (Vo).

1029 **Analytical ultracentrifugation: sedimentation velocity**

1030 Sedimentation velocity assays and subsequent raw data analysis were performed in the
1031 Molecular Interactions Facility of the Centro de Investigaciones Biológicas Margarita
1032 Salas. Samples (320 µL) in PBS containing 5% (v/v) glycerol and 1 mM β-
1033 mercaptoethanol were loaded into analytical ultracentrifugation cells, which were run at
1034 20°C and 48,000 rpm in a XL-I analytical ultracentrifuge (Beckman-Coulter Inc.)
1035 equipped with UV-VIS absorbance and Raleigh interference detection systems, using an
1036 An-50Ti rotor, and 12 mm Epon-charcoal standard double-sector centerpieces.
1037 Sedimentation profiles were recorded at 230 nm. Differential sedimentation coefficient
1038 distributions were calculated by least-squares boundary modelling of sedimentation
1039 velocity data using the continuous distribution *c(s)* Lamm equation model as
1040 implemented by SEDFIT(Schuck, 2000). Experimental Svedberg coefficient values were
1041 corrected to standard conditions ($s_{20,w}$: water, 20°C, and infinite dilution) using
1042 SEDNTERP software

1043 **Dynamic Light Scattering, DLS**

1044 DLS experiments were carried out in a Protein Solutions DynaPro MS/X instrument at
1045 20C using a 90° light scattering cuvette. DLS autocorrelation functions, average of at
1046 least 18 replicates, were collected with Dynamics V6 software. Analysis evidenced in
1047 most cases the presence of two diffusing species, one with faster diffusion corresponding
1048 to a discrete major species and a second with substantially slower diffusion,
1049 corresponding to higher order species, with a minor contribution to the whole population
1050 within the sample. Exceptions were the globular domain GHD that appeared as a single
1051 species, and the coiled-coil construct with a larger contribution of the higher order
1052 species. Dynamics software was also employed to export the data as text files for parallel
1053 analysis using user-written scripts and functions in MATLAB (Version 7.10, MathWorks,
1054 Natick, MA). A double exponential decay model was fit to the data *via* nonlinear least
1055 squares, using as starting values the translational diffusion coefficients and relative
1056 amounts of the two different species, using as starting values those from the
1057 regularization analysis and their masses (those of the discrete species as estimated by
1058 the Svedberg equation). These values were compatible with the experimental data,

1059 rendering a similar best-fit value of the diffusion coefficient for the major species and
1060 allowing to assess its probability distribution.

1061 **Estimate of molar mass from hydrodynamic measurements.**
1062 The apparent molar masses of Uso1 and its mutants were calculated via the Svedberg
1063 equation, using the *s*- and *D*-values of the major species independently measured by
1064 sedimentation velocity and DLS, respectively.

1065 **Fluorescence Microscopy**
1066 *A. nidulans* hyphae were cultured in Watch Minimal Medium WMM (Peñalva, 2005).
1067 Image acquisition equipment, microscopy culture chambers and software have been
1068 detailed (Pinar et al., 2022; Pinar and Peñalva, 2020). Simultaneous visualization of
1069 green and red emission channels was achieved with a Gemini Hamamatsu beam splitter
1070 coupled to a Leica DMi8 inverted microscope. Z-Stacks were deconvolved using
1071 Huygens Professional software (version 20.04.0p5 64 bits, SVI). Images were contrasted
1072 with Metamorph (Molecular Devices). Statistical analysis was performed with GraphPad
1073 Prism 8.02 (GraphPad). Uso1-GFP time of residence in cisternae was estimated from
1074 3D movies consisting of middle planes with 400 photograms at 2 fps time resolution.
1075 Each Uso1 puncta considered in the analysis was tracked manually with 3D (x,y,t)
1076 representations generated with Imaris software (Oxford Instruments) combined with
1077 direct observation of photograms in movies and kymograph representations traced
1078 across >25 px-wide linear ROI covering the full width of the hyphae.

1079 **AlphaFold predictions**
1080 AlphaFold2 (Jumper et al., 2021) predictions were run using versions of the program
1081 installed locally and on ColabFold (Mirdita et al., 2022) with the
1082 AlphaFold2_advanced.ipynb notebook and the MMseqs2 MSA option. In all cases, the
1083 five solutions predicted by AlphaFold2 by default were internally congruent, and we
1084 always chose the one ranked first by the software. Uso1 GHD (1-674), Bos1, Bet1 and
1085 RAB1 were initially submitted as hetero-oligomers. Subsequently, predictions were
1086 submitted as 1:1 complexes of Uso1 GHD with Bos1, Bet1 and RAB1, as described in
1087 the table below. The solutions were also very similar when comparing the different
1088 combinations displayed in the table were fed to the software, strongly supporting the
1089 validity of the results.
1090

AlphaFold2 runs, subunits included	
Uso1 GHD	Bet1

Uso1 GHD	Bet1	Bos1	
Uso1 GHD	Bet1	Bos1	Rab1
Uso1 GHD	Bet1 (1-49)		
Uso1 GHD (N-terminal)	Bet1 (1-49)		
Uso1 GHD	Bet1 (1-49)	Bos1 Habc (1-126)	
Uso1 GHD E6K/G540S	Bet1 (1-49)	Bos1 Habc (1-126)	
Uso1 GHD		Bos1	
Uso1 GHD		Bos1 Habc (1-126)	
Uso1 GHD dimer		Bos1 Habc (1-126)	
Uso1 GHD E6K/G540S		Bos1	
Uso1 GHD E6K/G540S		Bos1 Habc (1-126)	
Uso1			
Uso1 dimer			
Uso1 dimer E6K/G540S			
Bet1	Bos1	Sec22	Sed5
Rud3 dimer			
Coy1 dimer			
Grh1	Bug1		

Acknowledgements

We thank Juan R. Luque (Molecular Interactions Facility, Centro de Investigaciones Biológicas) for his help with the analytical ultracentrifuge experiments, Manuel Sánchez-Berges for HA3-tagged SNARE strains, Sara Abib and Elena Reoyo for skillful technical assistance. Thanks are due to Spain's Ministerio de Ciencia e Innovación for grants RTI2018-093344-B100 (MAP) and predoctoral contract BES-2016-077440 (IB.-P/MAP), and to the Comunidad de Madrid for grant S2017/BMD-3691 (MAP). Grants were co-funded by European Regional Development and European Social Funds. The authors declare that they do not have any competing financial interests.

Additional information

Competing interests

The authors declare that there are no competing interests

Availability statement

All DNA molecules used here may reconstructed by standard techniques using primers listed in supplemental Table II. All strains listed under supplemental Table I are available for academic purposes upon reasonable request to the corresponding author. They are deposited and maintained by the corresponding laboratory in the so-denoted Madrid (MAD) collection.

Funding

Funding Agency	Grant reference number	Principal Investigator
Agencia Estatal de Investigación, Ministerio de Ciencia e Innovación, Spain	RTI2018-093344-B100	Miguel A. Peñalva
Agencia Estatal de Investigación, Ministerio de Ciencia e Innovación, Spain	predoctoral contract BES-2016-077440	Ignacio Bravo-Plaza
Agencia Estatal de Investigación, Ministerio de Ciencia e Innovación, Spain	PID2021-124278OB-I00	Miguel A. Peñalva & Eduardo A. Espeso, co-IPs
Comunidad de Madrid	S2017/BMD-3691	Miguel A. Peñalva
Grants co-funded by European Regional Development and European Social Funds		

Author contributions

Ignacio Bravo Plaza, Conceptualization, Data curation, Formal analysis, Validation, Investigation, Visualization, Writing — review and editing; Víctor G. Tagua, Data curation, Formal analysis, Validation, Investigation; Herbert N. Arst, Jr., Conceptualization, Data curation, Formal analysis, Validation, Investigation, Supervision, Writing — review and editing; Ana M. Alonso, Data curation, Formal analysis, Validation, Investigation; Mario Pinar, Conceptualization, Data curation, Formal analysis, Validation, Investigation, Supervision, Writing — review and editing ; Begoña Monterroso, Conceptualization, Data curation, Formal analysis, Validation, Supervision, Writing — review and editing; Antonio Galindo, Conceptualization, Data curation, Formal analysis, Validation, Investigation, Visualization, Writing — review and editing and Miguel Á. Peñalva, Conceptualization, Data curation, Formal analysis, Validation, Investigation, Supervision, Funding acquisition, Visualization, Writing – original draft, Writing — review and editing.

Authors ORCIDs

Ignacio Bravo-Plaza (0000-0003-0934-9084) - ORCID
Victor García-Tagua (0000-0003-1494-6895) - ORCID
Ana M. Alonso (0000-0002-1228-7331) - ORCID
Mario Pinar (0000-0002-2415-8721) - ORCID
Begoña Monterroso (0000-0003-2538-084X)- ORCID
Antonio Galindo (0000-0002-1108-652X) - ORCID
Miguel A. Peñalva (0000-0002-3102-2806)- ORCID

1144

1145 ## Legends to figures

1146 **Figure 1. Characterization of mutations bypassing the essential role of RAB1.**
1147 (A). Genetic map in the region surrounding *uso1* with genetic markers used as landmarks
1148 for mapping.
1149 (B). Molecular identification of the nucleotide changes in *suArab1ts* strains
1150 (C) and (D): growth tests showing *rab1ts*- and *rab1*Δ-rescuing phenotypes, respectively,
1151 of individual mutations, and synthetic positive interaction between E6K and G540S.
1152 Strains produce either green or white conidiospores (conidiospore colors are used as
1153 genetic markers). In (C), strains were point-inoculated. In (D) conidiospores were spread
1154 on agar plates to give individual colonies.

1155 **Figure 1—figure supplement 1: E6K/G540S do not rescue lethality resulting from**
1156 ***arf1*Δ, *sly1*Δ or *sed5*Δ.**
1157 Top, *uso1* is an essential gene. Singly-nucleated conidiospores derived from a
1158 heterokaryotic strain in which one class of nuclei carries a deficient *pyrG* uracil
1159 biosynthetic gene whereas the second class contains a *uso1*Δ allele tagged with
1160 functional *pyrG* were unable to grow on medium lacking pyrimidines at any of the
1161 tested temperatures. Bottom: Similar experiments showing that unlike *rab1*Δ
1162 strains, strains carrying lethal *arf1*Δ, *sly1*Δ and *sed5*Δ alleles cannot be rescued by
1163 $uso1^{E6K/G540S}$. Top panel, strains with green conidiospores; bottom, strains with
1164 white conidiospores.

1165 **Figure 2: Localization of the amino acid substitutions within the Uso1**
1166 **AlphaFold2 structure**
1167 (A). AlphaFold2 cartoon representations of A. nidulans Uso1 in monomeric and dimeric
1168 forms. Confidence estimations for this and other models are detailed under extended
1169 data S2. Red, N-terminal tail; marine blue, globular head domain; gray, coiled-coil; green,
1170 limit of the CTR. The rest of the CTR is shown as surface representation.
1171 (B). Amino acid alignment of fungal sequences with mammalian p115 showing strong
1172 conservation within the CTR: ANIDU, *Aspergillus nidulans;* PRUBE, *Penicillium rubens*;
1173 TREES, *Thrichoderma ressei*; SSCLE, *Sclerotinia scleriotorum*; MORYZ, *Magnaporthe*
1174 *oryzae*; CIMM, *Coccidioides immitis;* BOVIN, *Bos taurus*.
1175 (C). Position of the Gly6Lys and Gly540Ser substitutions. Only the GHD of dimeric full-
1176 length Uso1 are shown. The two different chains are colored in green and yellow,
1177 respectively. Distances between mutated residues are displayed in armstrongs.
1178 (D). The N-terminal amphipathic α-helix affected by the Glu6Lys substitution.

1179 **Figure 2—figure supplement 1. AlphaFold2 predictions of Uso1**
1180 Ribbon representation of AlphaFold 2-predicted structures of full-length Uso1 (A)
1181 and Uso1 GHD (B), color-coded by pLDDT values. Graphs at the bottom are the
1182 corresponding plots of predicted aligned error of the residues (PAE).
1183

1184 **Figure 3: Determining molecular masses and oligomerization status of the**
1185 **different Uso1 constructs by velocity sedimentation analysis**
1186 The different panels display the sedimentation profiles of the protein being analyzed,
1187 with % of the main species, scheme of the different constructs and their limits and
1188 pictures of Coomassie stained-gels showing the purity of the protein preparations. The
1189 table below depicts biophysical parameters of the constructs used to obtain relative
1190 molecular masses. s_{exp} is the experimentally determined Svedberg coefficient; D_{exp},
1191 translational diffusion coefficient of the main species; *Mr*, molecular mass deduced from
1192 Svedberg equation; M1 predicted molecular mass of the monomer; n = (*Mr* /M1).

1193 **Figure 3—figure supplement 1: GHD is a monomer across a range of**
1194 **concentrations**
1195 (A) and (B). Sedimentation velocity experiments with wild-type and E6K/G540S
1196 mutant GHD, respectively, showing that they behave as monomers at
1197 concentrations up to 5 μM.(C). Sedimentation velocity profile of E6K/G540S
1198 mutant GHD lacking the His-tag, showing that the presence of the latter does not
1199 interfere with oligomerization, and a picture of a Coomassie stained gel showing
1200 the purity of the protein preparation on the right.

1201 **Figure 4: Subcellular localization of Uso1**
1202 (A). Uso1-GFP localizing to punctate cytoplasmic structures, 3D shaded by software.
1203 (B). Sections of a deconvolved Z-stack and its corresponding MIP. Uso1-GFP in inverted
1204 greyscale for clarity
1205 (C). Kymograph showing the transient recruitment of Uso1 to punctate cytoplasmic
1206 structures.
1207 (D). Average time of residence of Uso1 in these structures. Error bars, 95% CI.
1208 (E). Example of one such structures visualized with a kymograph and with the
1209 corresponding movie frames (Movie 4).
1210

1211 **Figure 4—figure supplement 1: Methodology for tracking the half-life of**
1212 **Uso1-GFP on punctate structures.**

1213 (1) 3D movies were acquired by streaming pictures to the computer RAM at 2 fps.
1214 Appropriate reduction of excitation light intensity permitted acquisition of 400
1215 frames without apparent phototoxicity.
1216 (2) The behavior of punctate structures over time was represented in kymographs,
1217 in which vertical lines represent the time of residence of Uso1 on membranes.
1218 (3). As vertical lines frequently overlapped, jeopardizing the quality of this analysis,
1219 we imported the time series into a 3D viewer as if they were (x, y, z) series. Rotation
1220 across the different axes facilitated unambiguous tracking of the trajectories across
1221 time.
1222 (4) The length of the trajectories was measured and converted to time units.
1223 Bottom graphs display examples of time trajectories.
1224

1225 **Figure 5: Uso1 puncta do not colocalize with ERESs**
1226 (A). Low extent co-localization of Sec13 ERES and Uso1 structures. Z-stacks for the two
1227 channels were acquired simultaneously, deconvolved and represented as MIPs. Two
1228 rare examples of colocalization are arrowed.
1229 (B). Photograms of a dual channel Z-stack with a Sec13-labeled nuclear envelope
1230 focused in the middle plane, illustrating that while some puncta show colocalization, the
1231 red Sec13 signal and the green Uso1 signal do not usually overlap.
1232 (C). A MIP of the same z-stack showing orthogonal views with some overlapping puncta
1233 (arrows).
1234 (D). A ts mutation in the *sarA* gene encoding the $SarA^{Sar1}$ GTPase governing ER exit
1235 markedly reduces the number of Uso1-GFP puncta upon shifting cells to restrictive
1236 conditions. Box-and-whisker plots: Statistical comparison was made using one-way
1237 ANOVA with Dunn's test for multiple comparisons. Whiskers are in Tukey's style: Only
1238 significant differences were indicated, using asterisks.
1239

1240 **Figure 6: Uso1 localizes to RAB1-containing Golgi cisternae**
1241 (A). Tip cells showing Uso1 colocalization with the indicated subcellular markers. Images
1242 are MIPs of deconvolved Z-stacks.
1243 (B). Magnified images of the color-coded shaded regions of the cells shown in A.
1244 (C). Pearson's coefficients of the different combinations.
1245

1246 **Figure 7: Uso1 localization to punctate structures is dependent on RAB1**
1247 (A). Complete de-localization of Uso1-GFP to the cytosol by rab1ts and relocalization by
1248 E6K/G540S.
1249 (B). Uso1-GFP and *rab1ts* show a synthetic negative interaction that is rescued by the
1250 E6K/G540S double substitution. Strains in lanes 7 and 8 carry the *wA2* mutation resulting
1251 in white conidiospores.
1252

1253 **Figure 8. Genetic evidence showing that the CTR region of Uso1 contributes to**
1254 **its recruitment to membranes.**
1255 (A). Top, scheme of the predicted interactions. Bottom, engineering a gene-replaced
1256 allele lacking the CTR domain by homologous recombination.
1257 (B). The Bug1 C-terminal residues fit into the groove formed between the two Grh1 PDZ
1258 domains and into the pocket of the N-terminal PDZ domain (PDZ1).
1259 (C). A gene-replaced *uso1ΔCTR* allele encoding a protein truncated for the CTR domain
1260 shows a synthetic negative interaction with *rab1ts*.
1261 (D). Western blot analysis. Removal of the CTR does not result in Uso1 instability.
1262 (E). *bug1Δ* and *grh1Δ* show a synthetic negative interaction with *rab1ts* that is rescued
1263 by the double E6K/G540S substitution in Uso1

1264 **Figure 8—figure supplement 1: AlphaFold2 modelling of Grh1-Bug1.**
1265 (A). Cartoon, with alpha-helices shown as cylinders, of the nearly N-terminal PDZ
1266 domains of Grh1
1267 (B). AlphaFold 2 prediction of a 1:1 Grh1-Bug1 complex, trimmed of disordered
1268 regions
1269 (C). complete AlphaFold2 model of Grh1-Bug1 with color-coded model
1270 confidences values.

1271 **Figure 9: The GHD of Uso1 is sufficient to support cell viability**
1272 (A). Gene-replaced *uso1^{GHD}* allele carrying the double E6K/G540S substitution is
1273 sufficient to rescue viability at 30°C, but not at higher temperatures. (B). The Uso1 GHD
1274 is a monomer in vivo. Fractions collected from Superose columns loaded with the
1275 indicated protein extracts and reference His-tagged proteins were collected and
1276 analyzed by western blotting with α-HA and α-His antibodies. (C) Truncating Uso1 after
1277 the GHD results in markedly reduced protein levels, as determined by α-Uso1 GHD
1278 western blotting. The band (yellow asterisks) moving slower than Uso1 (magenta
1279 asterisk) and at nearly the same position of Uso1 ΔCTR (blue asterisk) represents cross-
1280 reacting contaminants unrelated to Uso1. The right panel shows a longer exposure for

1281 the indicated region, to reveal the faint GHD band (green dot). (D). Overexpression of
1282 Uso1, wild-type and E6K/G540S mutant, under the control of the *inuA* promoter, which
1283 is turned off on glucose and induced on sucrose. Western blots reacted with α-Uso1
1284 GHD antiserum. (E). Overexpressed GHD, be it E6K/G540S or wild-type, as the only
1285 source of Uso1 supports viability.
1286

1287 **Figure 10: Screening the preferential association of proteins acting in the**
1288 **ER/Golgi interface with E6K/G540S Uso1.**
1289 (A). S-tagged baits (Uso1, wt and E6K/G540S, and the unrelated protein BapH),
1290 expressed after gene replacement, were captured with their associated polypeptides on
1291 S-protein agarose beads. Candidate associates, also expressed after gene replacement,
1292 were tagged with HA3. (B). Schematic depiction of the proteins listed in these
1293 experiments showing their sites of action.(C). Anti-HA3 western blot analysis of the
1294 indicated S-bait and HA3-prey combinations. Equal loading of Uso1 proteins was
1295 confirmed by silver staining of precipitates. Note that BapH, chosen as negative control,
1296 is expressed at much higher levels than Uso1 proteins. Each panel is a representative
1297 experiment of three experimental replicates.

1298 **Figure 10—figure supplement 1.**
1299 (A) AlphaFold2 model, with PAE plot, of the GRIP domain of A. nidulans RUD3,
1300 predicted to be a dimer.
1301 (B) AlphaFold2 model of Coy1, calculated as a monomer. TMH is the nearly C-
1302 terminal transmembrane helix that contributes to its recruitment to membranes

1303 **Figure 10—figure supplement 2: Growth phenotypes of null mutants of genes**
1304 **encoding golgins.**
1305 (A). Ablation of individual golgins Bug1/Grh1 and Rud3 does not result in
1306 detectable growth defects. *coy1*Δ strains have a subtle growth phenotype.
1307 (B). Negative effects of *grh1*Δ, *bug1*Δ, coy1Δ and *rud3*Δ on the ability of
1308 *uso1*$^{E6K/G540S}$ to rescue *rab1*Δ. Note that *coy1*Δ and *rab1*Δ *uso1*$^{E6K/G540S}$ are
1309 synthetically lethal. For convenience, this set of strains carried a mutation resulting
1310 in white conidiospores, as opposed to the wild-type green color.
1311

1312 **Figure 11: The Uso1 GHD interacts directly with Bos1 and Bet1 SNAREs acting in**
1313 **the ER/Golgi interface**
1314 (A). Purified fusion proteins in which the cytosolic domains of the indicated SNAREs
1315 have been fused to GST were used in pulldown experiments with His-tagged, purified

1316 wild-type and E6K/G540S Uso1. The plasma membrane Qa syntaxin Sso1 was used as
1317 negative control. Pulled-down material was analyzed by anti-His western blotting. (B).
1318 Quantitation of the above experiment; significance was determined by unpaired *t*-student
1319 tests. Error bars represent S.E.M. (C). As in A, but using in vitro synthesized, HA3-tagged
1320 Sly1 as prey. Samples were analyzed by anti-HA western blotting. (D). As in A, but using
1321 wild-type and mutant GHD as preys, rather than full-length Uso1. (E). Quantitation of the
1322 experiment in D. (F). GST pull-down experiment comparing the ability of the GHD to
1323 interact with the early Golgi Qb and Qc SNAREs (Bos1 and Bet1), with that of their
1324 medial Golgi counterparts (Qb Gos1 and Qc Sft1).
1325

1326 **Figure 11—figure supplement 1. AlphaFold2 prediction of the ER/Golgi SNARE**
1327 **bundle.**
1328 (A) Sec5/Bos1/Bet1/Sec22 predicted SNARE bundle. (B) Quality control (pLDDT,
1329 color coded, and PAE) of the model.

1330 **Figure 12. AlphaFold2 models provide insight into the additive mode of**
1331 **suppression shown by E6K and G540S.**
1332 (A). Model of full length Uso1 bound to the ER/Golgi SNAREs Bos1 and Bet1.
1333 (B). Top, ribbon representation of the Bos1 N-terminal Habc domain and Uso1GHD.
1334 Bottom, Inset combining surface and ribbon depiction.
1335 (C). Increased binding of Bos1 to G540S Uso1 appears to involve insertion of Ser540
1336 into a pocket located in the Habc domain of the Qb SNARE. Partial view of the Bos1-
1337 Uso1 GHD surface of interaction in the wild type (left) and mutant (right) models. G540
1338 and S540 are annotated.
1339 (D). The N-terminal amphipathic α-helix of Uso1 comprising the E6K substitution lies
1340 within a flexible stretch of the protein that might facilitate its insertion into membranes.
1341 Alignment of six independent predictions, with Glu6 highlighted in red. The Uso1 GHD
1342 was modeled alone, in a complex with SNARE proteins or with Ypt1. The N-terminal a-
1343 helix (boxed) adopts different positions, suggesting high flexibility.

1344 **Figure 12—figure supplement 1. AlphaFold2 prediction of the Bet1-GHD**
1345 **interaction.**
1346 The putative binding surface of Bet1 and Uso1 as determined by AlphaFold2. Top
1347 images, cartoon of Bet1-GHD interactions, colored by pLDDT score. Alignment of
1348 four independent predictions involving the Bet1 N-terminal region and Uso1 GHD.
1349 A single model for Uso1 GHD is shown on the top representation for simplicity. In
1350 spite of the disordered nature of the N-terminal Bet1 region, the Bet1-Uso1 binding

interface is consistent among models. Bottom, surface representation of the N-terminal Bet1 region (orange) in complex with the GHD. Also indicated is the Habc domain of Bos1 (yellow) bound to the GHD.

Figure 12—figure supplement 2. AlphaFold 2 prediction of the RAB1 binding site on the Bet1/Bos1/Uso1 GHD complex.

(A) and (B): cartoon representation of the GHD-RAB1 complex. The model is depicted as pipes and planks

(C): Orthogonal views of the Uso1 GHD-RAB1-Bet1-Bos1Habc structural model. The Uso1 GHD is shown as surface to emphasize the distant binding sites of the Bos1 Habc domain, RAB1 and the Bet1 N-terminal region

(D): Ribbon representation of the model shown in C but including the full-length SNARE subunits, i.e. the GHD domain of Uso1, RAB1 and the SNARES Bet1 and Bos1. Proteins are in the correct orientation to connect membranes separated by 23 nm, counting from the SNARE TMDs to the prenylated RAB1 residues.

Figure 12—figure supplement 3. Quality control assessment of AlphaFold2 predictions for the indicated complexes.

Supplemental Table I

List and complete genotypes of *A. nidulans* strains used in this work

Supplemental Table II

Primers used for PCR-based genetic manipulations

Figure 8 source data

Raw images for western blots in panel D and uncropped pictures with used exposures and regions indicated.

Figure 9 source data

For panels B, C, D; raw images for western blots and uncropped pictures with used exposures and regions indicated.

Figure 10 source data

Raw images for western blots and silver-stained gels and uncropped pictures with used exposures and regions indicated.

1383 **Figure 11 source data**

1384 Raw images for western blots and Coomassie-stained gels and uncropped pictures
1385 with used exposures and regions indicated.

1386

1387 ## Rich file media

1388 **Video 1: Shaded 3D reconstruction of a hypha expressing Uso1-GFP**

1389 **Video 2: 4D acquisition showing the dynamics of Uso1-GFP.**
1390 4D (x, y, z, t) in which Z-stacks were acquired at a rate of 1 frame every 2.6 sec

1391 **Video 3: Dynamics of Uso1-GFP at 2 fps**
1392 3D acquisition (200 frames) showing the dynamics of Uso1-GFP. Time resolution, 2 fps

1393 **Video 4: Single Uso1-GFP cisterna tracked over time**
1394 Example of Uso1-GFP cisterna. The video contains 96 photograms acquired at 2fps

1395 **Video 5: ·3D reconstruction of a hypha expressing fluorescently labeled Uso1-**
1396 **GFP and Sec13-mCh**
1397 There is little colocalization between Uso1-GFP and Sec13 ERES

1398 **Video 6: ·4D video (1 fpm) of a hypha expressing fluorescently labeled Uso1-GFP**
1399 **and Sec7-mCh**
1400 Uso1 does not colocalize at all with the TGN marker Sec7
1401

1402

1403 **References**
1404
1405

1406 Allan, B.B., B.D. Moyer, and W.E. Balch. 2000. Rab1 recruitment of p115 into a cis-
1407 SNARE complex: programming budding COPII vesicles for fusion. *Science*.
1408 289:444-448. 10.1126/science.289.5478.444

1409 An, Y., C.Y. Chen, B. Moyer, P. Rotkiewicz, M.A. Elsliger, A. Godzik, I.A. Wilson, and
1410 W.E. Balch. 2009. Structural and functional analysis of the globular head
1411 domain of p115 provides insight into membrane tethering. *J Mol Biol*. 391:26-
1412 41. PM:19414022

1413 Anderson, N.S., I. Mukherjee, C.M. Bentivoglio, and C. Barlowe. 2017. The Golgin
1414 protein Coy1 functions in intra-Golgi retrograde transport and interacts with the
1415 COG complex and Golgi SNAREs. *Mol Biol Cell*. 10.1091/mbc.E17-03-0137

1416 Arst, H.N., Jr., M. Hernández-González, M.A. Peñalva, and A. Pantazopoulou. 2014.
1417 GBF/Gea mutant with a single substitution sustains fungal growth in the
1418 absence of BIG/Sec7. *FEBS Lett*. 588:4799-4786.
1419 10.1016/j.febslet.2014.11.014

1420 Baker, R.W., and F.M. Hughson. 2016. Chaperoning SNARE assembly and
1421 disassembly. *Nat Rev Mol Cell Biol*. 17:465-479. 10.1038/nrm.2016.65

1422 Baker, R.W., P.D. Jeffrey, M. Zick, B.P. Phillips, W.T. Wickner, and F.M. Hughson.
1423 2015. A direct role for the Sec1/Munc18-family protein Vps33 as a template for
1424 SNARE assembly. *Science*. 349:1111-1114. 10.1126/science.aac7906

1425 Barlowe, C.K., and E.A. Miller. 2013. Secretory protein biogenesis and traffic in the
1426 early secretory pathway. *Genetics*. 193:383-410.
1427 http://www.ncbi.nlm.nih.gov/pubmed/23396477

1428 Beard, M., A. Satoh, J. Shorter, and G. Warren. 2005. A cryptic Rab1-binding site in
1429 the p115 tethering protein. *J Biol Chem*. 280:25840-25848.
1430 10.1074/jbc.M503925200

1431 Behnia, R., F.A. Barr, J.J. Flanagan, C. Barlowe, and S. Munro. 2007. The yeast
1432 orthologue of GRASP65 forms a complex with a coiled-coil protein that
1433 contributes to ER to Golgi traffic. *J Cell Biol*. 176:255-261. PM:17261844

1434 Bentley, M., Y. Liang, K. Mullen, D. Xu, E. Sztul, and J.C. Hay. 2006. SNARE Status
1435 Regulates Tether Recruitment and Function in Homotypic COPII Vesicle
1436 Fusion*. *J Biol Chem*. 281:38825-38833.
1437 https://doi.org/10.1074/jbc.M606044200

1438 Bracher, A., and W. Weissenhorn. 2002. Structural basis for the Golgi membrane
1439 recruitment of Sly1p by Sed5p. *EMBO J*. 21:6114-6124. PM:12426383

1440 Brandon, E., T. Szul, C. Alvarez, R. Grabski, R. Benjamin, R. Kawai, and E. Sztul.
1441 2006. On and off membrane dynamics of the endoplasmic reticulum-golgi
1442 tethering factor p115 in vivo. *Mol Biol Cell*. 17:2996-3008. 10.1091/mbc.E05-09-
1443 0862

1444 Bravo-Plaza, I., M. Hernandez-Gonzalez, M. Pinar, J.F. Diaz, and M.A. Penalva. 2019.
1445 Identification of the guanine nucleotide exchange factor for SAR1 in the
1446 filamentous fungal model Aspergillus nidulans. *Biochim Biophys Acta Mol Cell*
1447 *Res*. 1866:118551. 10.1016/j.bbamcr.2019.118551

1448 Cai, H., S. Yu, S. Menon, Y. Cai, D. Lazarova, C. Fu, K. Reinisch, J.C. Hay, and S.
1449 Ferro-Novick. 2007. TRAPPI tethers COPII vesicles by binding the coat subunit
1450 Sec23. *Nature*. 445:941-944. PM:17287728

1451 Cao, X., N. Ballew, and C. Barlowe. 1998. Initial docking of ER-derived vesicles
1452 requires Uso1p and Ypt1p but is independent of SNARE proteins. *EMBO J*.
1453 17:2156-2165. 10.1093/emboj/17.8.2156

1454 Cove, D.J. 1966. The induction and repression of nitrate reductase in the fungus
1455 *Aspergillus nidulans. Biochim Biophys Acta*. 113:51-56. 10.1016/S0926-
1456 6593(66)80120-0

1457 Day, K.J., L.A. Staehelin, and B.S. Glick. 2013. A three-stage model of Golgi structure
1458 and function. *Histochem Cell Biol*. 140:239-249. 10.1007/s00418-013-1128-3

1459 Galindo, A., V.J. Planelles-Herrero, G. Degliesposti, and S. Munro. 2021. Cryo-EM
1460 structure of metazoan TRAPPIII, the multi-subunit complex that activates the
1461 GTPase Rab1. *Embo J*. 40:e107608.
1462 https://doi.org/10.15252/embj.2020107608

1463 Gillingham, A.K. 2018. At the ends of their tethers! How coiled-coil proteins capture
1464 vesicles at the Golgi. *Biochem Soc Trans*. 46:43-50. 10.1042/BST20170188

1465 Gillingham, A.K., and S. Munro. 2016. Finding the Golgi: Golgin Coiled-Coil Proteins
1466 Show the Way. *Trends Cell Biol*. 26:339-408.
1467 http://dx.doi.org/10.1016/j.tcb.2016.02.005

1468 Heo, Y., H.-J. Yoon, H. Ko, S. Jang, and H.H. Lee. 2020. Crystal structures of Uso1
1469 membrane tether reveal an alternative conformation in the globular head
1470 domain. *Scientific Reports*. 10:9544. 10.1038/s41598-020-66480-1

1471 Hernández-González, M., I. Bravo-Plaza, V. de Los Ríos, M. Pinar, A. Pantazopoulou,
1472 and M.A. Peñalva. 2019. COPI localizes to the early Golgi in *Aspergillus*
1473 *nidulans*. *Fungal Genet Biol*. 123:78-86. 10.1016/j.fgb.2018.12.003

1474 Hernández-González, M., A. Pantazopoulou, D. Spanoudakis, C.L.C. Seegers, and
1475 M.A. Peñalva. 2018. Genetic dissection of the secretory route followed by a
1476 fungal extracellular glycosyl hydrolase. *Mol Microbiol*. 109:781-800.
1477 doi:10.1111/mmi.14073

1478 Hu, F., X. Shi, B. Li, X. Huang, X. Morelli, and N. Shi. 2015. Structural basis for the
1479 interaction between the Golgi reassembly-stacking protein GRASP65 and the
1480 Golgi matrix protein GM130. *J Biol Chem*. 290:26373-26382.
1481 10.1074/jbc.M115.657940

1482 Jiang, Y., A. Scarpa, L. Zhang, S. Stone, E. Feliciano, and S. Ferro-Novick. 1998. A
1483 high copy suppressor screen reveals genetic interactions between BET3 and a
1484 new gene. Evidence for a novel complex in ER-to-Golgi transport. *Genetics*.
1485 149:833-841. 10.1093/genetics/149.2.833

1486 Joiner, A.M., B.P. Phillips, K. Yugandhar, E.J. Sanford, M.B. Smolka, H. Yu, E.A. Miller,
1487 and J.C. Fromme. 2021. Structural basis of TRAPPIII-mediated Rab1
1488 activation. *Embo J*. 40:e107607. https://doi.org/10.15252/embj.2020107607

1489 Jumper, J., R. Evans, A. Pritzel, T. Green, M. Figurnov, O. Ronneberger, K.
1490 Tunyasuvunakool, R. Bates, A. Zidek, A. Potapenko, A. Bridgland, C. Meyer,
1491 S.A.A. Kohl, A.J. Ballard, A. Cowie, B. Romera-Paredes, S. Nikolov, R. Jain, J.
1492 Adler, T. Back, S. Petersen, D. Reiman, E. Clancy, M. Zielinski, M. Steinegger,
1493 M. Pacholska, T. Berghammer, S. Bodenstein, D. Silver, O. Vinyals, A.W.
1494 Senior, K. Kavukcuoglu, P. Kohli, and D. Hassabis. 2021. Highly accurate
1495 protein structure prediction with AlphaFold. *Nature*. 596:583-589.
1496 10.1038/s41586-021-03819-2

1497 Lord, C., D. Bhandari, S. Menon, M. Ghassemian, D. Nycz, J. Hay, P. Ghosh, and S.
1498 Ferro-Novick. 2011. Sequential interactions with Sec23 control the direction of
1499 vesicle traffic. *Nature*. 473:181-186. 10.1038/nature09969

1500 Lupashin, V.V., and M.G. Waters. 1997. t-SNARE activation through transient
1501 interaction with a Rab-like guanosine triphosphatase. *Science*. 276:1255-1258.
1502 http://www.ncbi.nlm.nih.gov/pubmed/9157884

1503 Malsam, J., and T.H. Sollner. 2011. Organization of SNAREs within the Golgi stack.
1504 *Cold Spring Harb Perspect Biol*. 3:a005249. 10.1101/cshperspect.a005249

1505 McNew, J.A., F. Parlati, R. Fukuda, R.J. Johnston, K. Paz, F. Paumet, T.H. Sollner,
1506 and J.E. Rothman. 2000. Compartmental specificity of cellular membrane fusion
1507 encoded in SNARE proteins. *Nature*. 407:153-159. 10.1038/35025000.

1508 Mirdita, M., K. Schütze, Y. Moriwaki, L. Heo, S. Ovchinnikov, and M. Steinegger. 2022.
1509 ColabFold: making protein folding accessible to all. *Nature Methods*. 19:679-
1510 682. 10.1038/s41592-022-01488-1

1511 Muschalik, N., and S. Munro. 2018. Golgins. *Curr Biol.* 28:R374-R376.
1512 https://doi.org/10.1016/j.cub.2018.01.006

1513 Nakajima, H., A. Hirata, Y. Ogawa, T. Yonehara, K. Yoda, and M. Yamasaki. 1991. A
1514 cytoskeleton-related gene, uso1, is required for intracellular protein transport in
1515 Saccharomyces cerevisiae. *J Cell Biol*. 113:245-260. 10.1083/jcb.113.2.245

1516 Nayak, T., E. Szewczyk, C.E. Oakley, A. Osmani, L. Ukil, S.L. Murray, M.J. Hynes,
1517 S.A. Osmani, and B.R. Oakley. 2005. A versatile and efficient gene targeting
1518 system for *Aspergillus nidulans. Genetics*. 172:1557-1566.
1519 10.1534/genetics.105.052563

1520 Osmani, S.A., D.B. Engle, J.H. Doonan, and N.R. Morris. 1988. Spindle formation and
1521 chromatin condensation in cells blocked in interphase by mutation of a negative
1522 cell cycle control gene. *Cell*. 52:241-251. 10.1016/0092-8674(88)90513-2.

1523 Pantazopoulou, A., and B.S. Glick. 2019. A Kinetic View of Membrane Traffic
1524 Pathways Can Transcend the Classical View of Golgi Compartments. *Frontiers*
1525 *in Cell and Developmental Biology*. 7:153.
1526 https://www.frontiersin.org/article/10.3389/fcell.2019.00153

1527 Pantazopoulou, A., and M.A. Peñalva. 2011. Characterization of *Aspergillus nidulans*
1528 RabC^{Rab6}. *Traffic*. 12:386-406. 10.1111/j.1600-0854.2011.01164.x

1529 Parlati, F., O. Varlamov, K. Paz, J.A. McNew, D. Hurtado, T.H. Sollner, and J.E.
1530 Rothman. 2002. Distinct SNARE complexes mediating membrane fusion in
1531 Golgi transport based on combinatorial specificity. *Proc Natl Acad Sci USA*.
1532 99:5424-5429. 10.1073/pnas.082100899

1533 Pelham, H.R. 1999. SNAREs and the secretory pathway-lessons from yeast.
1534 *Experimental Cell Research*. 247:1-8. https://doi.org/10.1006/excr.1998.4356

1535 Pelham, H.R. 2001. SNAREs and the specificity of membrane fusion. *Trends Cell Biol*.
1536 11:99-101.

1537 Peng, R., and D. Gallwitz. 2002. Sly1 protein bound to Golgi syntaxin Sed5p allows
1538 assembly and contributes to specificity of SNARE fusion complexes. *J Cell Biol*.
1539 157:645-655. 10.1083/jcb.200202006

1540 Peñalva, M.A. 2005. Tracing the endocytic pathway of *Aspergillus nidulans* with FM4-
1541 64. *Fungal Genet Biol*. 42:963-975. 10.1016/j.fgb.2005.09.004

1542 Peñalva, M.A., E. Moscoso-Romero, and M. Hernández-González. 2020. Tracking
1543 exocytosis of a GPI-anchored protein in *Aspergillus nidulans*. *Traffic*. 21:675-
1544 688. https://doi.org/10.1111/tra.12761

1545 Pinar, M., A. Alonso, V. de los Ríos, I. Bravo-Plaza, Á. de la Gándara, A. Galindo, E.
1546 Arias-Palomo, and M.Á. Peñalva. 2022. The type V myosin-containing complex
1547 HUM is a RAB11 effector powering movement of secretory vesicles. *iScience*.
1548 25. 10.1016/j.isci.2022.104514

1549 Pinar, M., E. Arias-Palomo, V. de los Ríos, H.N. Arst, Jr., and M.A. Peñalva. 2019.
1550 Characterization of *Aspergillus nidulans* TRAPPs uncovers unprecedented
1551 similarities with metazoans and reveals the modular assembly of TRAPPII.
1552 *PLoS Genetics*. 15:e1008557. https://doi.org/10.1371/journal.pgen.1008557

1553 Pinar, M., H.N. Arst, Jr., A. Pantazopoulou, V.G. Tagua, V. de los Ríos, J. Rodríguez-
1554 Salarichs, J.F. Díaz, and M.A. Peñalva. 2015. TRAPPII regulates exocytic Golgi
1555 exit by mediating nucleotide exchange on the Ypt31 orthologue RabE/RAB11.
1556 *Proc Natl Acad Sci USA*. 112:4346-4351. 10.1073/pnas.1419168112

1557 Pinar, M., A. Pantazopoulou, H.N. Arst, Jr., and M.A. Peñalva. 2013. Acute inactivation
1558 of the *Aspergillus nidulans* Golgi membrane fusion machinery: correlation of
1559 apical extension arrest and tip swelling with cisternal disorganization. *Mol*
1560 *Microbiol*. 89:228-248. 10.1111/mmi.12280

1561 Pinar, M., and M.A. Peñalva. 2017. *Aspergillus nidulan*s BapH is a RAB11 effector that
1562 connects membranes in the Spitzenkörper with basal autophagy. *Mol Microbiol*.
1563 106:452-468. 10.1111/mmi.13777

1564 Pinar, M., and M.A. Peñalva. 2020. *En bloc* TGN recruitment of *Aspergillus* TRAPPII
1565 reveals TRAPP maturation as unlikely to drive RAB1-to-RAB11 transition. *J Cell*
1566 *Sci*. 133:jcs241141. 10.1242/jcs.241141

1567 Pinar, M., and M.A. Peñalva. 2021. The fungal RABOME: RAB GTPases acting in the
1568 endocytic and exocytic pathways of Aspergillus nidulans (with excursions to
1569 other filamentous fungi). *Mol Microbiol*. 116:53-70.
1570 https://doi.org/10.1111/mmi.14716

1571 Ren, Y., C.K. Yip, A. Tripathi, D. Huie, P.D. Jeffrey, T. Walz, and F.M. Hughson. 2009.
1572 A structure-based mechanism for vesicle capture by the multisubunit tethering
1573 complex Dsl1. *Cell*. 139:1119-1129. 10.1016/j.cell.2009.11.002

1574 Rexach, M.F., M. Latterich, and R.W. Schekman. 1994. Characteristics of endoplasmic
1575 reticulum-derived transport vesicles. *J Cell Biol*. 126:1133-1148.
1576 10.1083/jcb.126.5.1133

1577 Riedel, F., A. Galindo, N. Muschalik, and S. Munro. 2017. The two TRAPP complexes
1578 of metazoans have distinct roles and act on different Rab GTPases. *J Cell Biol*.
1579 217:601-617. 10.1083/jcb.201705068

1580 Rizo, J., and T.C. Sudhof. 2012. The membrane fusion enigma: SNAREs,
1581 Sec1/Munc18 proteins, and their accomplices--guilty as charged? *Annu Rev*
1582 *Cell Dev Biol*. 28:279-308. 10.1146/annurev-cellbio-101011-155818

1583 Sapperstein, S.K., V.V. Lupashin, H.D. Schmitt, and M.G. Waters. 1996. Assembly of
1584 the ER to Golgi SNARE complex requires Uso1p. *J Cell Biol*. 132:755-767.
1585 http://www.ncbi.nlm.nih.gov/pubmed/8603910

1586 Sapperstein, S.K., D.M. Walter, A.R. Grosvenor, J.E. Heuser, and M.G. Waters. 1995.
1587 p115 is a general vesicular transport factor related to the yeast endoplasmic
1588 reticulum to Golgi transport factor Uso1p. *Proc Natl Acad Sci USA*. 92:522-526.
1589 10.1073/pnas.92.2.522

1590 Schuck, P. 2000. Size-distribution analysis of macromolecules by sedimentation
1591 velocity ultracentrifugation and lamm equation modeling. *Biophys J*. 78:1606-
1592 1619. 10.1016/S0006-3495(00)76713-0

1593 Seog, D.H., M. Kito, K. Yoda, and M. Yamasaki. 1994. Uso1 protein contains a coiled-
1594 coil rod region essential for protein transport from the ER to the Golgi apparatus
1595 in Saccharomyces cerevisiae. *J Biochem*. 116:1341-1345.
1596 10.1093/oxfordjournals.jbchem.a124685

1597 Shorter, J., M.B. Beard, J. Seemann, A.B. Dirac-Svejstrup, and G. Warren. 2002.
1598 Sequential tethering of Golgins and catalysis of SNAREpin assembly by the
1599 vesicle-tethering protein p115. *J Cell Biol*. 157:45-62. 10.1083/jcb.200112127

1600 Sogaard, M., K. Tani, R.R. Ye, S. Geromanos, P. Tempst, T. Kirchhausen, J.E.
1601 Rothman, and T. Sollner. 1994. A rab protein is required for the assembly of
1602 SNARE complexes in the docking of transport vesicles. *Cell*. 78:937-948.
1603 10.1016/0092-8674(94)90270-4

1604 Striegl, H., Y. Roske, D. Kummel, and U. Heinemann. 2009. Unusual armadillo fold in
1605 the human general vesicular transport factor p115. *PLoS ONE*. 4:e4656.
1606 10.1371/journal.pone.0004656

1607 Szewczyk, E., T. Nayak, C.E. Oakley, H. Edgerton, Y. Xiong, N. Taheri-Talesh, S.A.
1608 Osmani, and B.R. Oakley. 2006. Fusion PCR and gene targeting in *Aspergillus*
1609 *nidulans*. *Nat Protoc*. 1:3111-3120. 10.1038/nprot.2006.405

1610 Thomas, L.L., A.M.N. Joiner, and J.C. Fromme. 2018. The TRAPPIII complex activates
1611 the GTPase Ypt1 (Rab1) in the secretory pathway. *J Cell Biol*. 217:283-298.
1612 10.1083/jcb.201705214

1613 Thomas, L.L., S.A. van der Vegt, and J.C. Fromme. 2019. A Steric Gating Mechanism
1614 Dictates the Substrate Specificity of a Rab-GEF. *Dev Cell*. 48:100-114.e109.
1615 https://doi.org/10.1016/j.devcel.2018.11.013

1616 Tilburn, J., C. Scazzocchio, G.G. Taylor, J.H. Zabicky-Zissman, R.A. Lockington, and
1617 R.W. Davies. 1983. Transformation by integration in *Aspergillus nidulans.*
1618 *Gene*. 26:205-211. 10.1016/0378-1119(83)90191-9.

1619 Todd, R.B., M.A. Davis, and M.J. Hynes. 2007. Genetic manipulation of Aspergillus
1620 nidulans : meiotic progeny for genetic analysis and strain construction. *Nat*
1621 *Protoc*. 2:811-821. 10.1038/nprot.2007.113.

1622 Tsui, M.M., W.C. Tai, and D.K. Banfield. 2001. Selective formation of Sed5p-containing
1623 SNARE complexes is mediated by combinatorial binding interactions. *Mol Biol*
1624 *Cell*. 12:521-538. http://www.ncbi.nlm.nih.gov/pubmed/11251068

1625 Wang, T., R. Grabski, E. Sztul, and J.C. Hay. 2014. p115-SNARE Interactions: A
1626 Dynamic Cycle of p115 Binding Monomeric SNARE Motifs and Releasing
1627 Assembled Bundles. *Traffic*. 10.1111/tra.12242

1628 Weigel, A.V., C.L. Chang, G. Shtengel, C.S. Xu, D.P. Hoffman, M. Freeman, N. Iyer, J.
1629 Aaron, S. Khuon, J. Bogovic, W. Qiu, H.F. Hess, and J. Lippincott-Schwartz.
1630 2021. ER-to-Golgi protein delivery through an interwoven, tubular network
1631 extending from ER. *Cell*. 184:2412-2429 e2416. 10.1016/j.cell.2021.03.035

1632 Yamakawa, H., D.H. Seog, K. Yoda, M. Yamasaki, and T. Wakabayashi. 1996. Uso1
1633 protein is a dimer with two globular heads and a long coiled-coil tail. *Journal of*
1634 *Structural Biology*. 116:356-365. 10.1006/jsbi.1996.0053

1635 Yu, I.M., and F.M. Hughson. 2010. Tethering factors as organizers of intracellular
1636 vesicular traffic. *Annu Rev Cell Dev Biol*. 26:137-156.
1637 10.1146/annurev.cellbio.042308.113327

1638 Zhang, Y., and F.M. Hughson. 2021. Chaperoning SNARE Folding and Assembly.
1639 *Annual Review of Biochemistry*. 90:581-603. 10.1146/annurev-biochem-
1640 081820-103615

1641 Zhang, Y., and J. Yang. 2020. Securing SNAREs for assembly. *J Biol Chem*.
1642 295:10136-10137. 10.1074/jbc.H120.014815

1643

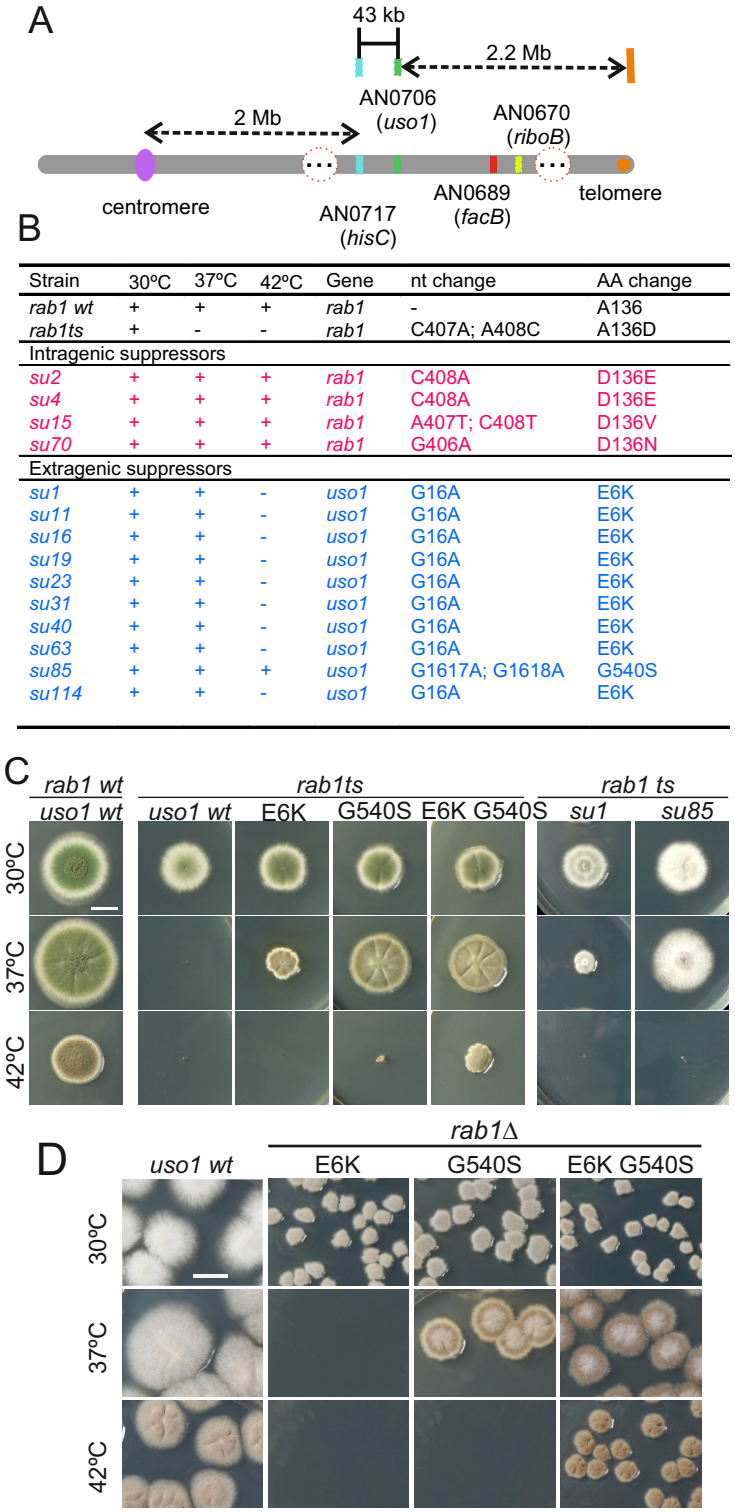

Strain	30ºC	37ºC	42ºC	Gene	nt change	AA change
rab1 wt	+	+	+	*rab1*	-	A136
rab1ts	+	-	-	*rab1*	C407A; A408C	A136D
Intragenic suppressors						
su2	+	+	+	*rab1*	C408A	D136E
su4	+	+	+	*rab1*	C408A	D136E
su15	+	+	+	*rab1*	A407T; C408T	D136V
su70	+	+	+	*rab1*	G406A	D136N
Extragenic suppressors						
su1	+	+	-	*uso1*	G16A	E6K
su11	+	+	-	*uso1*	G16A	E6K
su16	+	+	-	*uso1*	G16A	E6K
su19	+	+	-	*uso1*	G16A	E6K
su23	+	+	-	*uso1*	G16A	E6K
su31	+	+	-	*uso1*	G16A	E6K
su40	+	+	-	*uso1*	G16A	E6K
su63	+	+	-	*uso1*	G16A	E6K
su85	+	+	+	*uso1*	G1617A; G1618A	G540S
su114	+	+	-	*uso1*	G16A	E6K

Figure 1. Characterization of mutations bypassing the essential role of RAB1
(A). Genetic map in the region surrounding *uso1* with genetic markers used as landmarks for mapping.B). Molecular identification of the nucleotide changes in *suArab1*^{ts} strains
(C) and (D): growth tests showing *rab1*^{ts}- and *rab1*Δ-rescuing phenotypes, respectively, of individual mutations, and synthetic positive interaction between E6K and G540S. Strains produce either green or white conidiospores (conidiospore colors are used as genetic markers). In (C), strains were point-inoculated. In (D) conidiospores were spread on agar plates to give individual colonies.

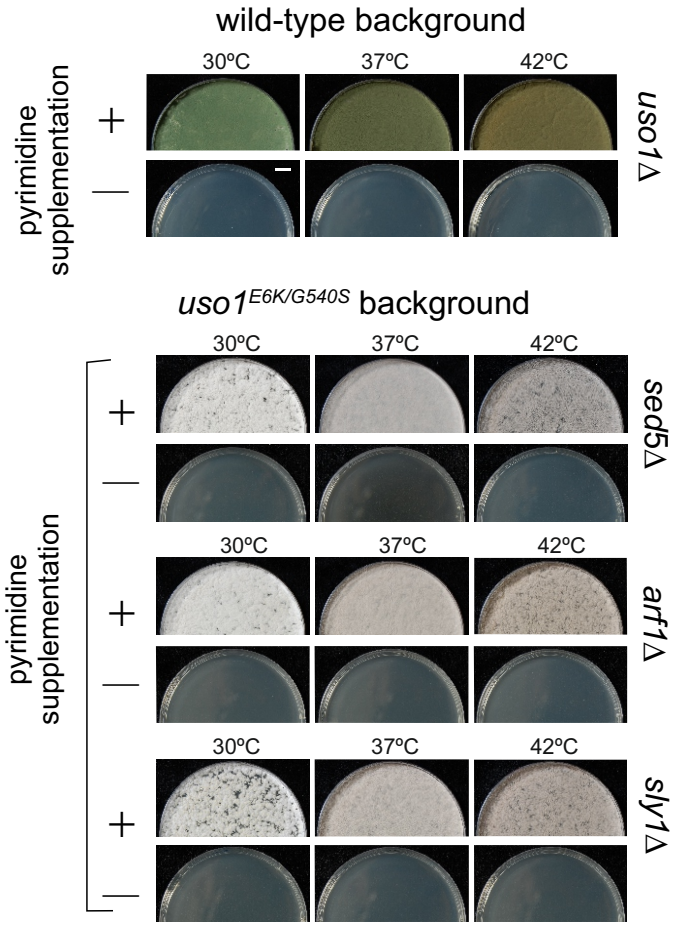

Figure 1—figure supplement 1: E6K/G540S do not rescue lethality resulting from *arf1*Δ, *sly1*Δ or *sed5*Δ.

Top, *uso1* is an essential gene. Singly-nucleated conidiospores derived from a heterokaryotic strain in which one class of nuclei carries a deficient *pyrG* uracil biosynthetic gene whereas the second class contains a *uso1*Δ allele tagged with functional *pyrG* were unable to grow on medium lacking pyrimidines at any of the tested temperatures. Bottom: Similar experiments showing that unlike *rab1*Δ strains, strains carrying lethal *arf1*Δ ,*sly1*Δ and *sed5*Δ alleles cannot be rescued by *uso1*$^{E6K/G540S}$. Top panel, strains with green conidiospores; bottom, strains with white conidiospores.

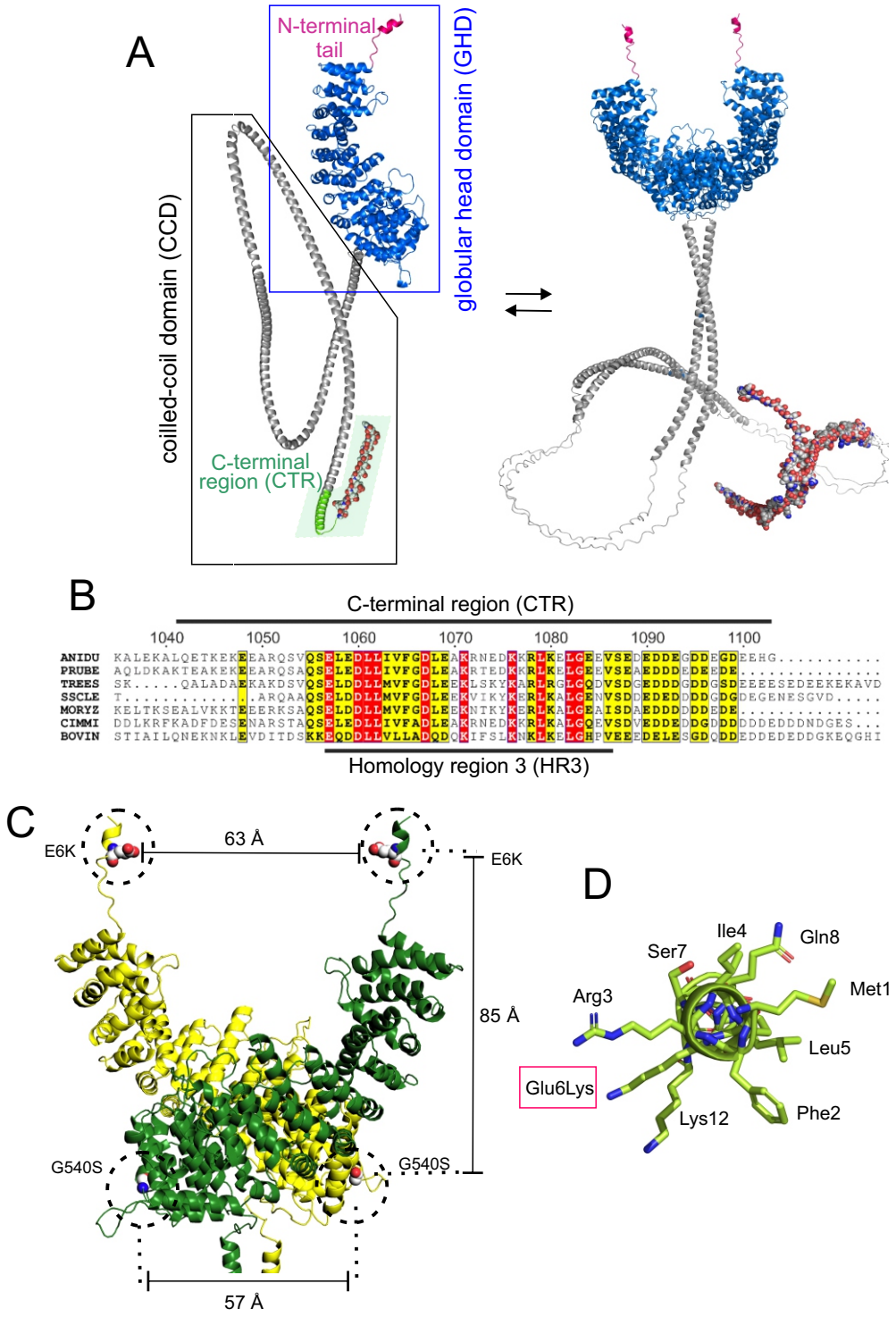

Figure 2: Localization of the amino acid substitutions within the Uso1 AlphaFold2 structure
(A). AlphaFold2 cartoon representations of *A. nidulans* Uso1 in monomeric and dimeric forms. Red, N-terminal tail; marine blue, globular head domain; gray, coiled-coil; green, limit of the CTR. The rest of the CTR is shown as surface representation.
(B). Amino acid alignment of fungal sequences with mammalian p115 showing strong conservation within the CTR: ANIDU, *Aspergillus nidulans*; PRUBE, *Penicillium rubens*; TREES, *Thrichoderma ressei;* SSCLE, *Sclerotinia scleriotorum*; MORYZ, *Magnaporthe oryzae*; CIMM, *Coccidioides immitis*; BOVIN, *Bos taurus*.
©. Position of the Gly6Lys and Gly540Ser substitutions. Only the GHD of dimeric full-length Uso1 are shown. The two different chains are colored in green and yellow, respectively. Distances between mutated residues are displayed in armstrongs.
(D). The N-terminal amphipathic α–helix affected by the Glu6Lys substitution.

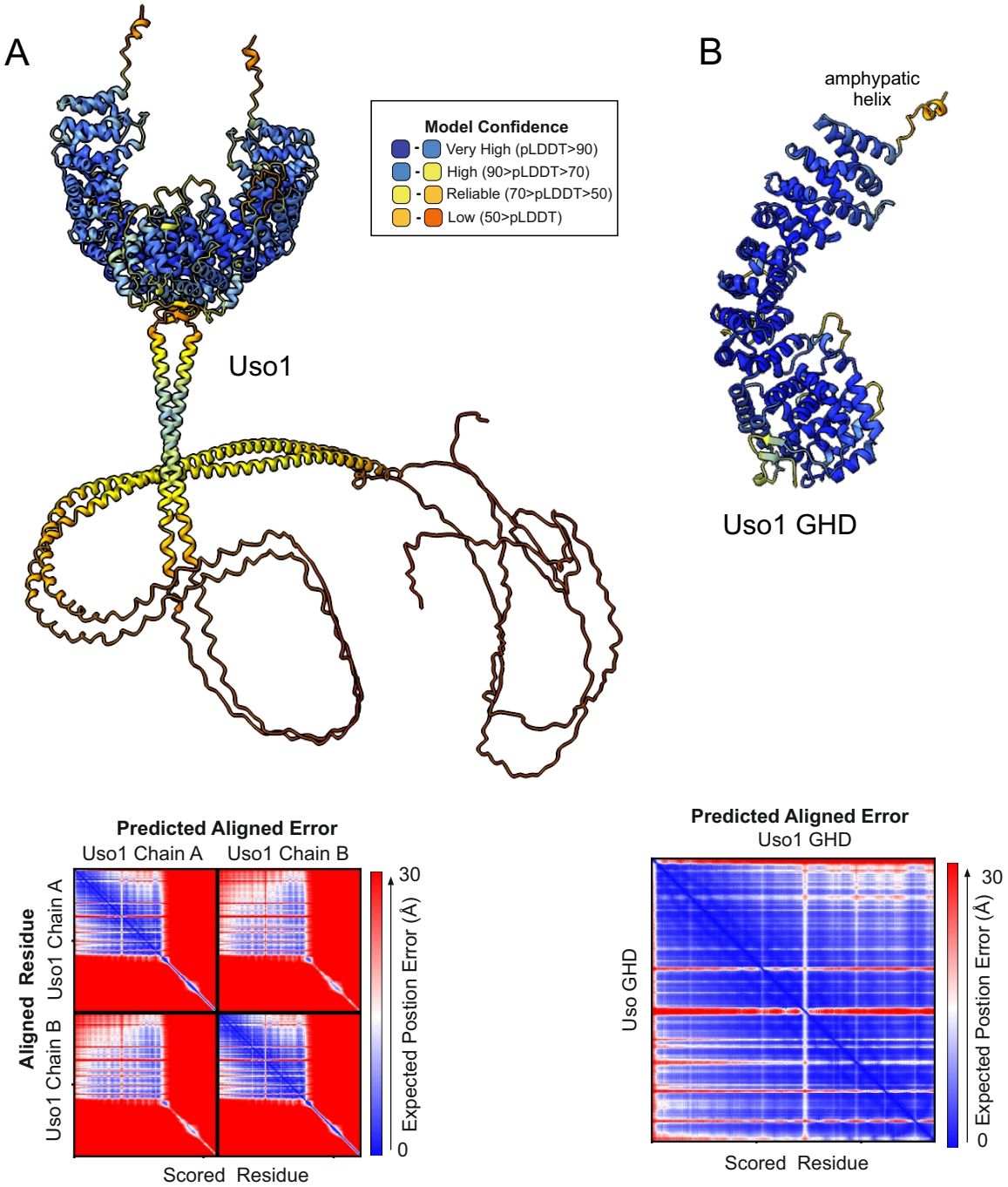

Figure 2— figure supplement 1. AlphaFold2 predictions of Uso1
Ribbon representation of AlphaFold 2-predicted structures of full-length Uso1 (A) and Uso1 GHD (B), color-coded by pLDDT values. Graphs at the bottom are the corresponding plots of predicted aligned error of the residues (PAE).

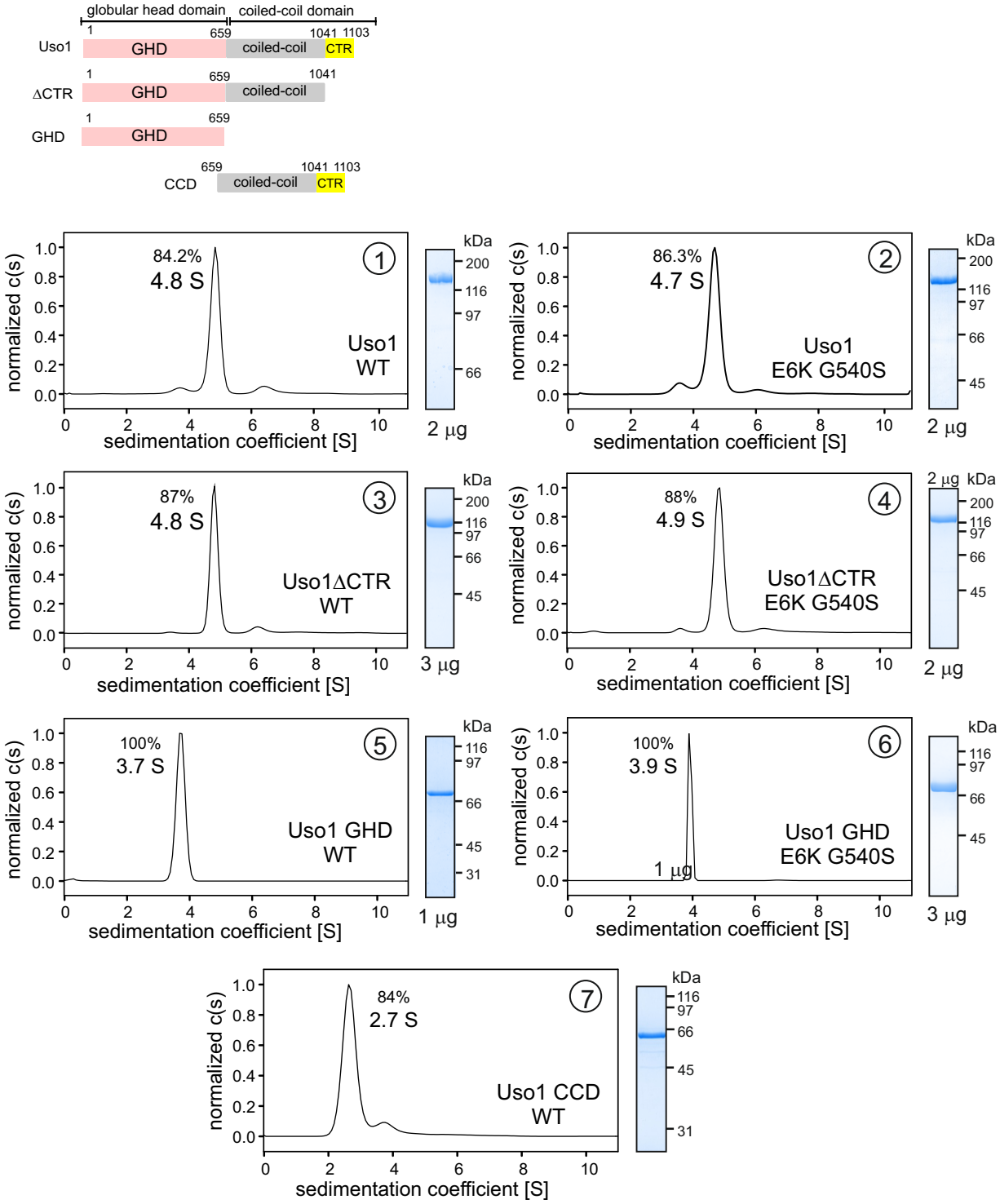

Figure 3: Determining molecular masses and oligomerization status of the different Uso1 constructs by velocity sedimentation analysis

The different panels display the sedimentation profiles of the protein being analyzed, with % of the main species, scheme of the different constructs and their limits and pictures of Coomassie stained-gels showing the purity of the protein preparations. The table below depicts biophysical parameters of the constructs used to obtain relative molecular masses. s_{exp} is the experimentally determined Svedberg coefficient; D_{exp}, translational diffusion coefficient of the main species; *Mr*, molecular mass deduced from Svedberg equation; M_1predicted molecular mass of the monomer; $n = (M_r/M_1)$

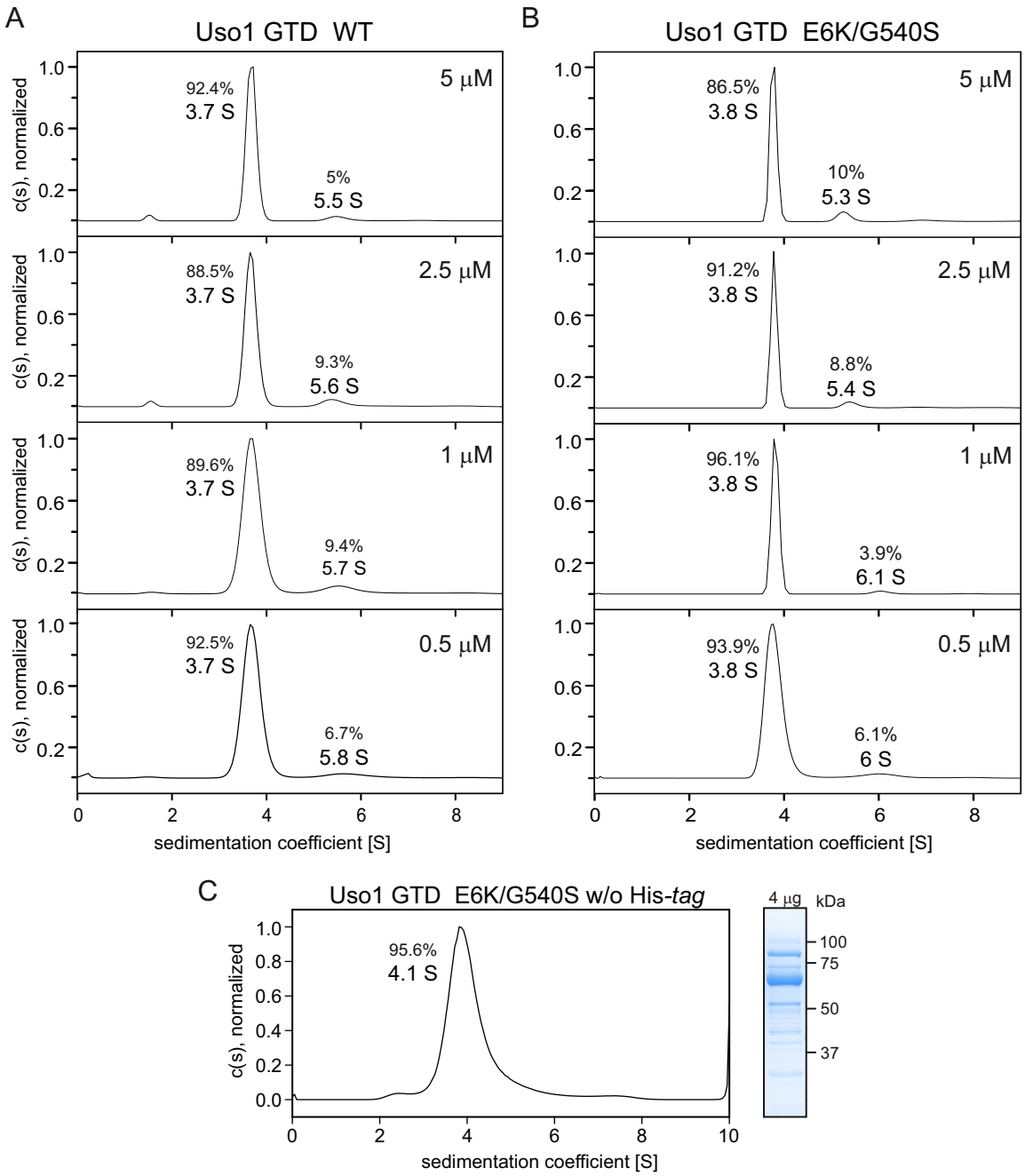

Figure 3—figure supplement 1: GHD is a monomer across a range of concentrations (A) and (B). Sedimentation velocity experiments with wild-type and E6K/G540S mutant GHD, respectively, showing that they behave as monomers at concentrations up to 5 μM.(C). Sedimentation velocity profile of E6K/G540S mutant GHD lacking the His-tag, showing that the presence of the latter does not interfere with oligomerization, and a picture of a Coomassie stained gel showing the purity of the protein preparation on the right.

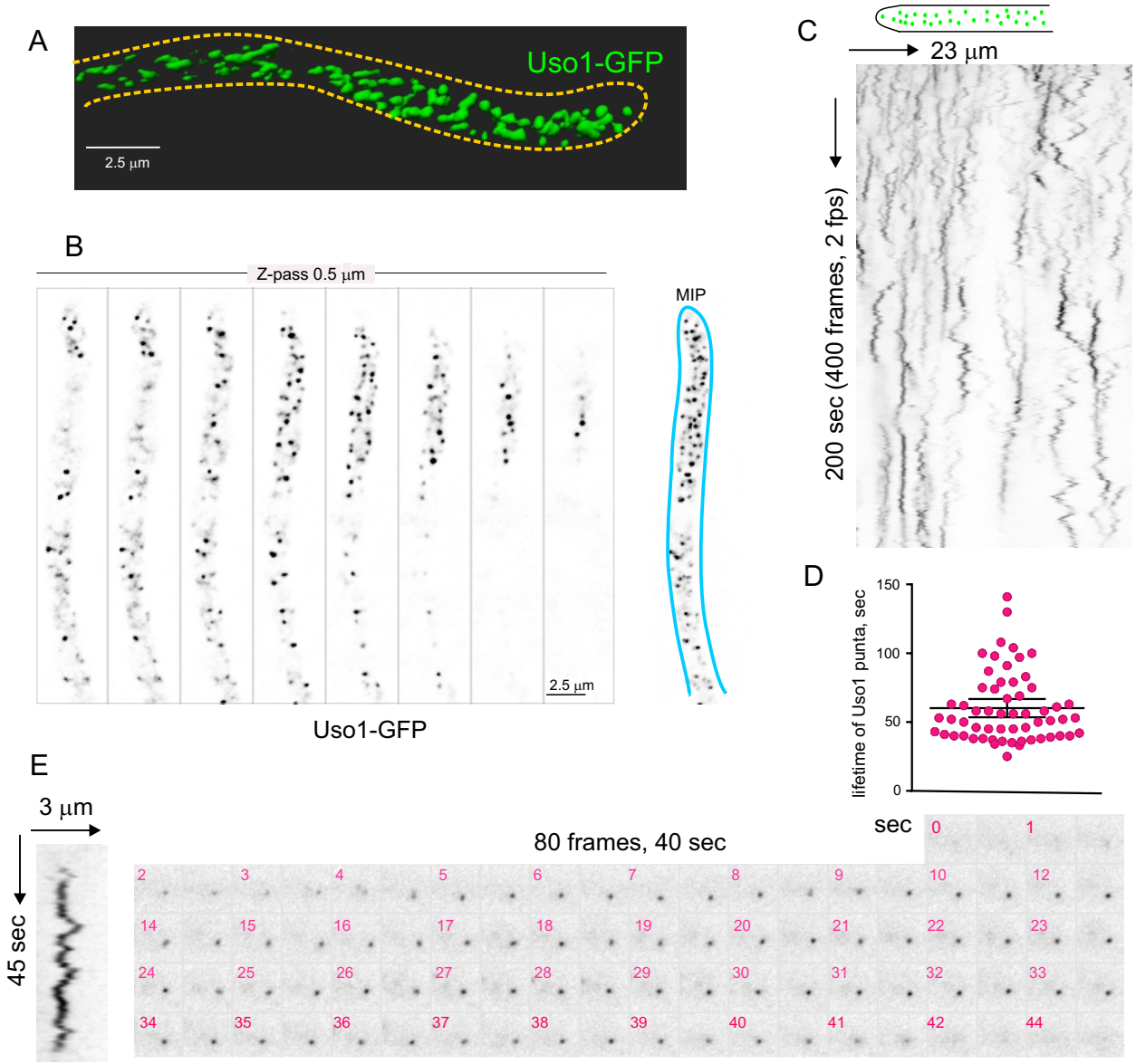

Figure 4: Subcellular localization of Uso1
(A). Uso1-GFP localizing to punctate cytoplasmic structures, 3D shaded by software.
(B). Sections of a deconvolved Z-stack and its corresponding MIP. Uso1-GFP in inverted greyscale for clarity
(C). Kymograph showing the transient recruitment of Uso1 to punctate cytoplasmic structures.
(D). Average time of residence of Uso1 in these structures. Error bars, 95% CI.
(E). Example of one such structures visualized with a kymograph and with the corresponding movie frames (Movie 4).

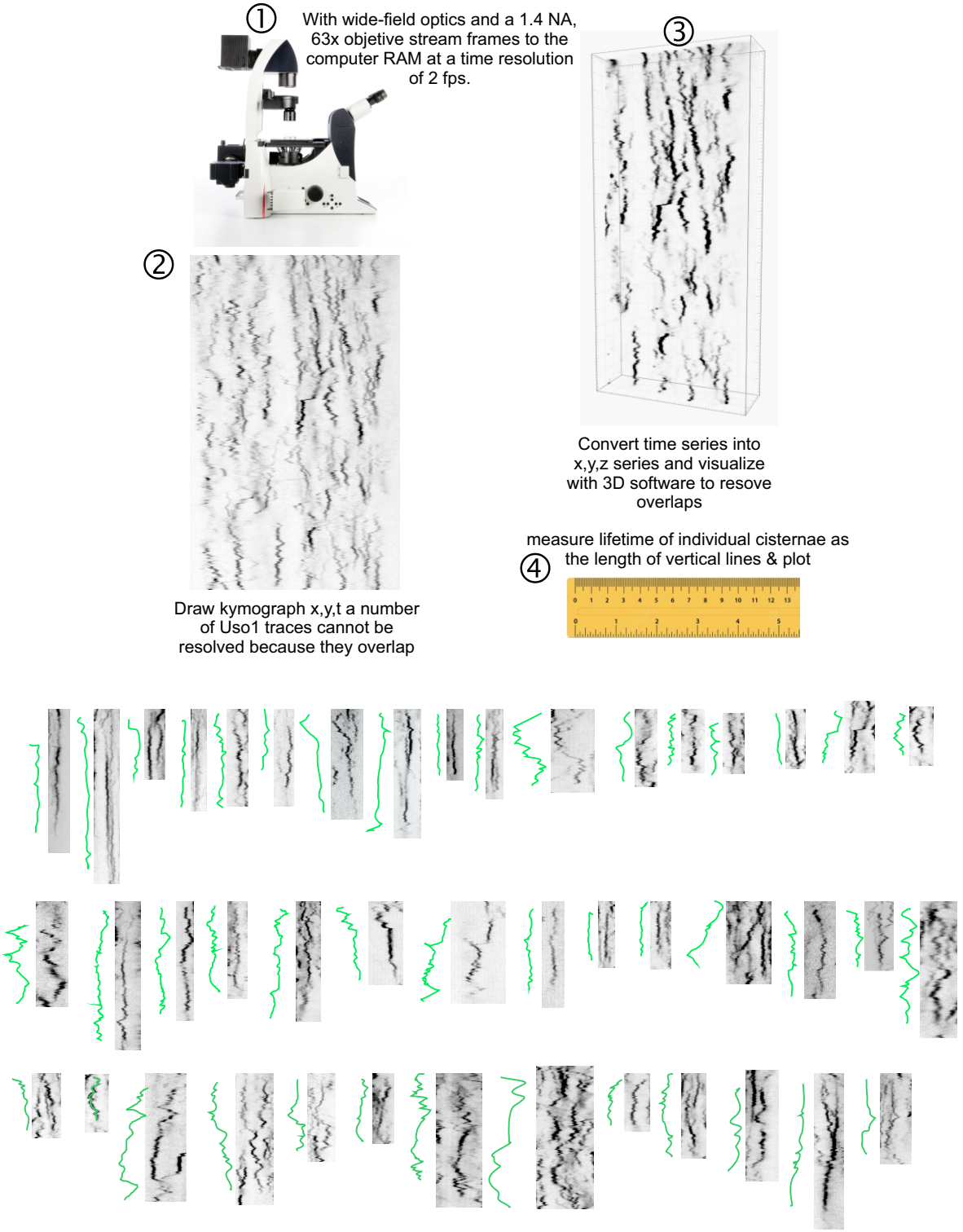

Figure 4—figure supplement 1: Methodology for tracking the half-life of Uso1-GFP on punctate structures.

1) 3D movies were acquired by streaming pictures to the computer RAM at 2 fps. Appropriate reduction of excitation light intensity permitted acquisition of 400 frames without apparent phototoxicity.

2) The behavior of punctate structures over time was represented in kymographs, in which vertical lines represent the time of residence of Uso1 on membranes.

3). As vertical lines frequently overlapped, jeopardizing the quality of this analysis, we imported the time series into a 3D viewer as if they were (x, y, z) series. Rotation across the different axes facilitated unambiguous tracking of the trajectories across time.

4) The length of the trajectories was measured and converted to time units. Bottom graphs display examples of time trajectories.

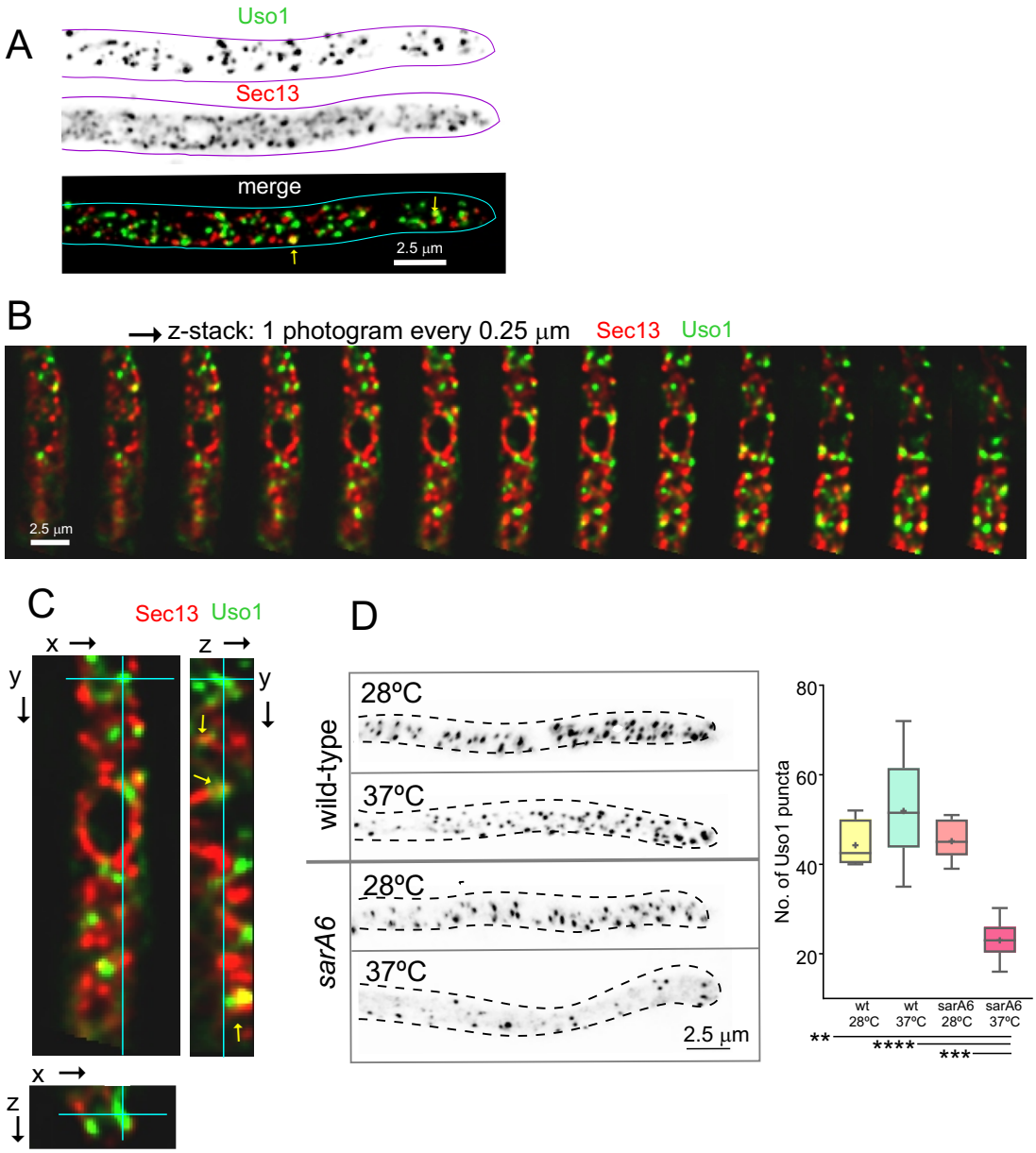

Figure 5: Uso1 puncta do not colocalize with ERESs
(A). Low extent co-localization of Sec13 ERES and Uso1 structures. Z-stacks for the two channels were acquired simultaneously, deconvolved and represented as MIPs. Two rare examples of colocalization are arrowed.
(B). Photograms of a dual channel Z-stack with a Sec13-labeled nuclear envelope focused in the middle plane, illustrating that while some puncta show colocalization, the red Sec13 signal and the green Uso1 signal do not usually overlap.
(C). A MIP of the same z-stack showing orthogonal views with some overlapping puncta (arrows).
(D). A *ts* mutation in the *sarA* gene encoding the SarA^{Sar1} GTPase governing ER exit markedly reduces the number of Uso1-GFP puncta upon shifting cells to restrictive conditions. Box-and-whisker plots: Statistical comparison was made using one-way ANOVA with Dunn's test for multiple comparisons. Whiskers are in Tukey's style: Only significant differences were indicated, using asterisks.

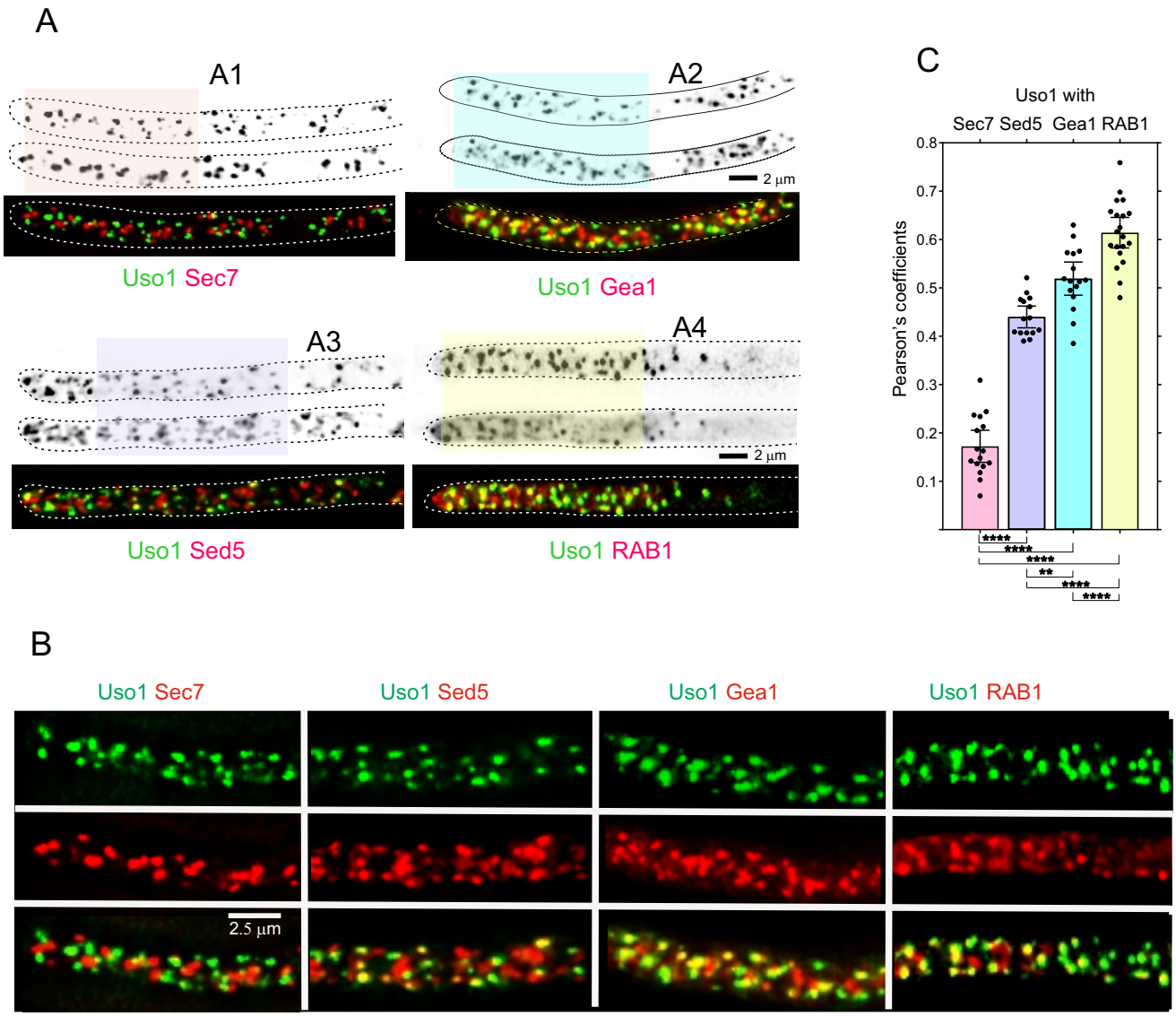

Figure 6: Uso1 localizes to RAB1-containing Golgi cisternae
(A). Tip cells showing Uso1 colocalization with the indicated subcellular markers. Images are MIPs of deconvolved Z-stacks.
(B). Magnified images of the color-coded shaded regions of the cells shown in A.
©. Pearson's coefficients of the different combinations

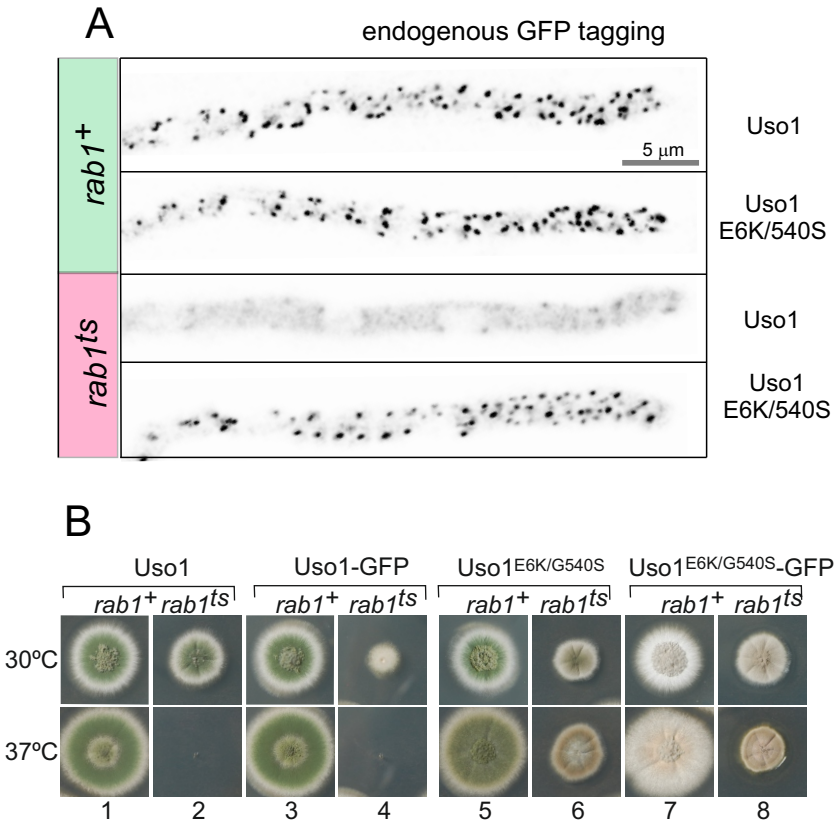

Figure 7: Uso1 localization to punctate structures is dependent on RAB1

(A). Complete de-localization of Uso1-GFP to the cytosol by *rab1ts* and relocalization by E6K/G540S.

(B). Uso1-GFP and *rab1ts* show a synthetic negative interaction that is rescued by the E6K/G540S double substitution. Strains in lanes 7 and 8 carry the *wA2* mutation resulting in white conidiospores.

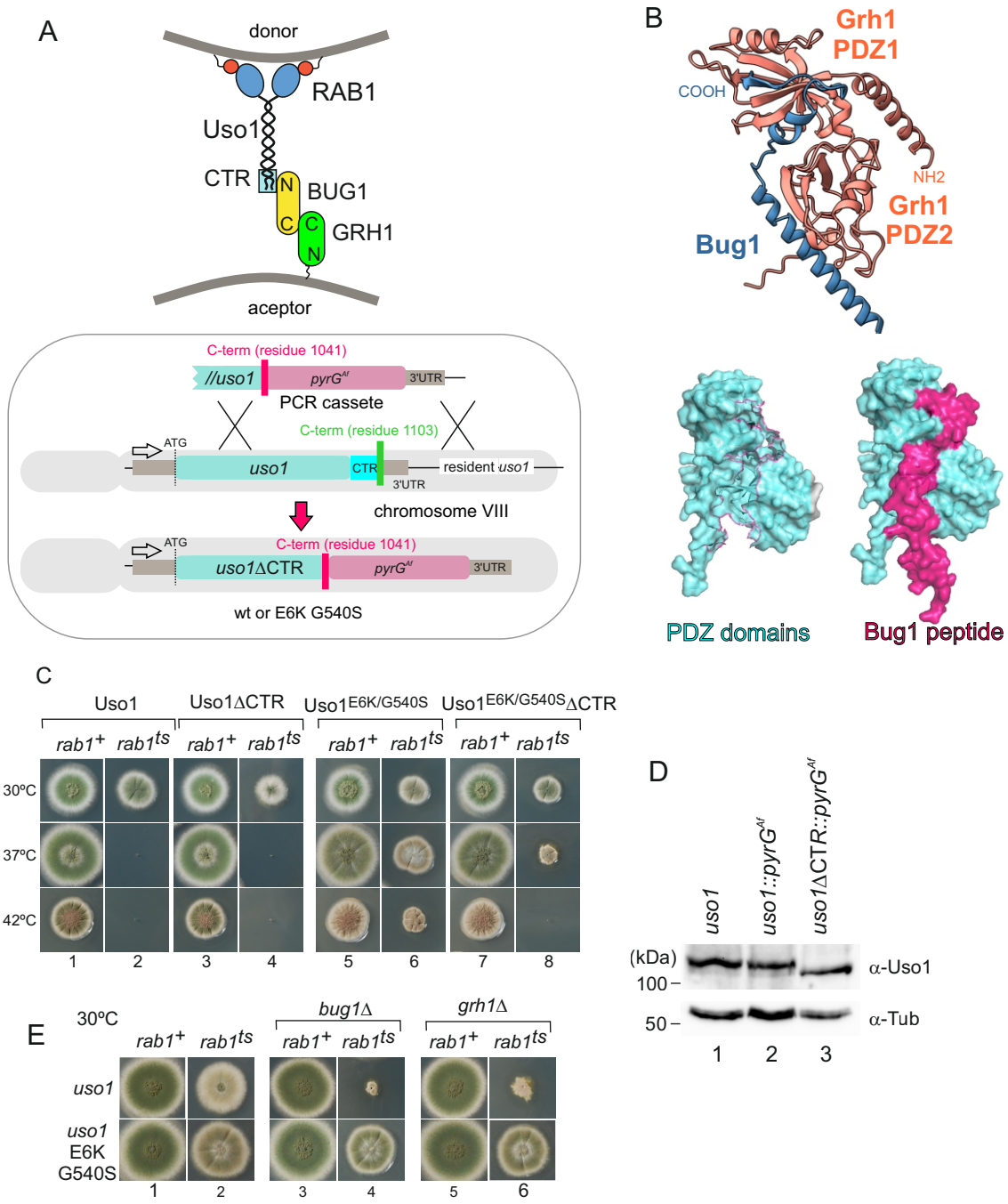

Figure 8. Genetic evidence showing that the CTR region of Uso1 contributes to its recruitment to membranes.
(A). Top, scheme of the predicted interactions. Bottom, engineering a gene-replaced allele lacking the CTR domain by homologous recombination.
(B). The Bug1 C-terminal residues fit into the groove formed between the two Grh1 PDZ domains and into the pocket of the N-terminal PDZ domain (PDZ1).
(C). A gene-replaced *uso1ΔCTR* allele encoding a protein truncated for the CTR domain shows a synthetic negative interaction with *rab1ts.*
(D). Western blot analysis. Removal of the CTR does not result in Uso1 instability.
(E). *bug1Δ* and *grh1Δ* show a synthetic negative interaction with *rab1ts* that is rescued by the double E6K/G540S substitution in Uso1

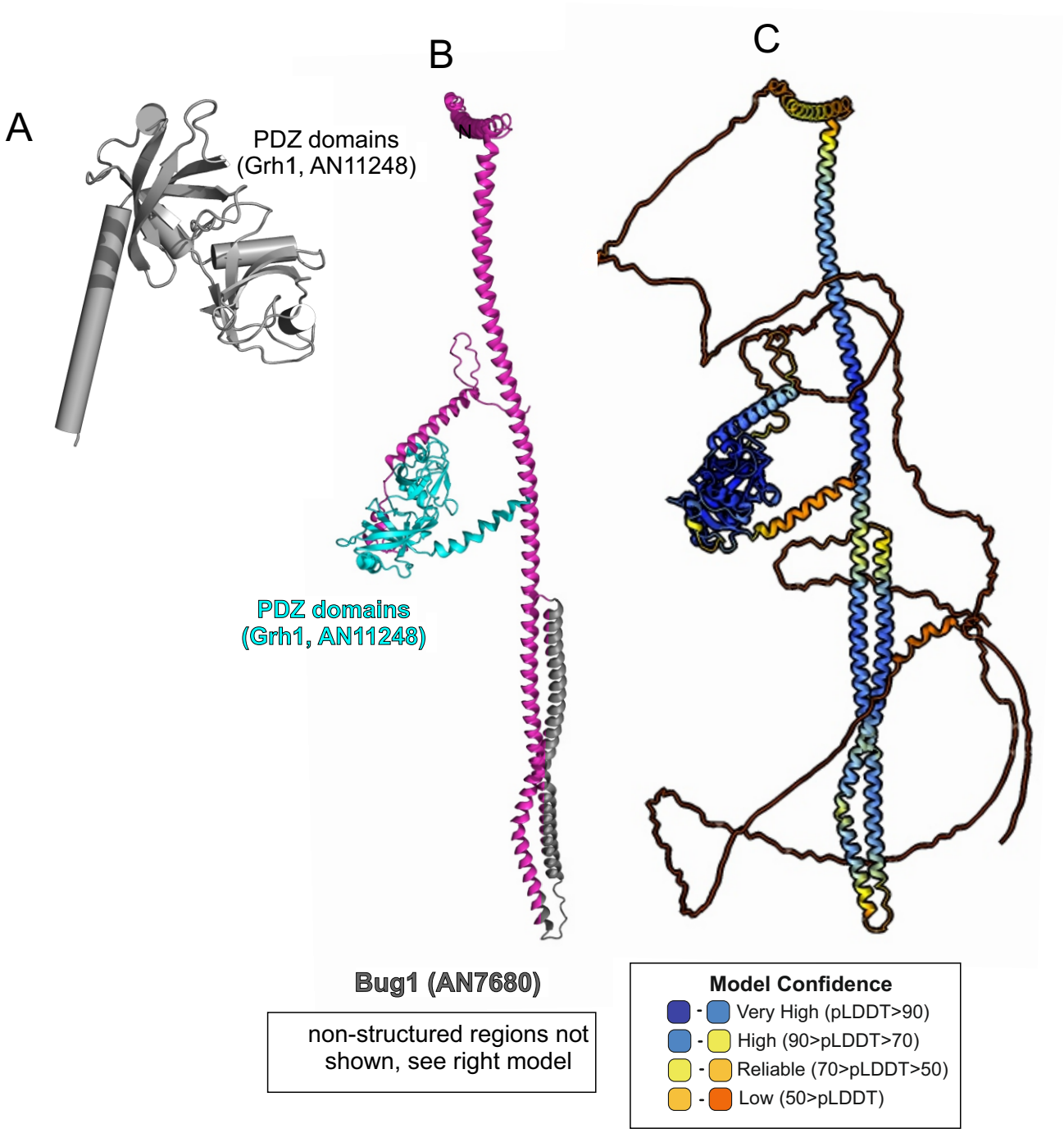

Figure 8 —figure supplement 1: AlphaFold2 modelling of Grh1-Bug1.
(A). Cartoon, with alpha-helices shown as cylinders, of the nearly N-terminal PDZ domains of Grh1
(B). AlphaFold 2 prediction of a 1:1 Grh1-Bug1 complex, trimmed of disordered regions
©. complete AlphaFold2 model of Grh1-Bug1 with color-coded model confidence values.

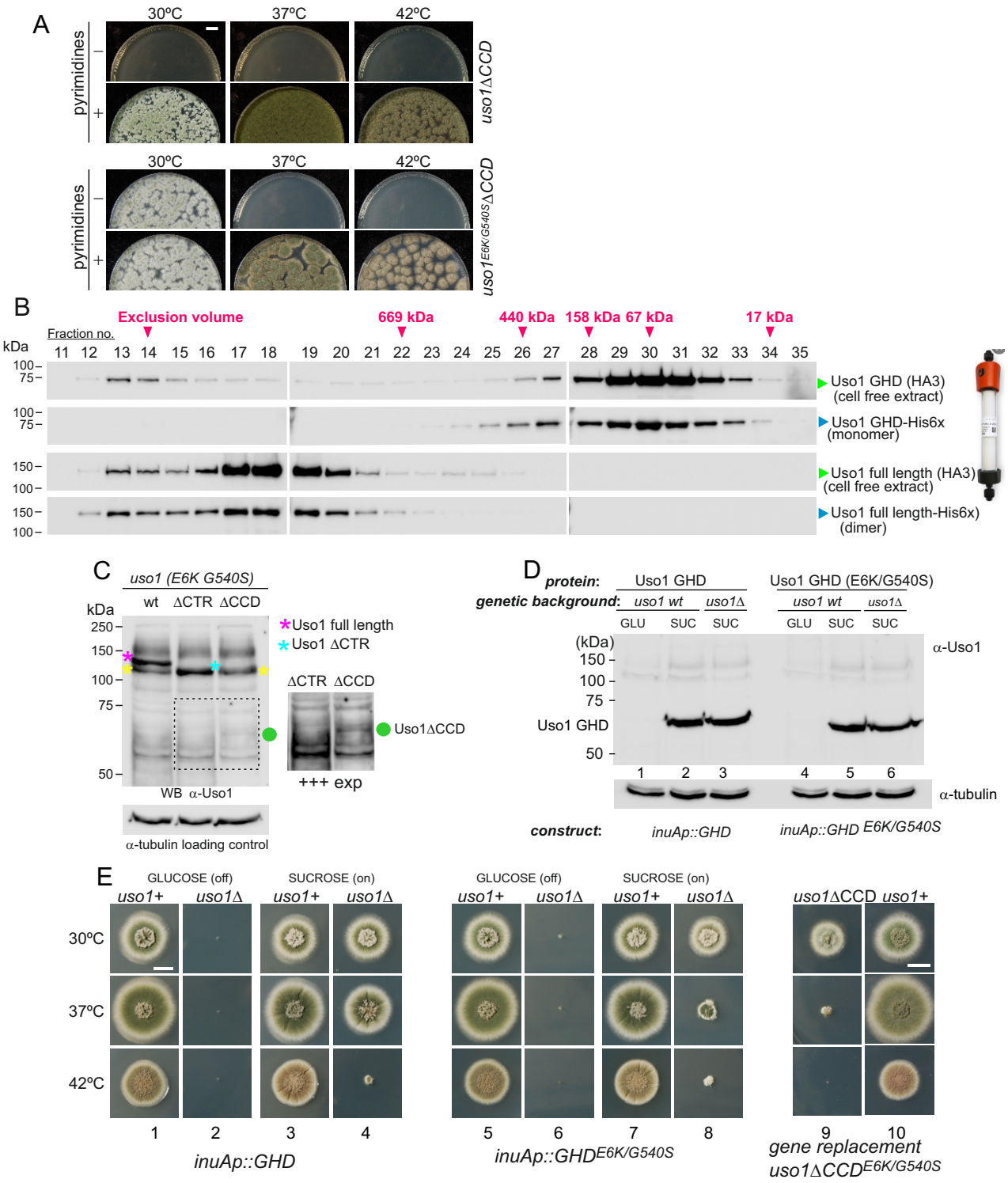

Figure 9: The GHD of Uso1 is sufficient to support cell viability
(A). Gene-replaced *uso1*^{GHD} allele carrying the double E6K/G540S substitution is sufficient to rescue viability at 30°C, but not at higher temperatures. (B). The Uso1 GHD is a monomer in vivo. Fractions collected from Superose columns loaded with the indicated protein extracts and reference His-tagged proteins were collected and analyzed by western blotting with α–HA and α–His antibodies. (C) Truncating Uso1 after the GHD results in markedly reduced protein levels, as determined by α-Uso1 GHD western blotting. The band (yellow asterisks) moving slower than Uso1 (magenta asterisk) and at nearly the same position of Uso1 ΔCTR (blue asterisk) represents cross-reacting contaminants unrelated to Uso1. The right panel shows a longer exposure for the indicated region, to reveal the faint GHD band (green dot). (D). Overexpression of Uso1, wild-type and E6K/G540S mutant, under the control of the *inuA* promoter, which is turned off on glucose and induced on sucrose. Western blots reacted with α–Uso1 GHD antiserum. (E). Overexpressed GHD, be it E6K/G540S or wild-type, as the only source of Uso1 supports viability.

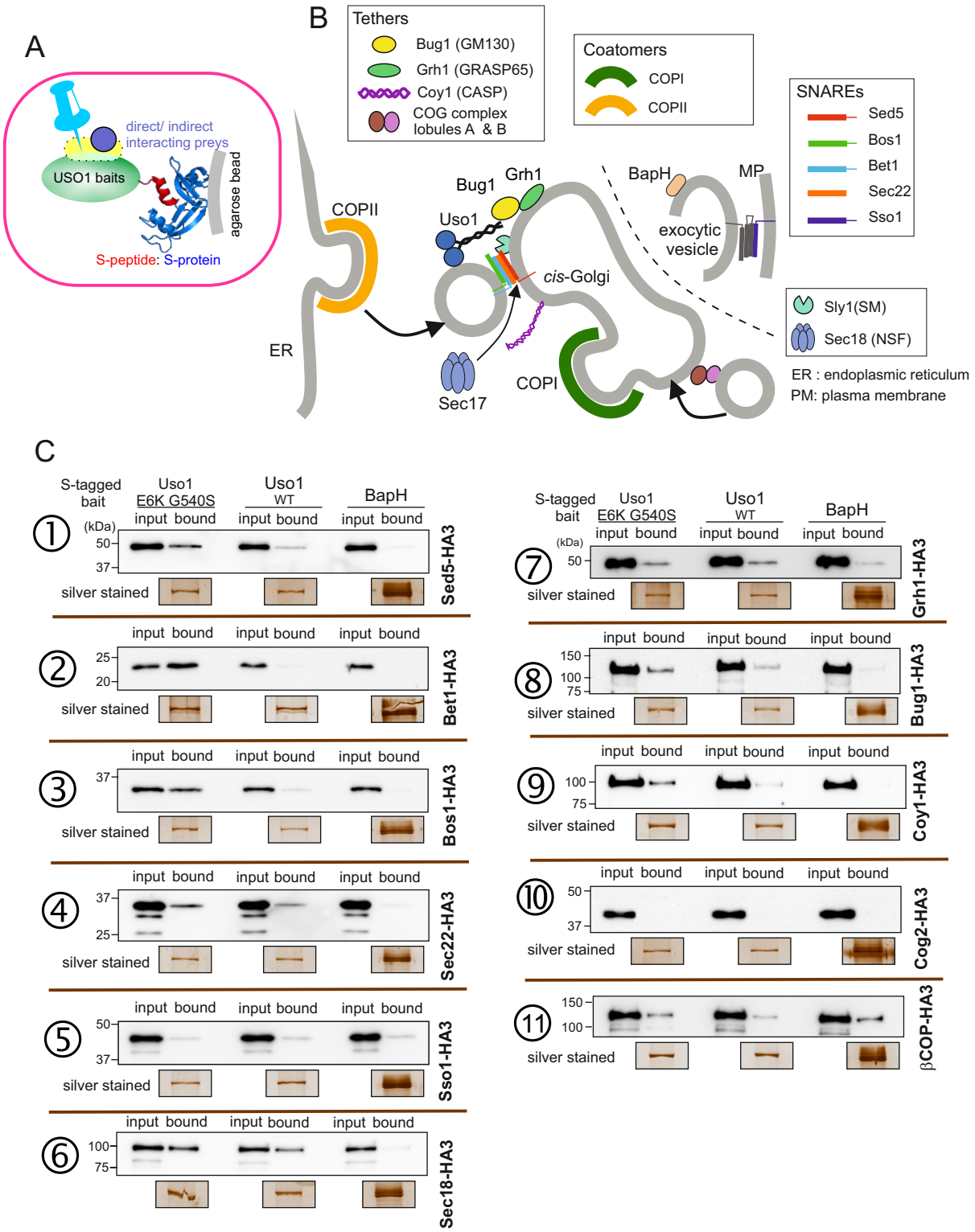

Figure 10: Screening the preferential association of proteins acting in the ER/Golgi interface with E6K/G540S Uso1.
(A). S-tagged baits (Uso1, wt and E6K/G540S, and the unrelated protein BapH), expressed after gene replacement, were captured with their associated polypeptides on S-protein agarose beads. Candidate associates, also expressed after gene replacement, were tagged with HA3. (B). Schematic depiction of the proteins listed in these experiments showing their sites of action.(C). Anti-HA3 western blot analysis of the indicated S-bait and HA3-prey combinations. Equal loading of Uso1 proteins was confirmed by silver staining of precipitates. Note that BapH, chosen as negative control, is expressed at much higher levels than Uso1 proteins. Each panel is a representative experiment of three experimental replicates.

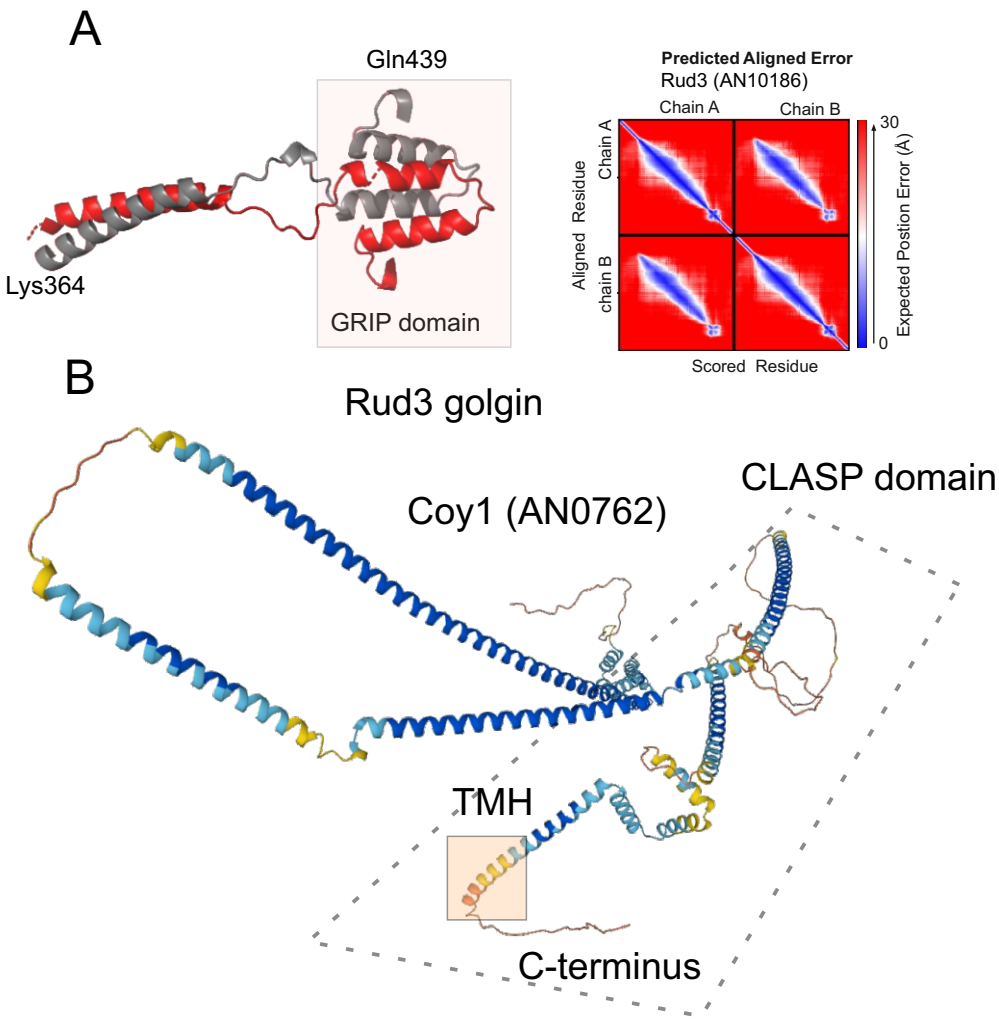

Figure 10—figure supplement 1.
/A) AlphaFold2 model, with PAE plot, of the GRIP domain of *A. nidulans* RUD3, predicted to be a dimer.
(B) AlphaFold2 model of Coy1, calculated as a monomer. TMH is the nearly C-terminal transmembrane helix that contributes to its recruitment to membranes

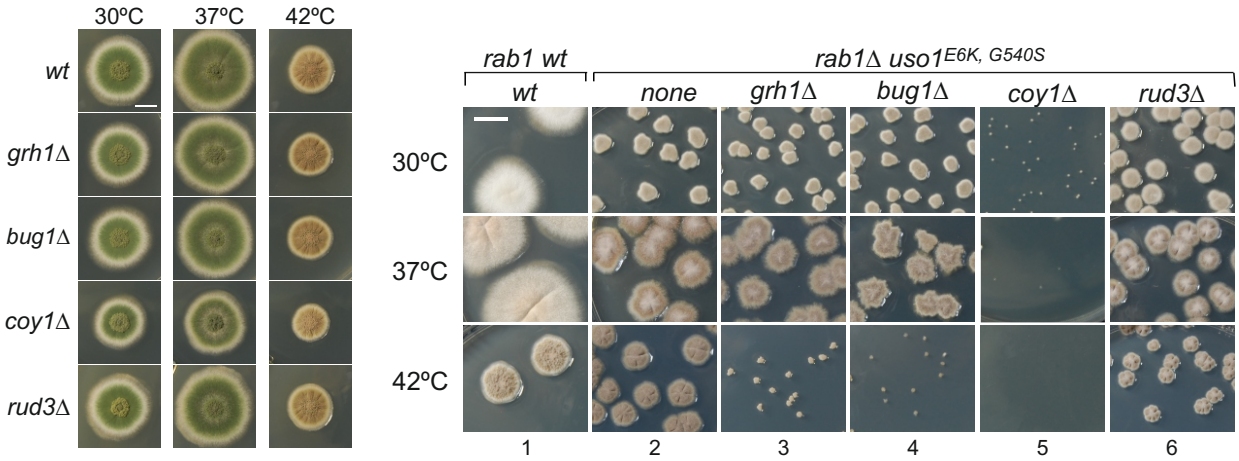

Figure 10—figure supplement 2: Growth phenotypes of null mutants of genes encoding golgins.
(A). Ablation of individual golgins Bug1/Grh1 and Rud3 does not result in detectable growth defects. *coy1*Δ strains have a subtle growth phenotype.
(B). Negative effects of *grh1*Δ*, bug1*Δ*, coy1*Δ and *rud3*Δ on the ability of *uso1*$^{E6K/G540S}$ to rescue *rab1*Δ*.* Note that *coy1*Δ and *rab1*Δ *uso1*$^{E6K/G540S}$ are synthetically lethal. For convenience, this set of strains carried a *wA1* mutation resulting in white conidiospores, as opposed to the wild-type green color.

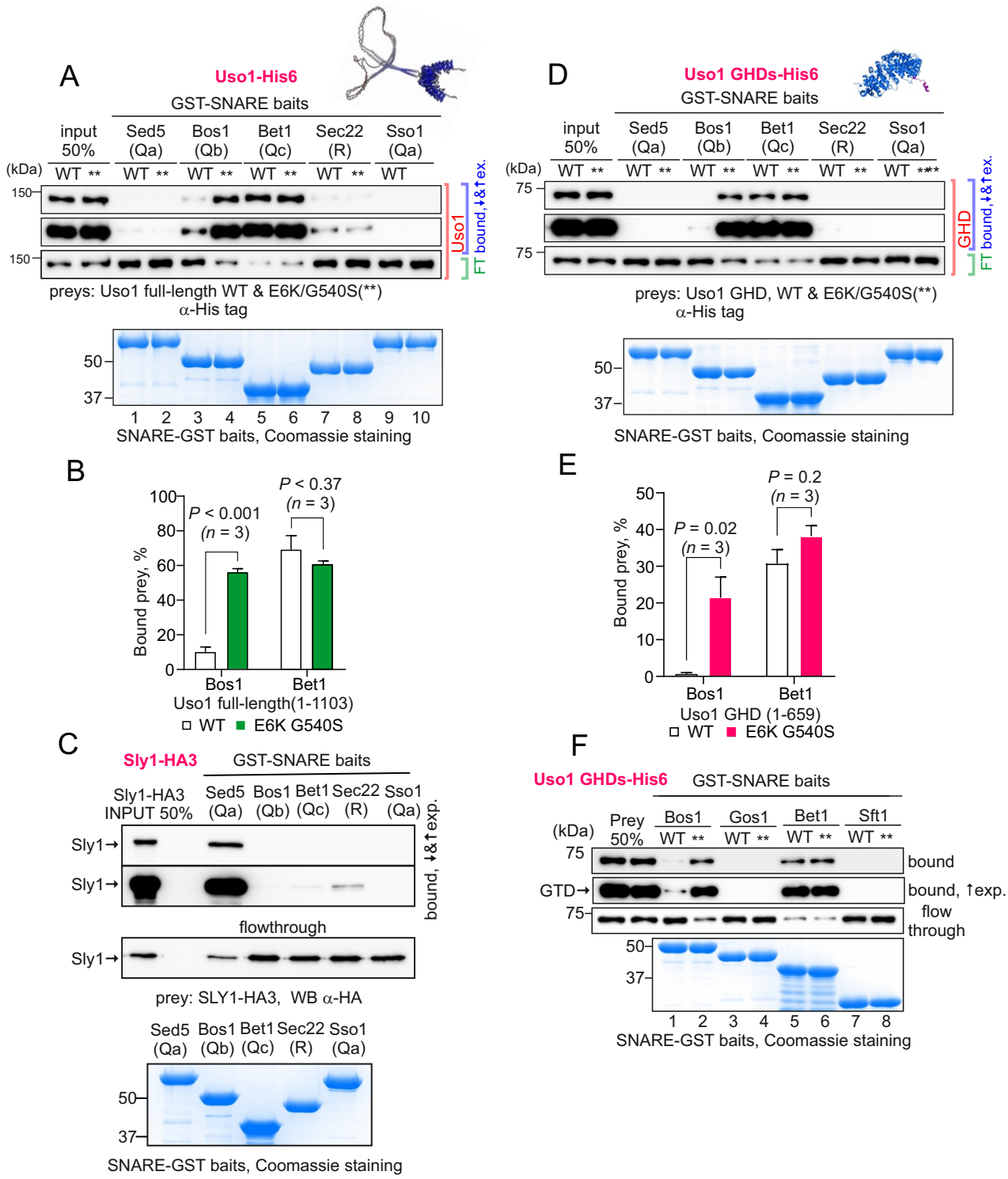

Figure 11: The Uso1 GHD interacts directly with Bos1 and Bet1 SNAREs acting in the ER/Golgi interface

(A). Purified fusion proteins in which the cytosolic domains of the indicated SNAREs have been fused to GST were used in pulldown experiments with His-tagged, purified wild-type and E6K/G540S Uso1. The plasma membrane Qa syntaxin Sso1 was used as negative control. Pulled-down material was analyzed by anti-His western blotting. (B)**.** Quantitation of the above experiment; significance was determined by unpaired *t*-student tests. Error bars represent S.E.M. (C). As in A, but using in vitro synthesized, HA3-tagged Sly1 as prey. Samples were analyzed by anti-HA western blotting. (D). As in A, but using wild-type and mutant GHD as preys, rather than full-length Uso1. (E). Quantitation of the experiment in D. **(F)**. GST pull-down experiment comparing the ability of the GHD to interact with the early Golgi Qb and Qc SNAREs (Bos1 and Bet1), with that of their medial Golgi counterparts (Qb Gos1 and Qc Sft1).

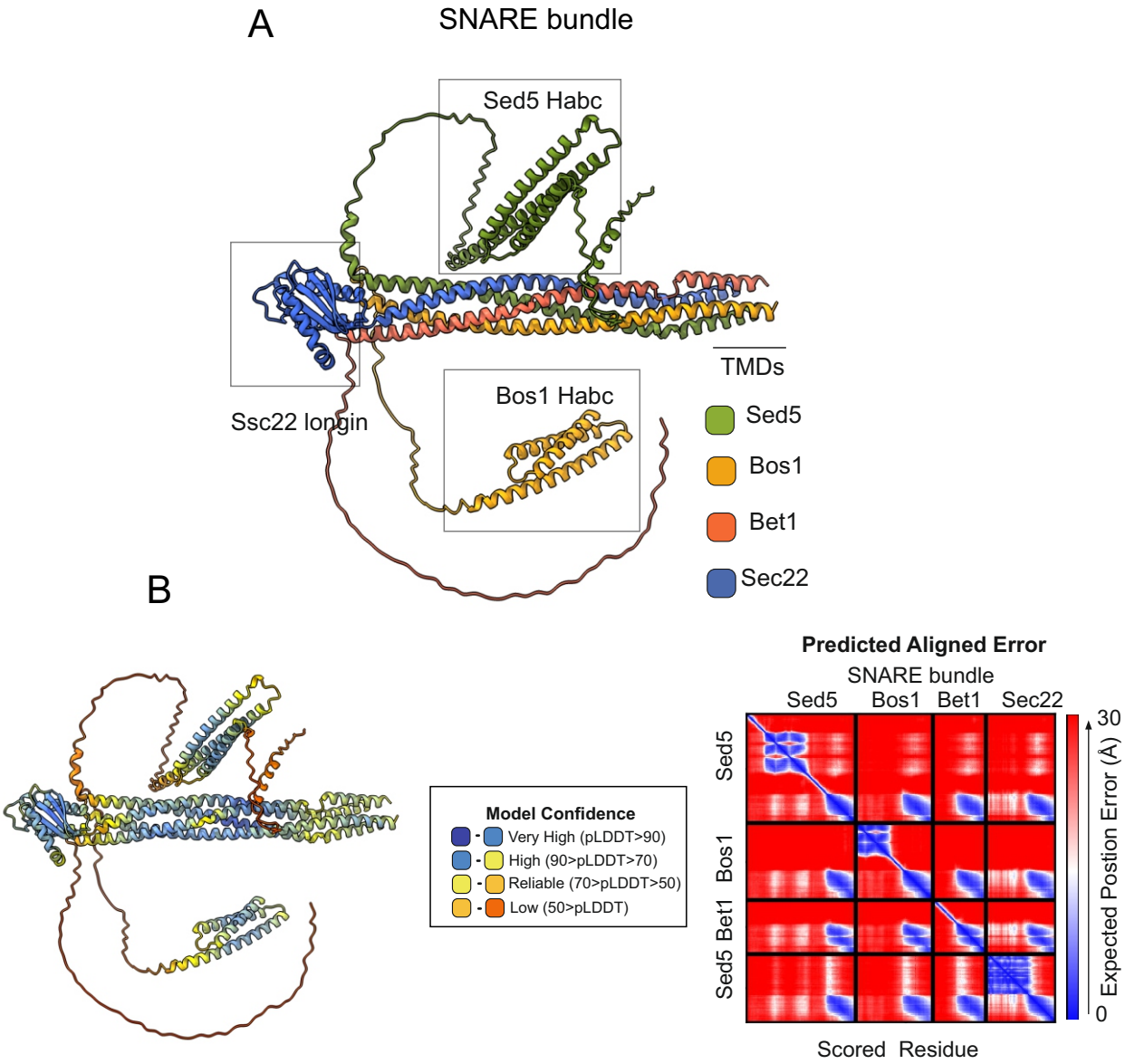

Figure 11—figure supplement 1. AlphaFold2 prediction of the ER/Golgi SNARE bundle.
(A) Sec5/Bos1/Bet1/Sec22 predicted SNARE bundle.
(B) Quality control (pLDDT, color coded, and PAE) of the model.

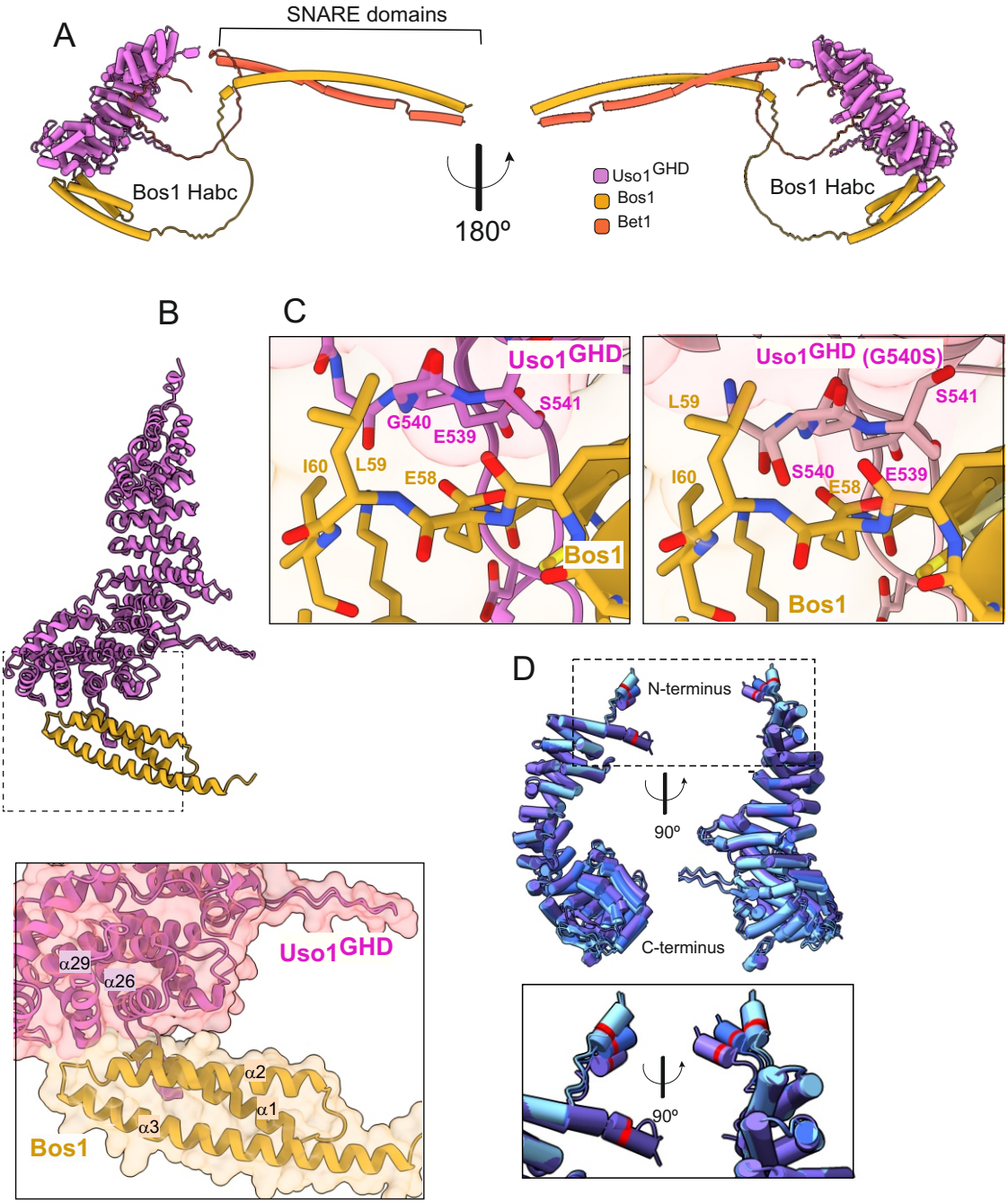

Figure 12. AlphaFold2 models provide insight into the additive mode of suppression shown by E6K and G540S.

(A). Model of full length Uso1 bound to the ER/Golgi SNAREs Bos1 and Bet1.

(B). Top, ribbon representation of the Bos1 N-terminal Habc domain and Uso1GHD. Bottom, Inset combining surface and ribbon depiction.

(C). Increased binding of Bos1 to G540S Uso1 appears to involve insertion of Ser540 into a pocket located in the Habc domain of the Qb SNARE. Partial view of the Bos1-Uso1 GHD surface of interaction in the wild type (left) and mutant (right) models. G540 and S540 are annotated.

(D). The N-terminal amphipathic α-helix of Uso1 comprising the E6K substitution lies within a flexible stretch of the protein that might facilitate its insertion into membranes. Alignment of six independent predictions, with Glu6 highlighted in red. The Uso1 GHD was modeled alone, in a complex with SNARE proteins or with Ypt1. The N-terminal α-helix (boxed) adopts different positions, suggesting high flexibility.

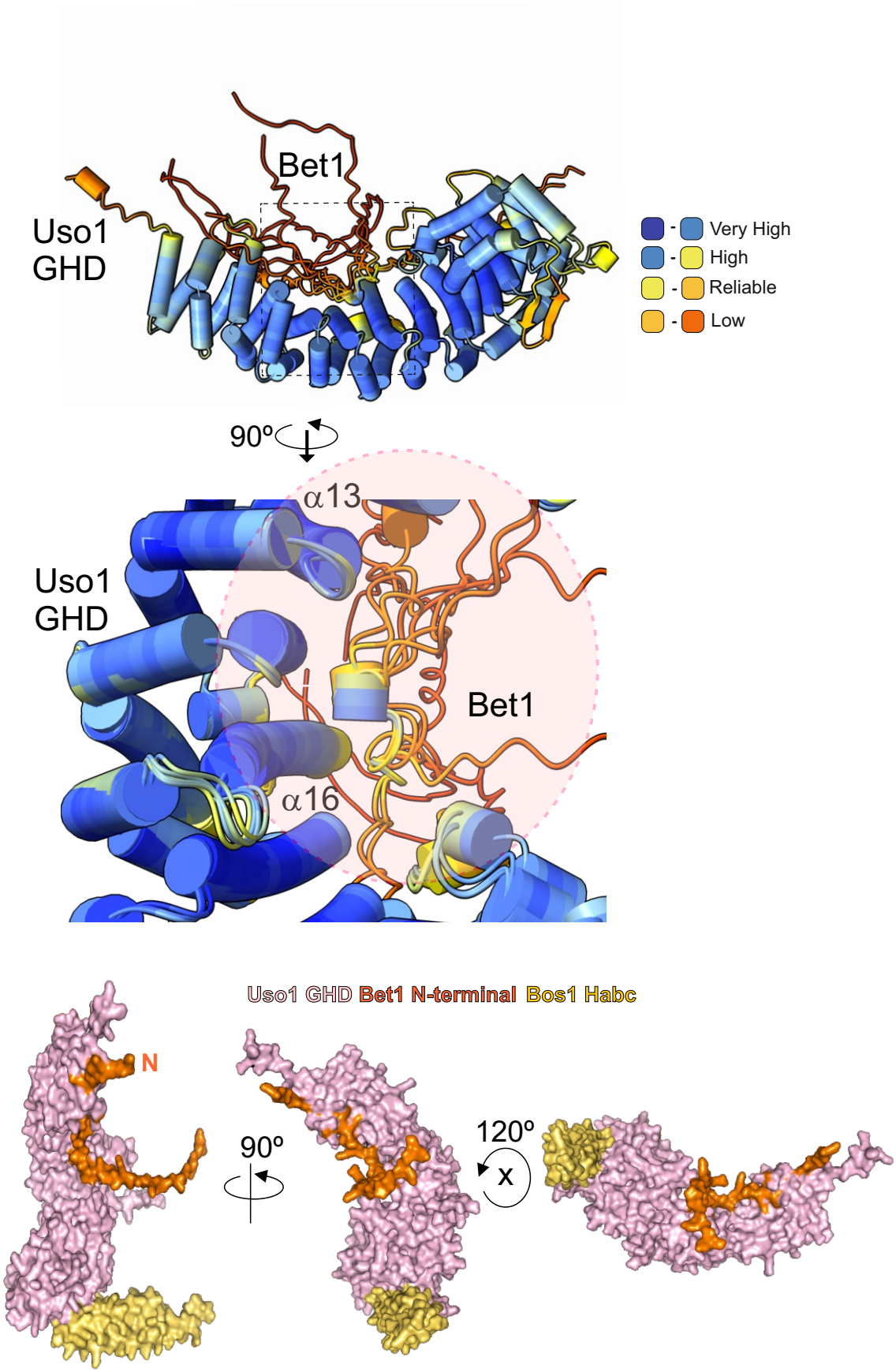

Figure 12—figure supplement 1. AlphaFold2 prediction of the Bet1-GHD interaction. The putative binding surface of Bet1 and Uso1 as determined by AlphaFold2. Top images, cartoon of Bet1-GHD interactions, colored by pLDDT score. Alignment of four independent predictions involving the Bet1 N-terminal region and Uso1 GHD. A single model for Uso1 GHD is shown on the top representation for simplicity. In spite of the disordered nature of the N-terminal Bet1 region, the Bet1-Uso1 binding interface is consistent among models. Bottom, surface representation of the N-terminal Bet1 region (orange) in complex with the GHD. Also indicated is the Habc domain of Bos1 (yellow) bound to the GHD.

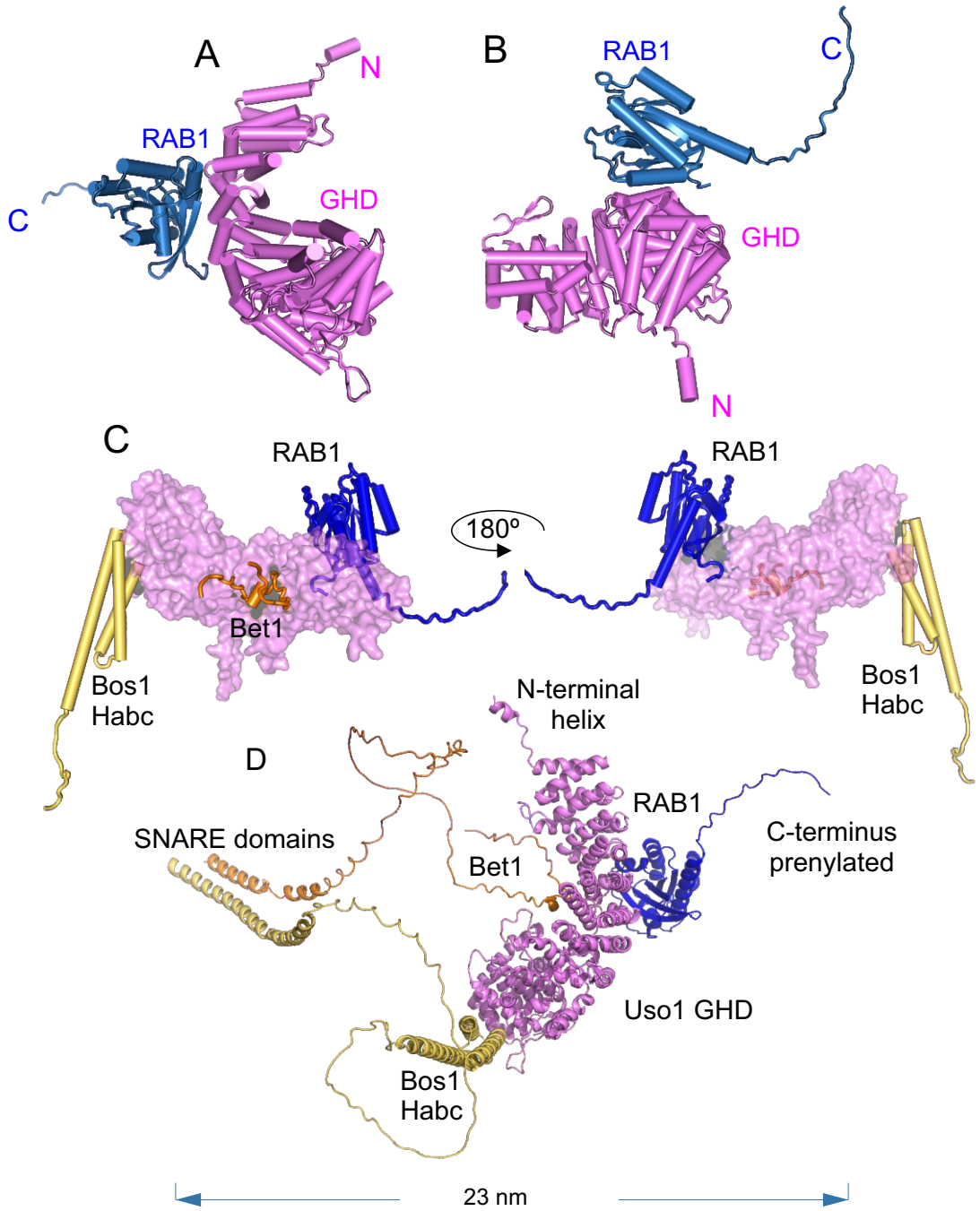

Figure 12—figure supplement 2. AlphaFold 2 prediction of the RAB1 binding site on the Bet1/Bos1/Uso1 GHD complex.
(A) and (B): cartoon representation of the GHD-RAB1 complex. The model is depicted as pipes and planks
(C): Orthogonal views of the Uso1 GHD-RAB1-Bet1-Bos1Habc structural model. The Uso1 GHD is shown as surface to emphasize the distant binding sites of the Bos1 Habc domain, RAB1 and the Bet1 N-terminal region
(D): Ribbon representation of the model shown in C but including the full-length SNARE subunits, i.e. the GHD domain of Uso1, RAB1 and the SNARES Bet1 and Bos1. Proteins are in the correct orientation to connect membranes separated by 23 nm, counting from the SNARE TMDs to the prenylated RAB1 residues.

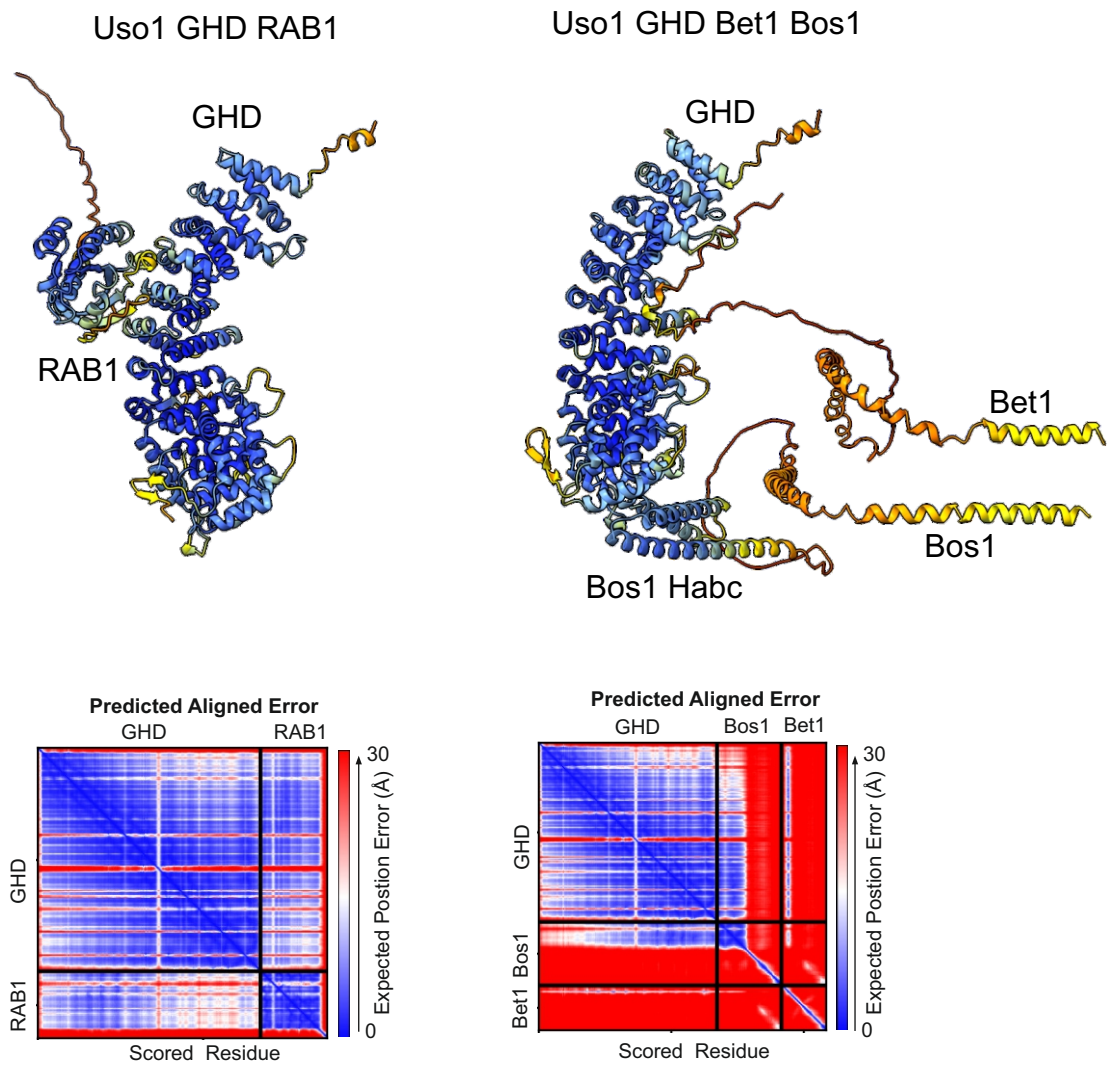

Figure 12—figure supplement 3. Quality control assessment of AlphaFold2 predictions for the indicated complexes.